Mechanisms that Promote Metastatic Progression in Nasopharyngeal Carcinoma

A dissertation

submitted by

David Merritt

In partial fulfillment of the requirements
for the degree of

Doctor of Philosophy

in

Immunology

TUFTS UNIVERSITY

Sackler School of Graduate Biomedical Sciences

February 2012

ADVISER: David Thorley-Lawson

Mechanisms that Promote Metastatic Progression in Nasopharyngeal Carcinoma

Abstract

Nasopharyngeal carcinoma (NPC) is a cancer of the head and neck, and is particularly common in Southern China. The non-keratinizing forms of NPC are associated with infection of the Epstein-Barr virus (EBV). These forms of NPC have been subdivided by the World Health Organization (WHO) into two classes based on histology: type II (poorly differentiated), and type III (undifferentiated). We developed a xenograft model of NPC in immunodeficient mice and found that tumors established with an NPC type III cell line (C666-1) frequently metastasize to distant tissues, whereas tumors established with an NPC type II cell line (HONE Akata) do not. This suggests that the distinction that separates type II and type III may be critical for metastatic progression in NPC. Our analysis of gene expression data from an Affymetrix study of type II and type III NPC using the Connectivity Map suggests that the PI3K-Akt-mTOR pathway may be more highly activated in NPC type III. The array data may also reflect differential sensitivity between type II and type III to PI3K-Akt-mTOR pathway inhibitors. When mice are treated with Rapamycin, an mTOR inhibitor, the growth of metastases is significantly reduced. Taken together, this suggests that the activation of the PI3K-Akt-mTOR pathway may provide a molecular basis for the distinction between NPC type II and NPC type III, and may be important for metastatic progression in NPC. It may also provide prognostic and therapeutic implications for more efficacious treatment specifically targeting metastatic NPC.

Using microarray analysis, we found that the EBV-encoded protein, LMP1, induces the transcription of the gene that encodes the chemokine CCL5/RANTES in

epithelial cells. The induction of this chemokine, which attracts lymphocytes, including T cells and macrophages, may provide a possible explanation for the extensive lymphocytic infiltrate seen in NPC tumors. RANTES has also been reported to play a causative role in promoting metastasis in models of lung and breast cancer. We therefore also investigated whether LMP1-induced expression of RANTES drives invasion and metastasis in NPC. Our data suggest that RANTES enhances the motility of NPC-derived cell lines and primary cells from NPC biopsies *in vitro* and may contribute to invasion and metastasis in our model of NPC *in vivo*.

Contents

Chapter 1

Introduction

Nasopharyngeal carcinoma

Nasopharyngeal carcinoma (NPC) is a cancer of the head and neck that is prevalent in southern China and Southeast Asia. In the endemic areas of China, including Guangdong province, the incidence is as high as 30 cases out of 100,000 persons per year. This represents approximately 20% of all cancers. In Hong Kong, it is the leading cancer in men aged 20-44 years (Lee, 2003). Within China, frequency decreases from south to north, with only 2 cases out of 100,000 persons per year in the Northern provinces. Throughout Southeast Asia, including Vietnam, the Philippines, Malaysia and Singapore, incidence is relatively high, occurring in approximately 18 cases out of 100,000 persons per year in Singapore. In contrast, the incidence is low in neighboring countries, such as Japan and Korea (less than one case per 100,000 persons per year). Outside of Asia, frequency is also low with the exception of intermediate incidence levels in North Africa, the Middle East and among Alaskan Eskimos (approximately 10 cases out of 100,000 persons per year, Yu 2002). Given its prevalence in medically underserved areas and the likelihood that it is underreported in other parts of Asia, including Indonesia and India, NPC represents a significant world health problem.

NPC is a squamous cell carcinoma that develops from transformed epithelial cells of the nasopharynx, often in recessed areas of the fossa of Rosenmuller (Vokes, 1997). It has a prominent background of infiltrating stroma, predominantly T cells, monocytes and

macrophages, which comprise the majority of the tumor mass, and was previously referred to as a lymphoepithelioma.

The World Health Organization (WHO) classification system distinguishes three types of NPC based on the differentiation status of the tumor cells. NPC type I is a differentiated keratinizing squamous cell carcinoma, and represents approximately 25% of NPC cases in North America, and 2% in Southern China (Marks 1998). NPC type II is a 'poorly' differentiated nonkeratinizing carcinoma that makes up 12% of cases in North America, and 3% in Southern China. In NPC type II tumors, there are clearly defined sections of transformed, malignant cells which retain the canonical cobblestone organization that is characteristic of epithelial cells. NPC type III is an undifferentiated carcinoma which represents 63% of cases in North America and 95% of cases in Southern China. In contrast with NPC type II, in NPC type III tumors, the transformed cancer cells appear more fibroblast-like and are interspersed sporadically among the infiltrating stroma.

Although the molecular basis for NPC pathogenesis is poorly understood, there are several prominent risk factors. First is the genetic predisposition among the Cantonese population. Epidemiological studies have reported that a high incidence of NPC is retained in subsequent generations of Cantonese people after they migrate to non-endemic areas, such as the United States (Jia, 2004). This suggests that there is a genetic component that increases the risk of developing NPC. Among environmental risk factors, the consumption of salted fish and other foods containing high concentrations of nitrosamines, a chemical carcinogen, is particularly notable (Yu, 2002). However, the most consistent environmental risk factor is infection with the Epstein-Barr virus (EBV).

The transformed epithelial cells in the non-keratinizing forms of NPC, types II and III, are 100% positive for EBV DNA, whereas the frequency of EBV infection of normal epithelium is extremely rare. Of note is that NPC type I is not associated with EBV infection.

Epstein-Barr virus

The Epstein-Barr virus is a B-lymphotropic gamma herpes virus and is associated with several types of human cancer, including Burkitt's lymphoma, Hodgkin's lymphoma, post-transplant lymphoproliferative disorder, gastric carcinoma and NPC. The association with both B cell lymphomas and epithelial carcinomas is a reflection of the dual tropism of the virus for B cells and epithelial cells as part of a life cycle that is exquisitely adapted to establish a latent infection in the human host.

The Epstein-Barr virus preferentially infects B cells through the binding of a viral glycoprotein, gp350, to the CD21 receptor on the surface of B cells (Nemerow, 1987). Fusion is mediated through the binding of another glycoprotein, gp42, to the MHC class II molecule HLA-DR1 as a co-receptor (Borza, 2002, Mullen, 2002). Infection of epithelial cells is less efficient and has recently been reported to require the binding of a complex of EBV glycoproteins, gHgL to integrins αvβ6 and αvβ8 on the surface of epithelial cells (Chesnokova, 2009).

EBV has the ability to transform resting B cells into latently infected lymphoblastoid cell lines (LCLs), providing valuable insight into the oncogenic potential of EBV-encoded gene products (Kieff, 2001). EBV transformed LCLs carry multiple copies of the viral episome and constitutively express a limited set of viral proteins and

transcripts, including six EBV nuclear antigens (EBNA1, EBNA2, EBNA3A, EBNA3B, EBNA3C and EBNA-LP), three latent membrane proteins (LMP1, LMP2A and LMP2B), transcripts from the *Bam*HIA region known as BART transcripts, and non-polyadenylated, non-coding RNAs called EBER1 and EBER2.

EBV-infected cells express virus encoded nuclear antigens that influence viral and cellular transcription. EBNA1 is expressed in all EBV infected cells and is critical to the maintenance of the viral episome. This is accomplished through sequence-specific binding to OriP, the viral plasmid origin of replication (Kieff, 2001). The protein is comprised of amino-terminal and carboxy-terminal domains separated by a glycine-alanine repeat sequence that appears to stabilize the mature protein and prevent its proteasomal degradation (Levitskaya, 1995). EBNA1 can influence the expression of viral nuclear antigens, including EBNA1 itself and LMP1 via interactions with viral promoters. Gene knockout studies suggest that apart from the maintenance of the episome, it plays no significant part in the transformation of B cells (Hume, 2003). Other studies, however, report that EBNA1 may have a role in oncogenesis since expression in B cells of transgenic mice induces the development of B cell lymphomas (Wilson, 1996).

EBNA2 is required for EBV-induced transformation of B cells *in vitro*. Evidence of its importance to transformation was first suggested by the inability of a viral strain, P3HR-1, to transform B cells *in vitro* (Kieff, 2001). This strain has a deletion that eliminates the gene that encodes EBNA2 and two exons of EBNA-LP. Restoration of EBNA2 in P3HR-1 confirmed the functional importance of EBNA2 in EBV-induced transformation (Hammerschmidt, 1989, Cohen, 1989). EBNA2 is responsible for the transcriptional activation of cellular genes, including CD23, as well as virus-encoded

genes, such as LMP1 and LMP2A, through interactions with a sequence-specific DNA binding protein, Jκ-recombination binding protein (RBP-Jκ) (Grossman, 1994, Hsieh, 1995). EBNA-LP interacts with EBNA2 and is required for efficient outgrowth of EBV-transformed B cells *in vitro* (Mannick, 1991, Sinclair, 1994).

The interaction of EBNA2 and EBNA-LP is moderated by the EBNA3A and EBNA3C proteins, which serve as negative regulators of EBNA2 (Roberston, 1996, Zhao, 1996). A role for EBNA3A and EBNA3C in transformation of B cells *in vitro* has been demonstrated using EBV recombinants (Tomkinson, 1993). EBNA3C has been shown to cooperate with RAS in classical rodent fibroblast transformation assays and disrupts cell cycle checkpoints (Parker, 1996, Parker, 2000). A role in transformation is further suggested by the ability of EBNA3A and EBNA3C to inhibit the expression of the pro-apoptotic protein BIM (Bcl2-like protein 11) (Anderton, 2008).

LMP1 is a transmembrane protein that functions as a classic oncogene in the rodent fibroblast transformation assay and is the main transforming protein encoded by the Epstein-Barr virus. LMP1 is essential for EBV-induced transformation of B cells *in vitro* (Wang, 1985, Kaye, 1993) and acts as a constitutively activated, ligand-independent member of the tumor necrosis factor receptor superfamily (TNFR) (Mosialos ,1995, Gires, 1997). Functionally, it is a homologue of CD40 and provides growth and differentiation signals in EBV-infected cells (Kilger, 1998). In support of this, LMP1 has been demonstrated to be able to partially substitute for CD40 in B cells (Uchida, 1999). LMP1 expression results in the activation of several signaling pathways, inducing the expression of anti-apoptotic proteins and cytokines, as well as modulating the expression of cell surface adhesion molecules.

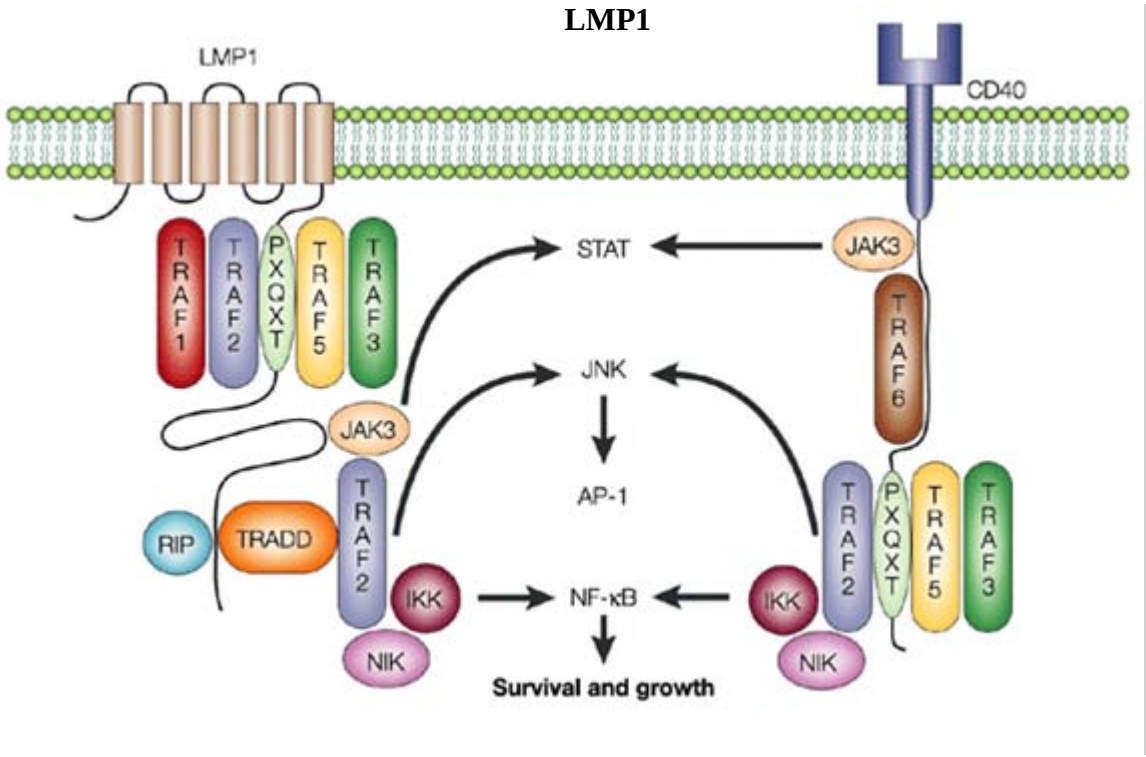

Figure 1. Latent membrane protein 1 (LMP1). LMP1 is a transmembrane protein consisting of cytoplasmic amino-terminal and carboxy-terminal domains linked by six transmembrane sequences. The carboxy-terminal signaling domain has significant functional homology with CD40. Both proteins contain consensus Tumor Necrosis Factor Receptor Associated Factor (TRAF) binding domains and interact with multiple signaling molecules. Both LMP1 and CD40 activate Nuclear Factor Kappa B (NF-κB), interact with Janus Activated Kinases (JAKs) and Signal Tranducers and Activators of Transcription (STATs), and activate Activator Protein 1 (AP-1) via the c-Jun N-Terminal Kinase (JNK) pathway. The net result is that both LMP1 and CD40 promote survival and proliferation. (Figure taken from Thorley-Lawson, 2001.)

LMP2A is a 12-span transmembrane proteins with no significant extracellular domain. It is not required for EBV-induced transformation of B cells *in vitro* (Longnecker, 2000). However, it has been reported to transform epithelial cells, enhance their motility and modulate their adhesion properties (Scholle, 2000). In infected B cells, LMP2A is a functional homologue for the B cell receptor and can drive proliferation and survival. In transgenic mice, it can substitute for the B cell receptor, allowing BCR-negative B lineage cells to bypass normal B cell development and colonize peripheral lymphoid organs (Caldwell, 1998).

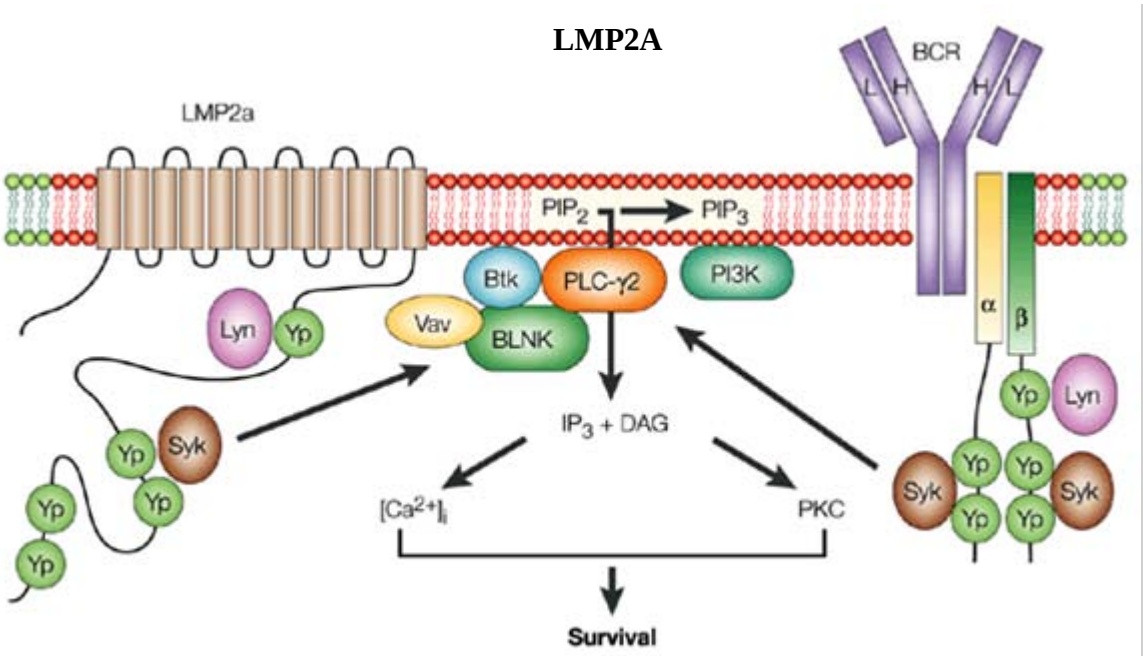

Figure 2. Latent Membrane Protein 2A (LMP2A.) LMP2A is a transmembrane protein consisting of amino-terminal and carboxy-terminal domains linked by twelve transmembrane sequences. The amino-terminal signaling domain of LMP2A contains immunoreceptor tyrosine-based activation motifs (ITAMs) similar to those of the B cell receptor (BCR). Both LMP2A and the BCR interact with the Src family tyrosine kinase Lyn. Phosphorylation of tyrosine residues in the ITAMs by Lyn allows the recruitment of the tyrosine kinase Syk and the corresponding downstream signaling, which promotes survival. (Figure taken from Thorley-Lawson, 2001.)

EBER1 and EBER2 are small non-coding RNAs that are transcribed in EBV-infected cells. EBERs are not required for EBV-induced transformation of B cells, however, expression in Burkitt's lymphoma cell lines has been reported to increase tumorigenicity, and promote cell survival (Ruf, 2000). A role for EBERs in EBV persistence has also been suggested. EBERs form a complex with the autoantigen La and ribosomal protein L22, and bind PKR, an interferon-inducible protein kinase believed to have a role in mediating the anti-viral effects of interferons (Nanbo, 2002).

*Bam*HIA rightward transcripts (BARTs) are RNAs encoded by the *Bam*HIA region of the EBV genome and are expressed in NPC, Burkitt's lymphoma, Hodgkin's lymphoma, and in EBV-infected B cells in the peripheral blood of healthy carriers. Several EBV-encoded microRNAs have been reported to be derived from these transcripts.

In NPC, a limited set of EBV-encoded gene products are expressed. EBNA1 and LMP2A are detected in all tumors, while LMP1 is detected in 50-60% of tumors (Busson, 1992, Heussinger, 2004). It is possible that LMP1 is expressed more frequently at early stages of neoplastic development and as the cancer progresses, it becomes dispensable for further tumor development. Several lines of evidence suggest that EBV plays a critical role in early NPC development. Primary epithelial cells from healthy carriers and premalignant NPC lesions contain EBV, suggesting that the virus is present prior to transformation (Pegtel, 2004, Pathmanathan, 1995). Furthermore, examination of the terminal repeat region of the virus demonstrates monoclonality of EBV in NPC. This suggests that EBV infection occurred before the clonal expansion of the tumor cells (Raab-Traub, 1986). Although it is not clear what the precise role of EBV is in NPC

development, given the tumorigenic properties of its encoded gene products and the fact that it is always present in premalignant lesions in the non-keratinizing forms of NPC, it is highly likely that EBV plays a critical role in driving tumor progression in NPC.

PI3K-Akt-mTOR Signaling

Among the common genetic abnormalities frequently detected in NPC samples is the dysregulation of PIK3CA, the gene that encodes the phosphoinositide 3-kinase (PI3K) alpha polypeptide. Comparative genomic hybridization (CGH) studies of NPC biopsies have shown that PIK3CA is frequently amplified and overexpressed (Hui, 2002, Or, 2005). PI3K activation initiates a signal transduction cascade that promotes cancer cell growth, survival and metabolism (Engelman, 2009).

Class I_A PI3Ks phosphorylate phosphatidylinositol-4,5-bisphosphate (PIP_2) on the plasma membrane to generate the second messenger, phosphatidylinositol-3,4,5-triphosphate (PIP_3) which activates many downstream molecules by binding to their pleckstrin homology domains (DiNito, 2003). The protein serine/threonine kinase Akt is the principal target of PIP_3 (Franke, 1997). Binding of Akt and PIP_3 results in the recruitment of Akt to the membrane surface and the subsequent phosphorylation of Akt by mTORC2 (Mammalian Target of Rapamycin, Complex 2) at serine 473 and PDK1 (3-phosphoinositide-dependent kinase) at threonin 308. This results in the full activation of Akt, which in turn, phosphorylates many downstream proteins which regulate a range of cellular functions, including cellular metabolism, cell cycle regulation, survival, protein synthesis and cell motility.

Several downstream targets of Akt operate together to promote tumorigenesis. Among these is the Mammalian Target of Rapamycin (mTOR)-raptor kinase complex, also called mTOR complex 1 (mTORC1). The mTOR-raptor kinase complex is a crucial regulator of cellular growth. Akt activates mTOR-raptor by directly phosphorylating Tuberous sclerosis protein 2 (TSC2), also known as tuberin. This inhibits the ability of the tuberin-hamartin complex (TSC1/TSC2) to function as a GTPase-activating protein (GAP) for the Ras-like GTP binding protein (RHEB) (Inoki, 2002, Potter, 2002). This allows RHEB to accumulate in the GTP-bound state, leading to the activation of the mTOR-raptor complex. This activation normally occurs in response to stimulation of receptor tyrosine kinases (RTKs) but can also occur constitutively in cancer with the aberrant activation of PI3K.

mTOR promotes protein synthesis through the activation of 4E-BP1 and p70S6 kinase. The importance of mTOR signaling in promoting PI3K-dependent tumorigenesis has been demonstrated by the finding that the mTOR-raptor inhibitor, Rapamycin abrogates Akt-driven prostate intraepithelial neoplasia in a transgenic model (Majumder, 2004). Furthermore, Rapamycin has been shown to inhibit tumorigenesis in PTEN-deficient cancer cell lines (Neshat, 2001, Podsypanina, 2001).

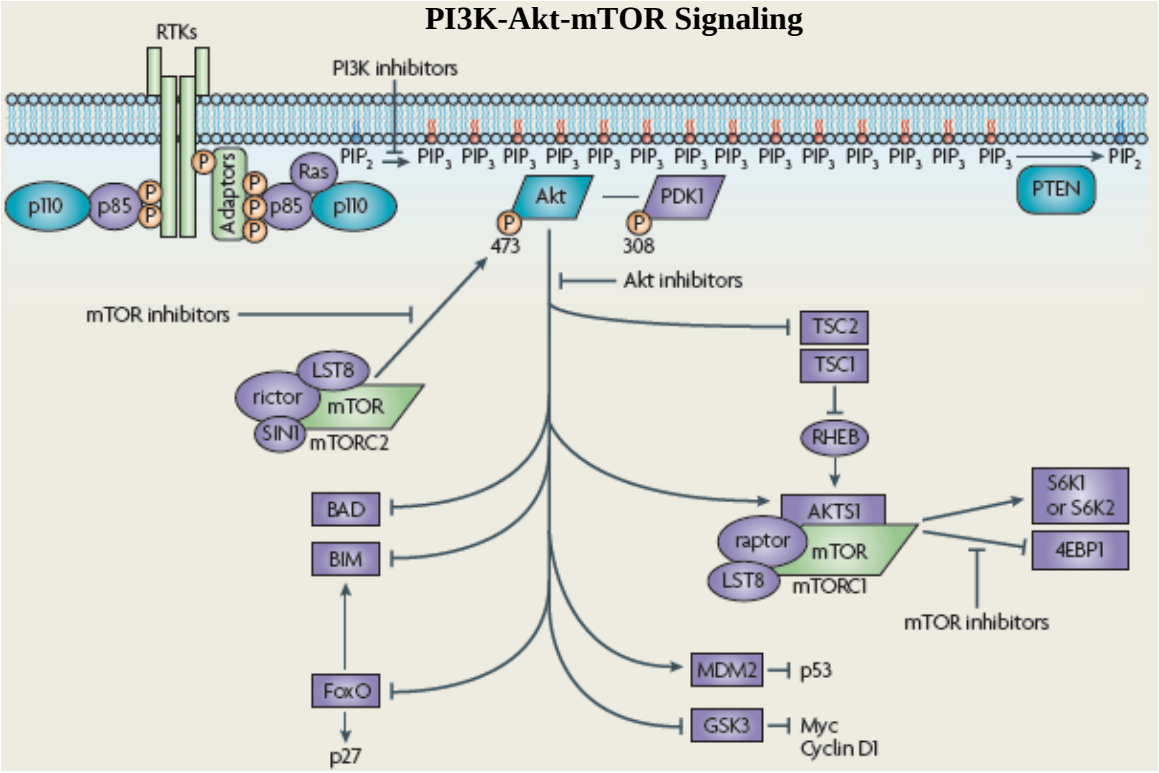

Figure 3. PI3K-Akt-mTOR signaling. Class IA PI3Ks phosphorylate phosphatidylinositol-4,5-bisphosphate (PIP_2) on the plasma membrane to generate the second messenger, phosphatidylinositol-3,4,5-triphosphate (PIP_3.) The 3' phosphatase PTEN dephosphorylates PIP_3, terminating PI3K signaling. Accumulation of PIP_3 on the surface leads to the recruitment of Akt and PDK1 to the membrane, where they bind directly to PIP_3. Phosphorylation of Akt at threonine 308 by PDK1 and serine 473 by the mTOR-rictor complex leads to full activation of Akt. Activated Akt phosphorylates several cellular proteins including GS3Kα, GS3Kβ, FoxO, MDM2, BIM and BAD, thereby promoting survival and regulating cell cycle entry. In addition, Akt phosphorylates and inactivates TSC2 (tuberin), which in turn allows RHEB to accumulate in the GTP-bound state, leading to the activation of the mTOR-raptor complex. (Figure taken from Engleman, 2009.)

Metastasis

Tumor progression from carcinoma *in situ* to metastatic carcinoma is frequently described as a multistep process in which tumor cells spread from the primary tumor to colonize distant organs (Gupta, 2006). Many genetic and epigenetic events that are critical to transformation have been shown to contribute to metastatic progression, including those which promote self-sufficiency of growth signals, evasion of apoptosis, alterations that provide unlimited replicative potential and events which promote an undifferentiated stem-like phenotype (Chambers, 2002). Tumor cells frequently remain addicted to the effects of these genetic lesions during later stages of tumor development, including metastasis. This is supported by evidence that lung metastases in a conditional Neu (also called HER2 and Erbb2) breast cancer mouse model regress when Neu expression eliminated (Moody, 2002), and by a report that shows that the progression-free survival of breast cancer patients with HER2-positive tumors improves under chemotherapy with the addition of Trastuzumab (Herceptin), a monoclonal antibody to HER2 (Slamon, 2001).

Transformation and primary tumor development, however, are not sufficient to confer the ability to metastasize. In order for malignant cells to traverse natural barriers and establish disseminated metastases in distant tissues, additional capabilities must be acquired. This is shown by the lack of metastases as a common feature in numerous cancer models based on genetically-modified mice (Minna, 2003). Furthermore, disseminated cancer cells can be detected in patients who do not develop metastases (Klein, 2003). The sequence of steps required for metastatic progression: local invasion,

intravasation, circulation, extravasation, and colonization, give insight to the required capabilities that must be acquired as a tumor progresses to metastatic disease.

Genes that drive tumor cells to invade local tissue and attract supportive stroma promote the motility and dispersion of cancer cells from the primary tumor. These genes have been described as metastasis-initiation genes (Nguyen, 2007) and may promote a number of activities, including epithelial-mesenchymal transition (EMT), extracellular matrix modification, angiogenesis, and bone marrow progenitor mobilization. EMT is a developmental program characterized by loss of cell adhesion, repression of E-cadherin expression and increased cell mobility and is essential for mesoderm formation and neurulation. EMT appears to be aberrantly activated in a number of cancers and is frequently driven by the expression of several genes that encode transcription factors, such as TWIST1, SNAI1 and SNAI2 (Yang, 2008). Other genes that promote invasion include MTDH, which encodes metadherin, in breast cancer (Hu, 2009) and MACC1 (metastasis-associated in colon cancer 1) in colon cancer (Stein, 2009). Metastatic growth can also be initiated by the suppression of microRNAs such as miR-126 in colorectal cancer (Gou, 2008) and miR-335 in breast cancer (Tavazoie, 2008).

The ability to passage through capillary walls, survive through transit in circulation, and survive in invaded parenchyma requires additional capabilities and allows tumor cells to invade distant organs. Malignant cells entering the circulation must have the genes that are required for this to already be dysregulated in the primary tumor, before dissemination. However, the effects in the distant site may be distinct from those in the primary tumor. These genes can be described as metastasis progression genes (Nguyen, 2007).

Since the composition of the capillary walls and underlying parenchyma will differ significantly in different tissue types, the molecular mechanisms and therefore, underlying genetic events, that are required for colonization will vary for different target organs. The expression of a set of genes in the primary tumor that promotes metastasis to a specific organ may provide prognostic markers that have a predictive value for the risk of metastatic relapse to the specific organ. This can be demonstrated by genes which promote metastasis specifically to bone but do not appear to confer a selective advantage to the primary tumor, such as PTHRP (parathyroid hormone related protein), which mobilizes osteoclasts (Yin, 1999), and IL-11 (interleukin-11) (Kang, 2003). These genes have been referred to as metastasis virulence genes (Nguyen, 2009).

Epithelial-Mesenchymal Transition

Epithelial-mesenchymal transition is a complex molecular and cellular program in which cells lose many of their differentiated characteristics and alter their phenotypes between epithelial and mesenchymal states. Cells typically shed canonical epithelial traits, such as cell-cell adhesion, planar and apical-basal polarity and instead, adopt mesenchymal features, such as increased motility, invasiveness and an increased resistance to apoptosis. EMT plays a prominent role in embryonic development, but its role in cancer development is particularly noteworthy (Baum, 2008, Yang, 2008). EMT has been determined to contribute to invasion, metastasis, and resistance to therapy. Cells progressively lose responsiveness to regulatory signals and gain a degree of plasticity in their differentiation status due to genetic and/or epigenetic instability. This frequently results in distinct subpopulations of cancer cells within tumors.

An EMT program can be initiated by multiple extracellular signals and there is frequent crosstalk between downstream intracellular signaling pathways and transcription factors which work in concert to promote the acquired mesenchymal characteristics (Thiery, 2006). Sustained activation of EMT-promoting signals can result in the progressive accumulation of epigenetic events which may be inherited in successive generations of cells, even after cessation of extracellular EMT promoting signals (Dumont, 2008). EMT is generally thought to be induced by signaling factors released by mesenchymal cells that constitute the stroma of normal and malignant tissue.

The transforming growth factor β (TGFβ) family of cytokines comprise the best characterized examples of EMT-promoting factors in embryonic development, wound healing, and neoplastic development (Yang, 2008, Massague, 2008). TGFβ can induce EMT through the phosphorylation of SMAD transcription factors and cytoplasmic proteins which regulate cell polarity and the maintenance of tight junctions, such as PAR6A. Phosphorylation of PAR6A results in the loss of cell adhesion and basal-apical polarity (Ozdamar, 2005). TGFβ signaling can also promote EMT through crosstalk with other pathways which promote EMT, such as Wnt and Notch.

Wnt signaling promotes EMT by increasing the levels of β-catenin. Wnt inhibits the glycogen synthase kinase 3β (GSK3β)-mediated phosphorylation and subsequent degradation of β-catenin. As a consequence, β-catenin levels increase. β-catenin then translocates to the nucleus where it serves as a subunit of a transcription factor that transactivates several genes, including EMT-promoting transcription factors (Vincan, 2008). Notch can promote EMT by modulating the activity of TGFβ and by activating NF-κB (Wang, 2006).

Several transcription factors have been identified which contribute to EMT during embryonic and neoplastic development. SNAI1, SNAI2 (also known as SLUG), ZEB2, and E47 are transcriptional repressors of E-cadherin. TWIST, ZEB1, FOXC1 and FOXC2 also promote EMT and confer stem cell characteristics to epithelial cells. In addition, several non-coding RNAs have been demonstrated to have a role in activating EMT. These include the miR-200 family, mir-205 and mir-335.

The Tumor Microenvironment

Tumors frequently develop as heterogeneous masses infiltrated with non-malignant stroma from the surrounding environment. In NPC, the majority of the tumor mass is composed of recruited cells of lymphoid and myeloid origin. The microenvironment can impose inhibitory effects on aggressive malignant cells. However, as the tumor progresses, it may acquire capabilities that allow it to circumvent these inhibitory signals and instead exploit the surrounding cells to enhance its ability for growth, invasion and eventually metastasis. Among the stromal cell types that have been reported to contribute to cancer pathogenesis are endothelial cells, fibroblasts and bone marrow derived cells (BMDCs), including macrophages, mast cells, neutrophils and mesenchymal stem cells (MSCs).

Tumors are frequently inundated with infiltrating lymphocytes. In the past this was perceived as a failed immune response to eliminate the tumor. However, in addition to being able to develop mechanisms to escape immune surveillance, tumors can also develop the ability to modulate the activity of certain inflammatory cell types, co-opting them to effectively become tumor-promoting instead of tumor-suppressing. Furthermore,

many inflammatory cell types that get recruited to the tumor are not responding as an anti-tumor response, but rather, as part of an inflammatory response due to the tissue disruption caused by the developing tumor. This is particularly notable in cancers associated with chronic inflammation, where the initial inflammatory response is not resolved, and instead, alterations evolve that promote the continued recruitment of BMDCs (Mantovani, 2008). This results in a cascade of events and interactions which amplify the tumor-promoting characteristics of the infiltrating stroma. Many of these activities may be the result of the aberrant activation of mechanisms that are normally used for wound healing or development (Medzhitov, 2008). Determining the specific contribution of BMDC cell types to tumor progression is complicated by the pleiotropic effects of their presence in the tumor. CD4+ T cells, macrophages and natural killer T cells (NKT) may exhibit either tumor-promoting or tumor-suppressing functions, depending on the tissue context and the extracellular stimuli from the surrounding environment (de Visser, 2006, Nozawa, 2006).

The induction of angiogenesis is critical to the development and growth of tumors. It is also crucial for the haematological spread of circulating tumor cells for metastasis. Macrophages, monocytes, neutrophils and mast cells have been reported to contribute to tumor development in part through their contributions to angiogenesis through the production of growth factors and cytokines (Lin, 2006). They can also modulate the local environment through the production of vascular endothelial growth factor A (VEGFA) and matrix metalloproteinases (MMPs).

Model of NPC pathogenesis

We can propose a model for the step-wise progression of genetic alterations and crucial events involved in the development of nasopharyngeal carcinoma that drives the progression from normal nasopharyngeal epithelium, to reversible hyperplasia, to severe dysplasia and carcinoma *in situ* and then finally to invasive carcinoma and metastasis. Loss of heterozygosity (LOH) can be detected early in high risk populations. Frequent deletions are found in regions of chromosomes 3p and 9p in cells of high risk individuals that lack EBV. In addition, promoter hypermethylation of several genes on chromosome 3p, including RASSF1A and retinoic-acid receptor B2, and on chromosome 9p, including p16 (INK4A), p15 (INK4B), and p19 (ARF) is frequently observed (Lo, 2002). This, in addition to exposure to environmental risk factors such as salted fish, results in a low grade hyperplasia that is susceptible to EBV infection. This is supported by the observation that monoclonality of the viral genome can be detected in EBV-infected cells prior to the expansion of the malignant cell clone (Raab-Traub, 1986).

After EBV infection, virus-encoded latent genes may provide signals that promote survival and growth advantages. Additional genetic lesions begin to accumulate, including LOH in chromosomes 11q, 13q and 14q (Lo, 2002). Cells may appear to dedifferentiate, resulting in carcinoma *in situ*. Further loss of additional tumor suppressors results in the dysregulation of the cell cycle, DNA damage recognition and repair mechanisms and pathways that regulate apoptosis. Eventually tumor cells gain the ability to invade beyond the basement membrane, leading to an invasive carcinoma, then eventually to metastasis (figure 4).

Figure 4. Proposed model of nasopharyngeal carcinoma pathogenesis

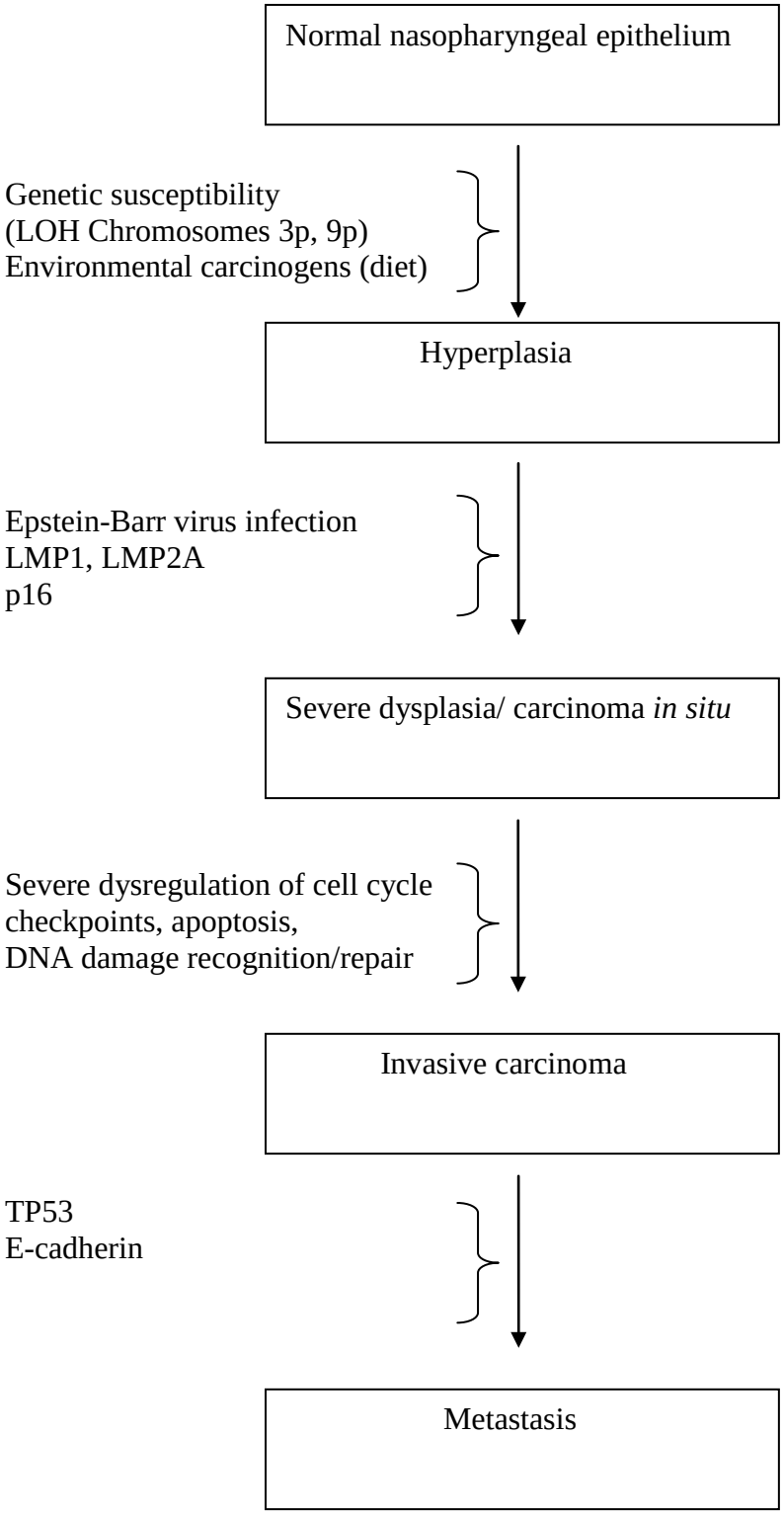

Clinical Presentation and Treatment

NPC normally originates in an area of the nasopharynx called the fossa of Rosenmuller. This is a clinically occult site and initial symptoms of disease, such as headaches, congestion and inner ear infections are nonspecific and are easily confused with the symptoms of the flu. As a result, early stages of the disease frequently go undetected. NPC is frequently missed even by endoscopic examination since the tumor spreads submucosally. As a result, by the time of diagnosis, over 90% of patients have advanced disseminated disease (Lee, 1997).

Primary NPC tumors are highly radiosensitive and radiotherapy remains the standard treatment of early stage disease. However, once the disease has spread to nearby tissue and lymph nodes, the survival rate declines rapidly (Cheng, 2000) and the chance of recurrence increases dramatically (Heng, 1999). Metastatic disease is essentially incurable and the treatment options are largely for palliative effect (Kwong, 2004). Therefore, there is a clinically relevant need to identify molecular pathways and biological processes that contribute to invasion and metastasis in NPC. The discovery of mechanisms that promote metastatic progression may provide potential targets for therapeutic intervention.

Chapter 2

Materials and Methods

I. Tissue Culture

Cell lines

The HaCaT epithelial cell line (ATCC) and the NPC type II cell lines, HONE-1 and HONE Akata (a gift from Ronald Glaser, Ohio State) were cultured in DMEM. The NPC type III cell line, C666-1 (provided by Fei Fei Lui, Ontario Cancer Institute, University of Toronto) was cultured in RPMI 1640. Media was supplemented with 10% heat-inactivated fetal bovine serum and maintained at 37° C in a 5% CO_2 and water-saturated environment.

Primary Cells and Biopsies

Human tonsils and NPC biopsies provided by Tufts Medical Center were sectioned and washed in DMEM/F12 supplemented with 10% FBS and Penicillin/Streptomycin with Amphotericin B. The explants were then placed under transwell devices in 10 cm tissue culture dishes and maintained in DMEM/F12. The transwell devices provided physical pressure that promoted epithelial cell adhesion to the tissue culture plate. After four days, the transwells were removed and the media was replaced with serum-free media supplemented with keratinocyte growth factor. This provided a growth advantage for the epithelial cells over fibroblasts. After the primary tonsillar epithelial cells or NPC biopsy cells grew to a significant number, the explants

were removed, and the cells were trypsinized and replated to form uniform monolayer cultures which could then be used for experiments.

Transfection

HONE Akata and C666-1 cells were transfected with a plasmid (pGL4.51 luc2.CMV/Neo, Promega) to express firefly luciferase. Electroporation was performed using a BTX High Throughput Electroporator (HT-200) with the following conditions: 2 pulses at 155 volts for 99 ms duration. In order to generate stable transfectants, cells were then selected by culturing transfected cells with media supplemented with G418 (Invitrogen).

Lentivirus infection

HONE Akata and C666-1 cells were infected with a lentivirus (pGreenFire1-CMV, TR011VA-1, System Biosciences) to express luciferase and GFP. Infected cells were selected by multiple rounds of sorting GFP positive cells. Cells were cultured for at least two weeks between sorting intervals. Luciferase expression was confirmed by adding luciferin (100 ng/ml) to cell cultures, then imaging cells using a Xenogen IVIS 200 biophotonic imager.

Adenovirus infection

Cell lines and primary cells were infected with adenoviruses in order to express the EBV latent proteins, either LMP1 or LMP2A, as well as GFP. Adenoviruses were created by cloning B95-8 LMP1 or LMP2A cDNA into the KpnI-NotI sites of the

polylinker of a pShuttle vector (fig. 5) containing an upstream ubiquitin promoter-EGFP cassette (Sutkowski, 2004). Recombinant adenovirus plasmids were produced by homologous recombination with the pAdEasy system (Quantum Biotechnologies) and provided to our lab by Brigitte Huber's lab at Tufts University. Adenoviruses were produced in 293 cells by the Gastroenterology Research on Absorptive and Secretory Processes (GRASP) facility at Tufts Medical Center. Infected cells expressed the gene of interest (either LMP1 or LMP2A) and EGFP. Control cells were infected with matched titres of a control adenovirus that expressed only EGFP.

Figure 5. Vector map of pShuttle plasmid used for cloning LMP1 and LMP2A adenovectors

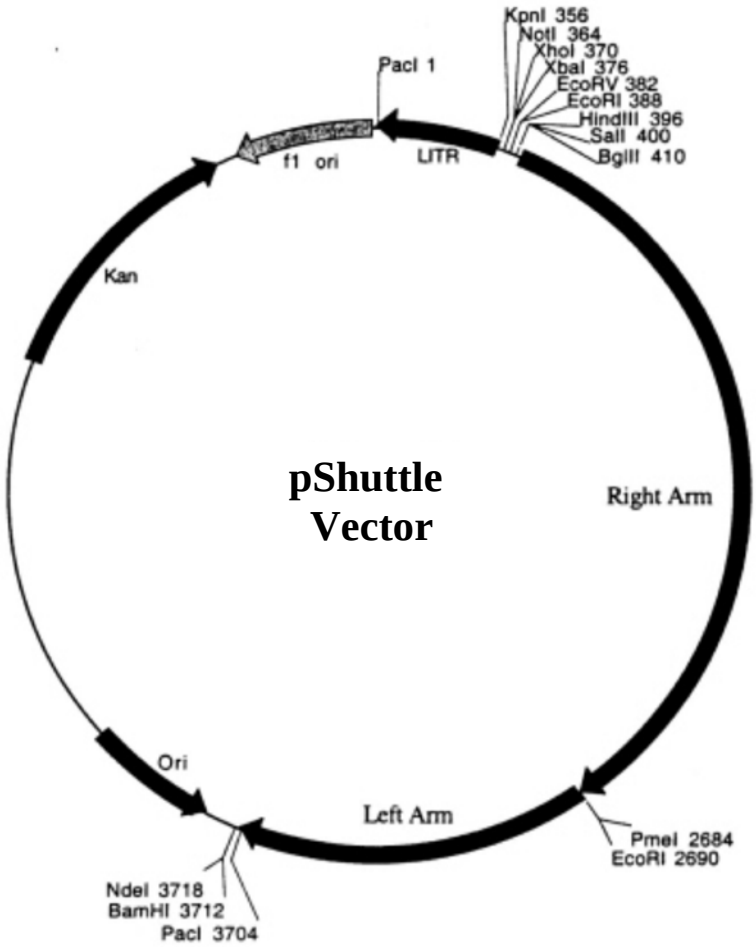

II. Mice

Injection of Cells to Establish Xenograft Tumors

The severely immunodeficient mouse strain, NOD.Cg-Prkdc^{scid} Il2rg^{tm1Wj1}/SzJ (NOD scid gamma) was used in all of our experiments. 5×10^5 tumor cells suspended in 100 µl of PBS were injected subcutaneously in the right flanks of mice. Tail vein

injections were performed by injecting 2×10^5 cells suspended in 300 µl of PBS. For orthotopic nasopharyngeal injections, the mice were first anaesthetized with a Ketamine (100 mg/kg)/Xylazine (16 mg/kg) formulation by intraperitoneal injection. They were then placed in a prone position with their mouths held open with forceps. A second set of forceps was used to pull the tongue to the side, allowing a clear view to the back of the oral cavity. 2.5×105 tumor cells suspended in 30 µl of PBS were then injected in the nasopharyngeal tissue of mice, distal and to the right of the hard palate.

Drug treatment

Rapamycin (LKT laboratories) was diluted in PBS containing 5% PEG300 and 5% Tween80 to a final dose of 5 mg/kg in 100 µl and administered to mice by IP injection each weekday (Monday to Friday) for the duration of the experiment. Placebo-treated mice received 100 µl of the PBS/PEG300/Tween80 formulation.

Antibody treatment

Mice were treated with 32 µg of anti-human CCL5/RANTES polyclonal antibody (AB-278-NA, R&D Systems), diluted to a volume of 100 µl, and then IP injected twice a week for the duration of the experiment. Control mice receiving the isotype control antibody were injected with 32 µg of normal goat control IgG (AB-108-C, R&D Systems) twice a week.

III. Protocols

In vivo imaging

Xenograft tumors in NOD scid gamma mice were imaged using a Xenogen IVIS 200 biophotonic imaging system. Mice were IP injected with 1 mg of luciferin, diluted in 100 μl of PBS, and then anesthetized with isoflurane. They were then imaged for luciferase activity with exposure times ranging from 10 seconds to 5 minutes. Since large primary tumors could be strong light sources that make detection of developing metastases difficult, images were also taken with the heads of the mice covered with heavy black construction paper, allowing for longer exposure times and greater sensitivity in detecting small, disseminated tumors.

Image analysis

Analysis of luciferase activity to estimate tumor size was performed using Living Image software (Caliper Lifesciences). For each tumor, a region of interest (ROI) is prescribed where the signal strength is at least 5% of the maximum intensity for that exposure. The photon flux (photons emitted per second) from that region is then calculated. This approximates the size of the tumor. Growth over time and response to drug treatment can then be followed over a period of several weeks.

Histology

Histological analysis of excised tissue was performed by the Department of Laboratory Animal Medicine (DLAM) at Tufts University or the Clinical Histology lab at Tufts Medical Center. Tissue sections and organs encompassing tumors were excised

from sacrificed mice using luciferase imaging to identify the locations of primary tumors and metastases. Tissues were fixed in 70% ethanol and stored at 4°C. Tissue processing, paraffin embedding and H&E staining were performed using standard techniques by the respective labs. Cytokeratin staining was performed with a AE1/AE3/PCK26 anti-Pan Keratin antibody (Ventana). *in situ* hybridization for EBER, an EBV encoded RNA, was also performed (INFORM EBER, Ventana).

Connectivity Map

Data from an Affymetrix study of 6 NPC type II biopsies and 8 NPC type III biopsies previously done in our lab were reanalyzed using the Connectivity Map, a bioinformatics algorithm developed at the Broad Institute. Conventional marker-selection techniques identified the 50 transcripts most differentially up-regulated and the 50 most differentially down-regulated between the type II and type III data sets on the basis of fold-change of RNA expression. This set of 100 genes was used to create a gene expression "signature" that indirectly describes the difference in the gene expression profiles of NPC type II and NPC type III which could then be used to query the Connectivity Map. The Connectivity Map is a database of genome-wide expression profiles of cultured human cell lines exposed to a large panel of bioactive small molecules with known biochemical mechanisms, along with a pattern-matching algorithm that ranks the similarity of gene expression responses to the bioactive molecules to a gene expression "signature" of interest. This can potentially provide insight into the underlying biological mechanisms that drive disease states, or the results of genetic alterations. The current version of the Connectivity Map (build 02) contains

genome-wide expression data for 7000 expression profiles, representing 1309 compounds. Enrichment of both the up- and down-regulated genes from a type III/type II signature in the thousands of treatment instances was estimated with a metric based on the Kolmogorov-Smirnov statistic (Lamb, 2006) and combined to produce a connectivity score. P-values were estimated by permutation testing. Further information can be found at (http://www.broadinstitute.org/cmap).

Gene Set Enrichment Analysis (GSEA)

We analyzed the Affymetrix data using an algorithm called Gene Set Enrichment Analysis (GSEA). Conventional marker selection techniques were applied to identify and rank genes that were up or down regulated in NPC type II or NPC type III based on fold change. We then used this gene profile to interrogate the GSEA data base of curated gene sets. GSEA is a general statistical method to test for the enrichment of set of genes in expression data. It contains a large collection of empirically defined gene sets (typically genes in the same functional class or signaling pathway) and provides a method to determine whether the members of these sets are overrepresented at the top (or bottom) of a gene profile, which has been rank-ordered by correlation with a specific phenotype (in this case, the relative expression level in NPC type II vs NPC type III biopsies). The output is a gene set enrichment score (ES) for each of the curated gene sets. To derive significance, the NPC type II vs NPC type III data set was permuted 1000 times, and random ES were calculated. Since none of the random enrichment scores exceeded the

observed ES, the P value was <0.001. Further information can be found at (http://www.broadinstitute.org/gsea).

Western Blot

Western blotting was performed using NuPAGE 4-12% Bis-Tris gels (NPO336, Invitrogen) employing standard protocols. We used primary antibodies against phosphorylated S473-Akt (4058, Cell Signaling), phosphorylated T308-Akt (4056, Cell Signaling), and β-actin (4970, Cell Signaling). For secondary antibodies, we used rabbit antibodies to mouse conjugated with horseradish peroxidase (7074, Cell Signaling), and developed the blots using ECL (Pierce).

MTS proliferation/survival assay

Proliferation assays of cells exposed to Rapamycin were performed using the CellTiter 96® AQ_{ueous} Assay (G3580 Promega), which uses the tetrazolium compound (3-(4,5-dimethylthiazol-2-yl)-5-(3-carboxymethoxyphenyl)-2-(4-sulfophenyl)-2H-tetrazolium, inner salt; MTS) and the electron coupling reagent, phenazine ethosulfate (PES). MTS is chemically reduced by cells into formazan, which is soluble in tissue culture medium. The measurement of the absorbance of the formazan can be carried out using 96 well microplates at 490nm. The assay measures dehydrogenase enzyme activity found in metabolically active cells. Since the production of formazan is proportional to the number of living cells, the intensity of the produced color is a good indication of the

viability of the cells. MTS solutions were prepared according to the manufacturer's instructions. NPC cell lines, cells cultured from NPC biopsies and primary epithelial cells were exposed to various concentrations of Rapamycin (9904, Cell Signaling) for 72 hours, then the assay was performed.

Microarray

Chemokines induced by the expression of EBV encoded proteins LMP1 and LMP2A were investigated by performing expression analysis using limited microarrays for chemokine gene expression. RNA from HaCaT cells infected with LMP1, LMP2A and control adenoviruses was prepared using TRIzol (Invitrogen Life Sciences). RNA was then reverse-transcribed with Biotin-16-dUTP (Roche) using the SuperArray TrueLabeling-RT Enzyme kit according to the manufacturer's protocol. The resulting biotinylated cDNA probe was hybridized overnight at 60° C to Human Chemokine and Chemokine Receptor arrays (SuperArray Biosciences). After washing and blocking array membranes, alkaline phosphatase-conjugated streptavidin was allowed to bind, and then CDP-Star substrate (SuperArray Biosciences) chemiluminescence was detected by exposure to film. The resulting film was matched to the array map and analyzed using the GEArray Expression Analysis Suite 2.0 (SuperArray Biosciences).

Real-time PCR

Quantitative Real-Time PCR was performed with a 7300 Real-Time PCR System (Applied Biosystems) using iTaq Supermix with Rox (172-5854, Rio-Rad) under standard protocols. FAM/MGB primer/probe combinations for CCL5/RANTES,

CCL17/TARC, CCL22/MDC and primer-limited Beta Actin Vic/TAMRA probes were provided by Applied Biosystems.

ELISA

The production of secreted chemokines was measured by ELISA for human CCL5/RANTES (DY278, R&D Systems), human CCL17/TARC (DY364, R&D Systems), and human CCL22/MDC (DY336).

Scratch Assay

Scratch assays were performed to study *in vitro* migration under various conditions. NPC cell lines (HONE-1, HONE Akata), cells from primary NPC biopsies and primary human tonsil epithelial cells were cultured in six well plates to form uniform monolayers. When cultures were approximately 90% confluent, a sterile 200 μl pipet tip would be used to create a straight line scratch across the center of the well. The wells would then be washed with PBS, and the media would be replaced. Certain wells would be supplemented with either anti-Human CCL5/RANTES neutralizing antibody (1000 ng/ml, AB-278-NA, R&D Systems) or recombinant human CCL5/RANTES (128 ng/ml, 278-RN-050, R&D Systems).

***In Vitro* Chemotaxis Assay**

To demonstrate the chemotaxis of T cells responding to the chemokine CCL5/RANTES induced by LMP1, we used ChemoTx plates from Neuroprobe. This assay is functionally similar to the standard Boyden chamber assay. Supernatants from

cultures of HaCaT cells expressing LMP1 were deposited in the lower chambers of a 96 well plate, fitted with a framed filter so that the media will be in contact with a permeable membrane. Above the filter, cell suspensions containing T cells (or a T cell line) were deposited. Secreted chemokines in the lower chambers attracted T cells in the cell suspensions and induced them to migrate into the membrane. Cells trapped in the membrane were then extracted by centrifugation, stained with MTS, and then quantified by a standard ELISA reader.

IV. Statistical Methods

Paired t Test

In order to determine the statistical significance of differences in the growth of primary tumors and metastases in mice under treatment with rapamycin compared to the tumors in mice receiving a placebo, we used a paired t test. The paired t test provides a hypothesis test of the difference between population means for a pair of random samples whose differences are approximately normally distributed. . A test of the null hypothesis that the difference between the two responses measured on the same statistical unit has a mean value of zero.

The test statistic is calculated as:

$$t = \frac{\bar{d}}{\sqrt{(s^2 / n)}}$$

where d bar is the mean difference, s^2 is the sample variance, n is the sample size and t is a Student t quantile with n-1 degrees of freedom.

Permutation Testing

The statistical significance of Connectivity Map and Gene Set Enrichment Analysis results was calculated by permutation testing. We estimated the statistical significance (nominal p value) of the enrichment score (ES*)* by using an empirical phenotype-based permutation test procedure that preserved the complex correlation structure of the gene expression data. Specifically, we permuted the phenotype labels and recomputed the ES of the gene set for the permuted data, which generated a null distribution for the ES. The empirical, nominal p value of the observed ES was then calculated relative to this null distribution. Importantly, the permutation of class labels preserved gene-gene correlations and, thus, provided a more biologically reasonable assessment of significance than would be obtained by permuting the genes.

Kaplan-Meier Statistics

Survival analysis of mice treated with an anti-RANTES antibody or an isotype control antibody were performed by generating a Kaplan-Meier plot and performing statistics. The Kaplan–Meier estimator is a statistic and several estimators are used to approximate its variance. One of the most common such estimators is the following:

$$\widehat{\operatorname{Var}}(\widehat{S}(t)) = \widehat{S}(t)^2 \sum_{t_i<t} \frac{d_i}{n_i(n_i - d_i)}.$$

A program, MedCalc, was used to generate the plot, calculate the significance, the hazard ratio and the 95% confidence interval.

Results – Part I: PI3K signaling promotes metastasis in NPC

Chapter 3: Development of an *in vivo* model of NPC

A clear molecular and genetic analysis of the factors that contribute to tumor development in nasopharyngeal carcinoma, within the malignant cells and in the local microenvironment, is lacking. This is in part because there is currently no mouse model of NPC that allows the *in vivo* study of tumor development that recapitulates the features of advanced disease, including invasion and metastasis. We therefore decided to develop an *in vivo* model of NPC based on existing NPC cell lines that we felt best retained features of NPC.

There are currently only a few established NPC cell lines which have their origins documented and confirmed. This is due in large part to the difficulty in culturing cells derived from NPC tumors *ex vivo*. In our own experience, I was able to maintain cells cultured from primary NPC tumors for several passages, up to six weeks *ex vivo*, but after that, the cultures were no longer viable. Transfection to express human telomerase (hTERT) extended the time the cell cultures remained viable, but I was never able to develop new NPC cell lines. Among the few cell lines that are available and widely used in NPC research are HONE-1 and C666-1. HONE-1 is EBV negative. Like many EBV associated cell lines, it lost the viral episome after multiple passages in culture. An EBV positive variant, HONE Akata, was produced by reinfecting the HONE-1 line *in vitro* by co-culturing HONE-1 cells with the EBV positive Akata B cell line. C666-1 is an NPC cell line which has retained the EBV episome for many years despite multiple passages.

NPC tumors are subclassified by the WHO according to histological criteria with "poorly differentiated" NPC type II comprised of well defined sections of transformed

epithelial cells maintaining tight junctions and canonical epithelial basolateral orientation (figure 6A, figure 6B), whereas "undifferentiated" NPC type III tumors are comprised of what appear to be dedifferentiated transformed epithelial cells interspersed among the infiltrating stroma (figure 6C). These morphological differences appear to be retained in NPC derived cell lines. The type II derived cell line, HONE Akata (figure 6E) has a similar contiguous epithelial arrangement, when cultured *in vitro*, as primary tonsil derived epithelial cells (figure 6D), whereas the type III derived cell line, C666-1 appears to be more fibroblast-like and lacks tight junctions between adjacent cells. Unlike most epithelial cell lines, like HONE Akata, C666-1 cells do not spread across tissue culture plates to form uniform monolayers. Instead, the cells tend to form clusters in vitro, and stack vertically. This would be lethal to most epithelial cell lines, however C666-1 cells display characteristics of anchorage independence. In fact, confluent C666-1 cultures frequently have clusters of cells in suspension. These clumps of cells floating in media can be split and remain viable after successive passages and retain the anchorage-independent phenotype. Anchorage independence has been reported to be a feature associated with increased metastatic potential (Mori 2009).

We developed an *in vivo* xenograft model of NPC in immunodeficient NOD scid gamma mice. Type II HONE Akata and type III C666-1 cells were infected with an HIV-based lentivirus that expresses both GFP and luciferase under the control of a CMV promoter (pGreenFire1, Systems Biosciences). Infected cells were selected by multiple rounds of FACS sorting for GFP expression over a period of four weeks, then confirmed for luciferase expression by adding luciferin to cell culture flasks and then observing luciferase bioluminescence using a Xenogen IVIS 200 imager. Once we had obtained

subclones of the HONE Akata and C666-1 cell lines that stably expressed luciferase, we then injected cells into mice to establish tumors. We could then track tumor development over time in each mouse using the Xenogen IVIS 200 bioluminescent imager. The mouse strain that we elected to use was the NOD scid gamma strain (NOD.Cg-*Prkdc*^{scid} *Il2rg*^{tm1Wjl}/SzJ, Jackson Labs). We chose this strain because it is severely immunocompromised, lacking B cells, T cells and NK cells. As a result, it is ideal for transplatation studies using human cells, including xenograft tumor experiments. We first started by injecting either $5x10^5$ HONE Akata cells or $5x10^5$ C666-1 cells into the flank of three week old female NOD scid gamma mice. Once a week, the mice would be injected with luciferin, then anesthetized by isofluorene and placed in the Xenogen IVIS 200 imager. We would then take exposures ranging in time between 30 seconds and 5 minutes to measure luciferase expression in the tumor cells at the primary tumor site, as well as metastases if they develop elsewhere in the mouse. When either HONE Akata or C666-1 cells were injected subcutaneously into the flank, tumors developed at the site of the injection and were large enough to be visualized by three to four weeks after injection (fig. 7). After the mice were sacrificed, sections including the tumor and the surrounding tissue were prepared, preserved, and mounted on slides. Histological examination confirmed that the tumors were of NPC origin, since they expressed human cytokeratins (fig 7C) and the EBV-encoded RNA transcript EBER1 (fig 7D). These tumors were well encapsulated and did not invade nearby tissue. Although we were able to establish tumors in the mice based on the human NPC cell lines, the mice remained healthy, and the development of the xenograft tumors did not recapitulate normal tumor development, particularly with respect to invasion and metastasis.

We reasoned that the physical site where the primary tumor is established may play an important role in tumor development. Interactions in the local microenvironment between the malignant cells and untransformed cells which may provide factors that promote local colonization and intravisation into the bloodstream or lymphatics can affect tumor progression and the development of advanced disease. We thought that some of the features of the local context of nasopharyngeal tissue may be retained between humans and mice, so there may be a value in establishing the primary tumor in the nasopharynx of the NOD scid gamma mice. We anesthetized three to four week old female NSG mice with Ketamine (100 mg/Kg) and Xylazine (16 mg/Kg) by intraperitoneal injection. The mouth of a mouse was then held open using a set of forceps, while another set of forceps was used to maneuver the tongue to the side, providing a clear view into the back of the mouse's oropharynx. 2.5x105 tumor cells (either HONE Akata or C666-1) suspended in 100ul of PBS were injected into mice, just behind the hard palette and to the right side. Care had to be given in the placement of the injection. If the needle penetrated the tissue down the centerline of the mouse too deep, the mouse would die instantly. After approximately an hour, the mice regained consciousness and were returned to the animal housing facility for normal care. At least once a week over the following two months, the mice were imaged for luciferase expression as described above. Compared to the subcutaneous flank injection, when we performed an orthotopic injection of tumor cells into the nasopharynx of the mice, tumor development much more closely resembled features of human disease. The NPC cells did invade into nearby tissue, the mice appeared cachectic, and their health rapidly declined. Importantly, we found that the type II HONE Akata cells (fig 8) rarely

metastasized (1 out of 42 mice, 2.5%) whereas the type III C666-1 cells (fig 9) metastasized efficiently to distant tissue (17 out of 48 mice, 35%). Furthermore, histological examination showed that the type III C666-1 cells crossed tissue planes and invaded nearby structures (fig 10 and 11). This suggests that the distinction that separates type II and type III may be associated with factors that promote metastatic progression in NPC.

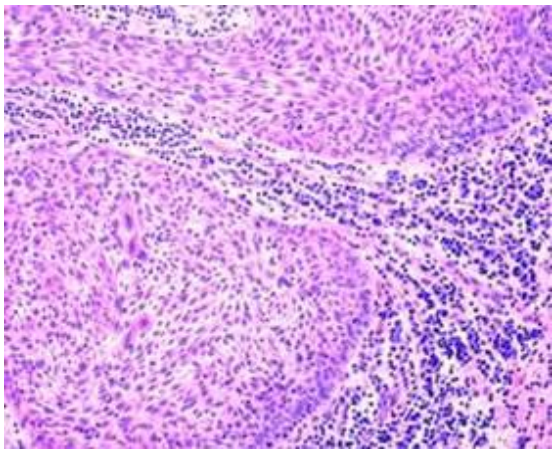

Fig 6A. Differentiated NPC type II

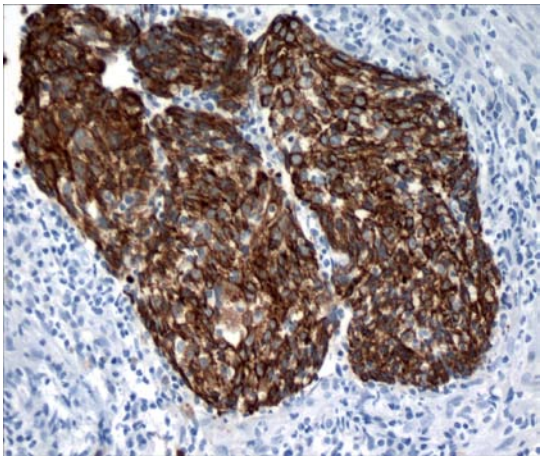

Fig 6B. Type II Pancytokeratin staining

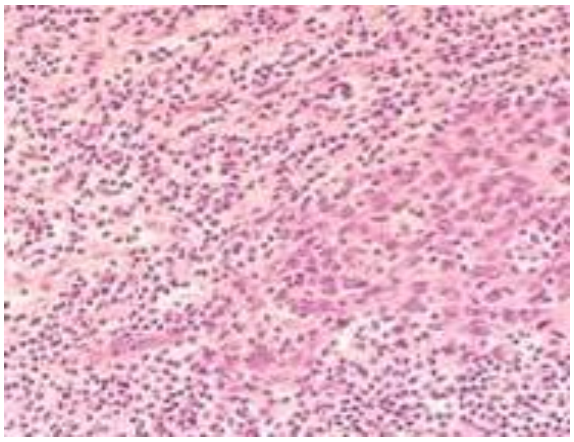

Fig 6C. Undifferentiated NPC type III

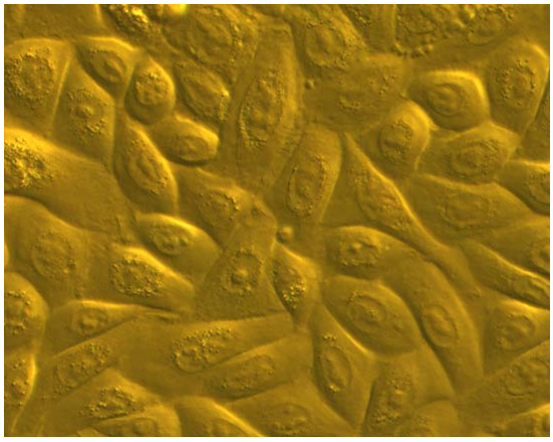

Fig 6D. Primary tonsil epithelial cells

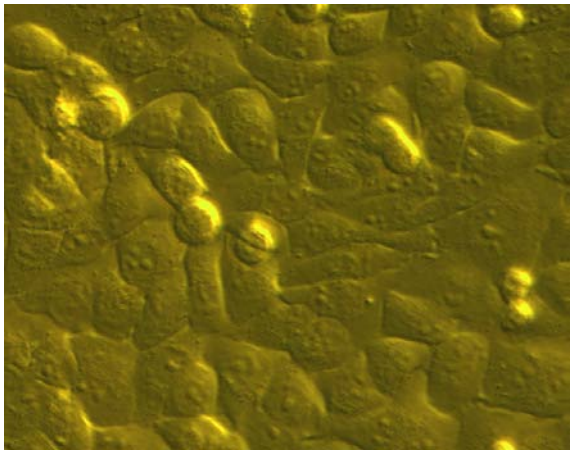

Fig 6E. HONE Akata (NPC type II)

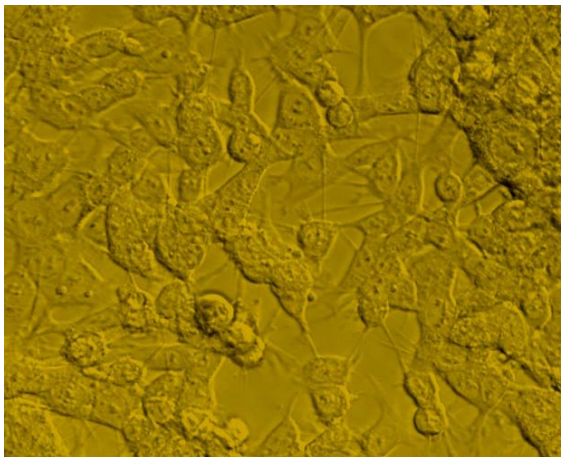

Fig 6F. C666-1 (NPC type III)

Figure 6. NPC type III demonstrates a dedifferentiated phenotype.

(A) An NPC type II biopsy, provided by Tufts Medical Center. Sections of malignant NPC cells can be clearly seen, separate from infiltrating stroma. Tight junctions are maintained between the transformed epithelial cells resulting in a relatively uniform organization. (B) Pancytokeratin staining clearly discriminates large sections of transformed cancer cells among the surrounding tissue and infiltrating stroma. (C) A type III biopsy, also provided by Tufts Medical Center, shows a much more disorganized heterogeneous composition, as the transformed NPC cells appear dedifferentiated, loose adhesion and are interspersed among non-malignant stroma. (D) Primary tonsil epithelial cells cultured *in vitro* form monolayers, display contact inhibition, and maintain cell-cell contacts and apical-basolateral polarity. (E) This phenotype is retained in the NPC type II derived cell line, HONE Akata, and is similar to the organization seen in type II biopsies in figures 6A and 6B. (F) The NPC type III derived cell line, C666-1, displays depolarization and loss of adhesiveness, similar to the type III biopsy in figure 6C. In culture, these cells lose contact inhibition and grow in disorganized clusters.

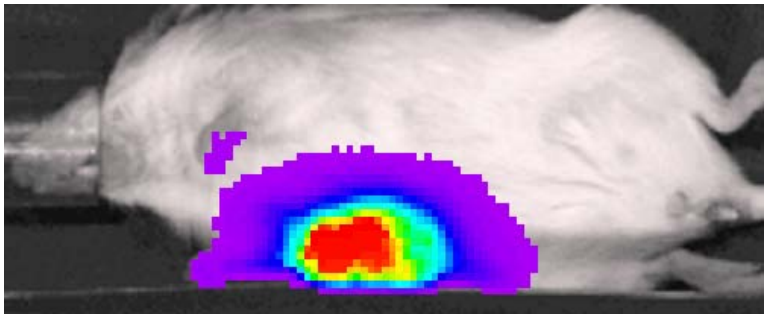

Fig 7A. Bioluminescence imaging of a subcutaneous tumor

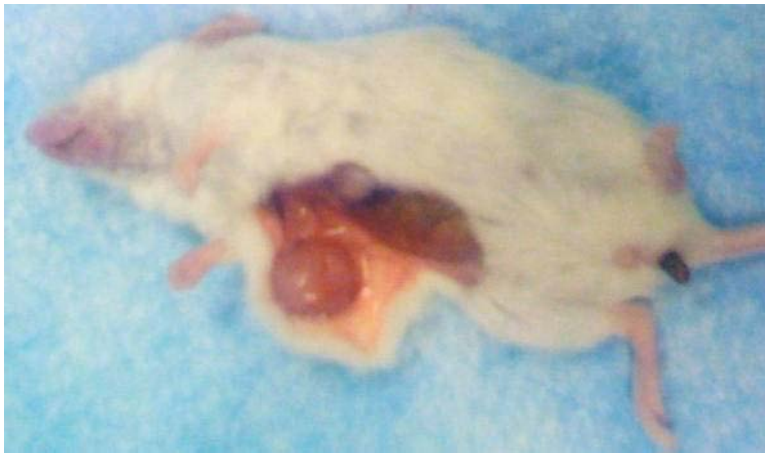

Fig 7B. Encapsulated subcutaneous tumor

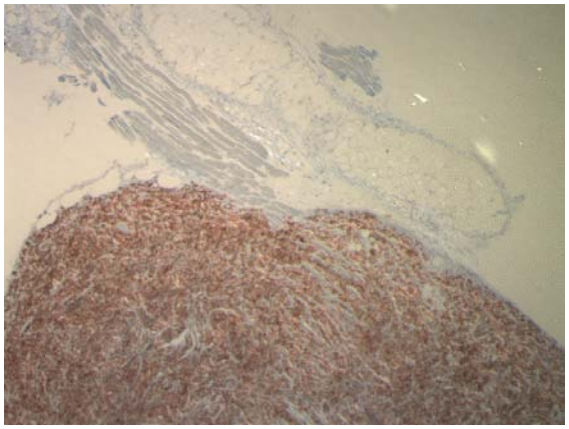

Fig 7C. Pan-cytokeratin stain of sub-cutaneous tumor

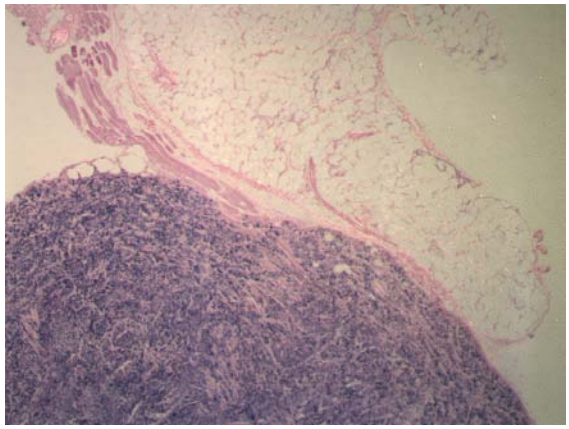

Fig 7D. EBER stain

Figure 7. NPC cells injected subcutaneously do not invade or metastasize.

NOD scid gamma mice were injected subcutaneously in the flank with either HONE Akata (type II) or C666-1 (type III) cells that were stably transfected to express luciferase. (A) Tumor growth in the flank of a C666-1 injected mouse is visualized using a IVIS 200 biophotonic imager (Xenogen.). (B) Dissection of the mouse after it is sacrificed confirms the presence of an encapsulated tumor. Histological examination confirms the origin of the tumor to be human NPC cells. (C) Immunohistochemistry of human keratins and (D) the EBV encoded RNA transcript, EBER1. The tumors that develop from subcutaneous injection maintain clearly defined borders and do not invade nearby tissue or metastasize. The same results are seen for both type II HONE Akata and type III C666-1 derived tumors.

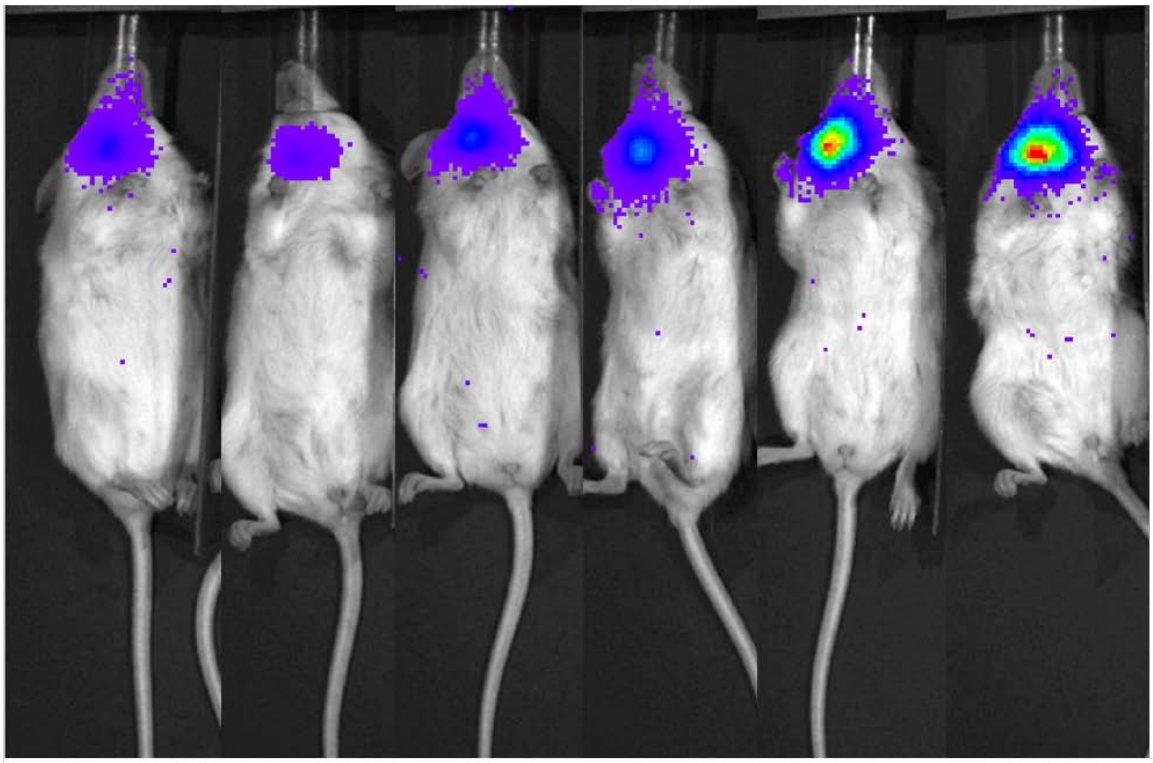

Figure 8. Orthotopic injection of NPC type II HONE Akata cells results in tumor at primary site only. NOD scid gamma mice were anaesthetized and injected with 2.5×10^5 HONE Akata cells in the oral cavity. Tumor development was followed over a period of up to eight weeks. Shown here is a representative time sequence with a 3-4 day interval between images. Mice injected with type II HONE Akata cells developed primary tumors but rarely metastasized (1 out of 42 mice, 2.5%.)

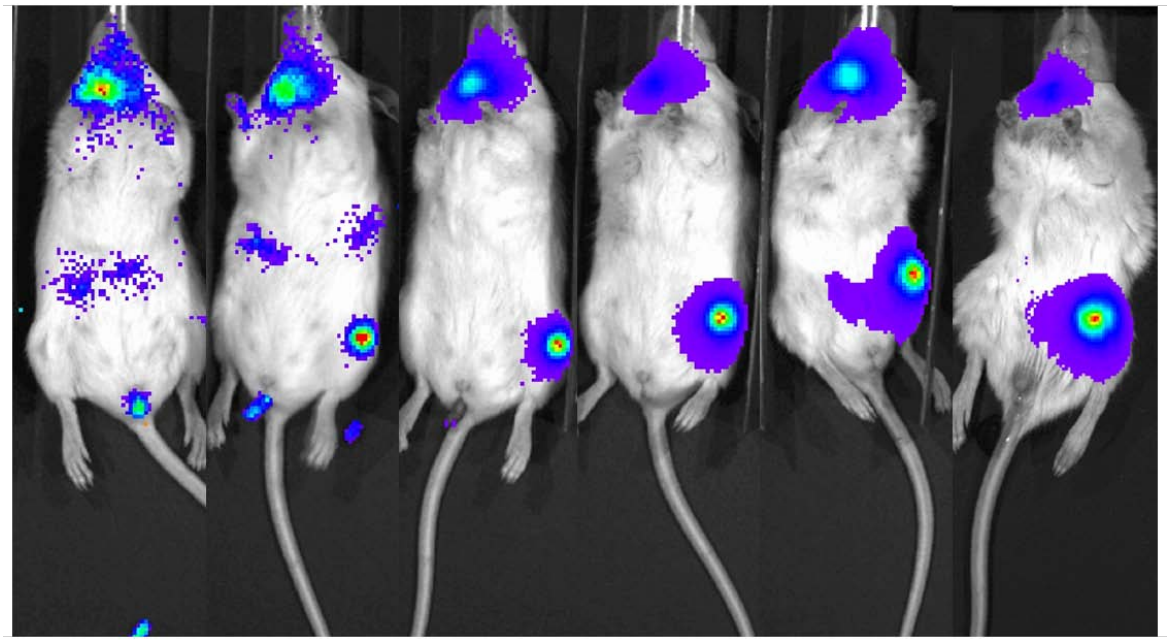

Figure 9. Orthotopic injection of NPC type III C666-1 cells results in development of primary tumor and metastases. . NOD scid gamma mice were anaesthetized and injected with 2.5×10^5 C666-1 cells in the oral cavity. Tumor development was followed over a period of up to eight weeks. In contrast to the HONE Akata mice, mice injected with type III C666-1 cells developed metastases efficiently (17 out of 48 mice, 35%) in addition to the primary tumor.

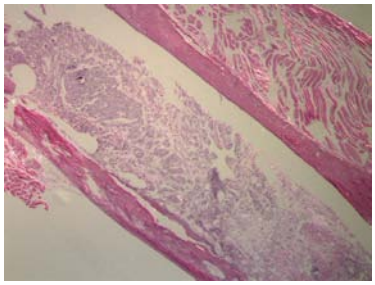

Fig. 10a H&E stain of femur met

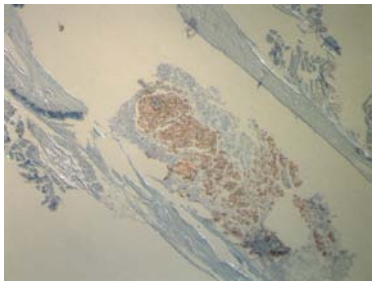

Fig.10b Pan-cytokeratin

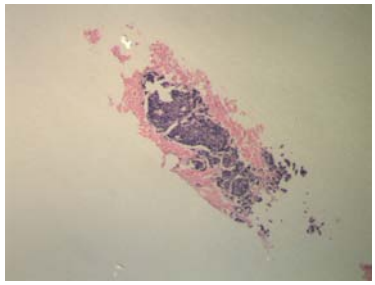

Fig. 10c EBER1

Figure 10. Histological examination of a metastasis in the femur of a C666-1 injected mouse.

Immunohistochemistry on the metastasis shown in figure 9 confirms that the origin of the tumor in the leg is NPC cells that had been injected in the oral cavity. (A) an H&E stain of the femur. (B) A pancytokeratin stain of an adjacent section shows the tumor is postitive for expression of human cytokeratins. (C) An EBER1 stain of a cross-section in the same series shows the tumor is positive for the EBV transcript EBER1.

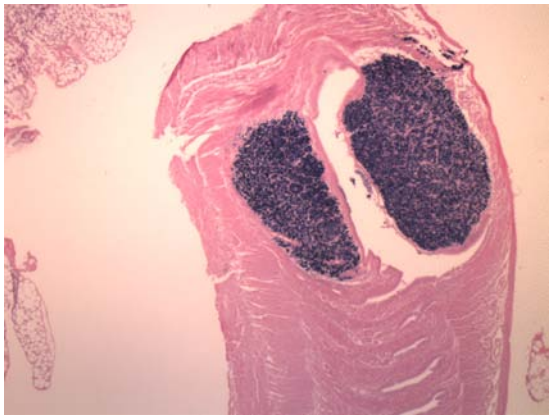

Fig. 11a Adrenal gland met

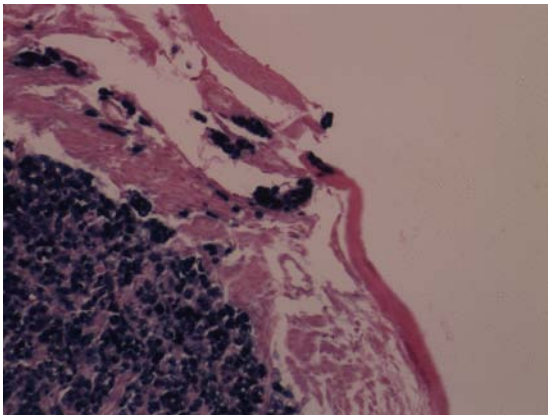

Fig. 11b Close-up showing invasion into nearby tissue

Figure 11. Histological examination of an adrenal metastasis shows that the type III C666-1 cells are invasive. (A) Metastases in C666-1 mice were broadly distributed in various tissue, including this adrenal gland. (B) A close-up image of EBER1 stained NPC type III C666-1 cells.

Chapter 4: PI3K signaling contributes to metastasis in NPC

In view of the difference in the propensity between the type III and type II cells to metastasize in our mice, we then wanted to see if we can determine molecular factors that separate NPC type III and type II that may contribute to metastatic progression. For this, we used data from an Affymetrix study of primary biopsies from 14 NPC patients (8 type III, 6 type II). We first constructed an expression signature that indirectly represents the molecular difference between NPC type III and type II (fig 12). This signature is comprised of the 50 genes most up-regulated based on relative expression between the NPC type III samples versus and the NPC type II samples and the 50 genes most down-regulated between the two sets. The identity of the specific genes and their molecular functions were not important to our analysis. Instead, we wanted a broad picture of the molecular differences that separate the two phenotypes. We then analyzed the NPC subtype expression profiles using the Connectivity Map, a reference database of genome-wide transcriptional profiles designed to enable the discovery of functional connections between drugs, genes and disease states (fig 13). The Broad Institute performed thousands of experiments in which various cell lines were exposed to small molecules, and then used Affymetrix experiments to determine effects of the drugs on the cell lines' gene expression profiles. The results of these experiments were entered into a database which could be interrogated by investigators using their own empirical data. The general principle is that the unknown underlying molecular pathways that separate two phenotypes, in our case, NPC type II and NPC type III, may be revealed by comparing the differential expression profile of those two states, represented by our signature set, to the results of the Broad experiments in the database. A close correlation of markers

between the ones found in our experimental data set and the closest matches in the Broad database may be due to the activation of the same molecular pathways. Therefore, if we could identify drugs with known biochemical functions in the Broad experiments that yielded similar up-regulated and down-regulated gene expression changes to our NPC type III versus NPC type II signature, we may be able to identify the molecular pathways that separate the type III and type II phenotypes. When we analyzed our data using the Connectivity Map, there was a striking correlation between our experimental data and three drug inhibitors of the same pathway. Sirolimus (Rapamycin), LY294002, and Wortmannin are all inhibitors of the PI3K-Akt-mTOR Pathway. Taken alone, each of these results would have been statistically significant, based on permutation testing ($p< 0.0001$). The implication that there may be a differential level of activation of the PI3K-Akt-mTOR pathway between the two EBV associated subtypes of NPC (type III and type II) is made even stronger by the fact that among the drugs with the highest correlation to our data, three of them affected this same pathway. These results suggest that the PI3K-Akt-mTOR axis may have a role in promoting metastatic progression in NPC.

Our next step was to determine if there were differences in PI3K-Akt-mTOR activity in NPC type III and NPC type II cells *in vitro*. We first began by analyzing the differences in the phosphorylation of Akt in our NPC cell lines. HONE-1, HONE Akata and C666-1 cells were cultured in 10 cm plates until they were 90% confluent. In order to confirm that the expected band at 60 kD was Akt, 293 control cultures were also prepared, and were either serum starved or insulin stimulated. Akt in the insulin stimulated sample would be expected to be more heavily phosphorylated than in the

serum starved samples. Lysates were prepared, and then ran on precast polyacrylamide gels (NuPage 4-12% Bis-Tris gels, Invitrogen). Proteins were then transferred to nitrocellulose membranes and blotted with antibodies specific to Akt phosphorylated at serine 473, Akt phosphorylated at threonine 308 and beta actin. Full activation of Akt has been reported to require the phosphorylation of both Ser 473 and Thr 308, however Thr 308 is considered to be the more important trigger for downstream activities. Western blotting of the NPC cell lines showed a greater intensity in the Thr 308 band for the C666-1 sample, compared to the HONE-1 and HONE Akata samples (fig 14), suggesting that the PI3K-Akt-mTOR pathway is more highly activated in NPC type III C666-1 cells versus NPC type II HONE Akata cells. Western blotting was performed eight times, the images shown are representative of the results.

We also wanted to deternine if the Connectivity Map results reflected a greater sensitivity to PI3K pathway inhibitors in NPC Type III compared to NPC type II. For this, I used an MTS proliferation assay. Type III C666-1 cells and type II HONE-1 and HONE Akata cells were grown in 96 well plates, and then exposed to different concentrations of LY294002 or Rapamycin for 72 hours. MTS was then added to the cultures. Respirating cells reduce the tetrazolian salt, MTS, to formazan, producing a color which can be quantified by a spectrometer. These readings were compared to a standard curve generated using known numbers of cells to determine the viability of cultures exposed to different concentrations of the two drugs, LY294002 and Rapamycin. The MTS proliferation assays showed that C666-1, the NPC Type III cell line, is more sensitive to PI3K and mTOR inhibitors *in vitro* than the type II cell lines, HONE-1 and HONE Akata. MTS assays were performed five times, with a minimum of six replicates

per condition. The results shown are representative of these experiments. Cells from a primary type III biopsy were also more sensitive to mTOR inhibition than primary tonsil epithelial cells (fig 15).

We then extended these studies into our mouse model. Tumors were established in the nasopharynx of NOD scid gamma mice. We then treated the mice with Rapamycin (5mg/Kg) or a placebo for up to two months and imaged the mice using the Xenogen IVIS 200 systems every three to four days. Using the Living Image Software (Caliper Lifesciences), I analyzed the tumor growth and estimated the relative size of each tumor in each mouse from timepoint to timepoint. We saw a reduction in the growth rate of the primary tumors in the Rapamycin treated mice, compared to the placebo mice (fig 16). However, there was a much more dramatic effect on the metastases. Figure 17 shows the progression of metastases in the spine of a NOD scid gamma mouse treated with placebo over the period of several weeks. This can be compared to a representative example of a metastasis in a mouse treated with Rapamycin, in figure 18. The interval between each photograph in each of these series is three to four days. Analysis of the luciferase imaging allowed us to quantify the growth of the tumors, which is plotted in figure 19. Whereas metastases grew at an exponential rate in placebo mice, the rates were significantly reduced in the Rapamycin treated mice (fig 20). In several cases, such as the one illustrated in figure 18, we saw a reduction in the size of the metastases after Rapamycin treatment until they were no longer detectable ($p=0.04$).

These results suggest that the PI3K-Akt-mTOR axis may provide a molecular basis for the distinction between NPC type II and NPC type III and may be important for

metastatic progression in NPC. Our results also suggest that PI3K-Akt-mTOR pathway inhibitors may have therapeutic potential for treatment of metastatic NPC.

We also analyzed the Affymetrix data using an algorithm called Gene Set Enrichment Analysis (GSEA). This is a computational method that determines whether an empirically derived set of genes shows statistically significant, concordant differences between two biological states. (In this case, NPC type III and NPC type II.) The results are illustrated in figure 21. The enrichment plot includes a color bar that depicts phenotype correlation based on ranking metric scores. Ranked from left to right (red to dark blue) is the rank-ordered gene list determined by the Affymetrix study, with genes highly up-regulated in type III NPC vs. type II to the far left, genes down-regulated in type III vs. type II to the far right. The location of genes that comprise an experimentally derived set of coordinately regulated genes along the rank-ordered gene list is indicated by the vertical black lines. If a set of genes is strongly correlated with one of the phenotypes versus the other (such as type III vs. type II), the genes in that set will be skewed towards one side of the rank-ordered gene list.

With our analysis of NPC type III versus type II, the two most statistically significant enriched gene sets ($p < 0.01$) were both comprised of genes that are up-regulated during epithelial-mesenchymal transition (EMT). EMT is an important process during development by which epithelial cells acquire mesenchymal, fibroblast-like properties and show reduced intercellular adhesion and increased mobility. EMT plays a significant role in tumor progression and malignant transformation, endowing transformed cells with invasive and metastatic properties.

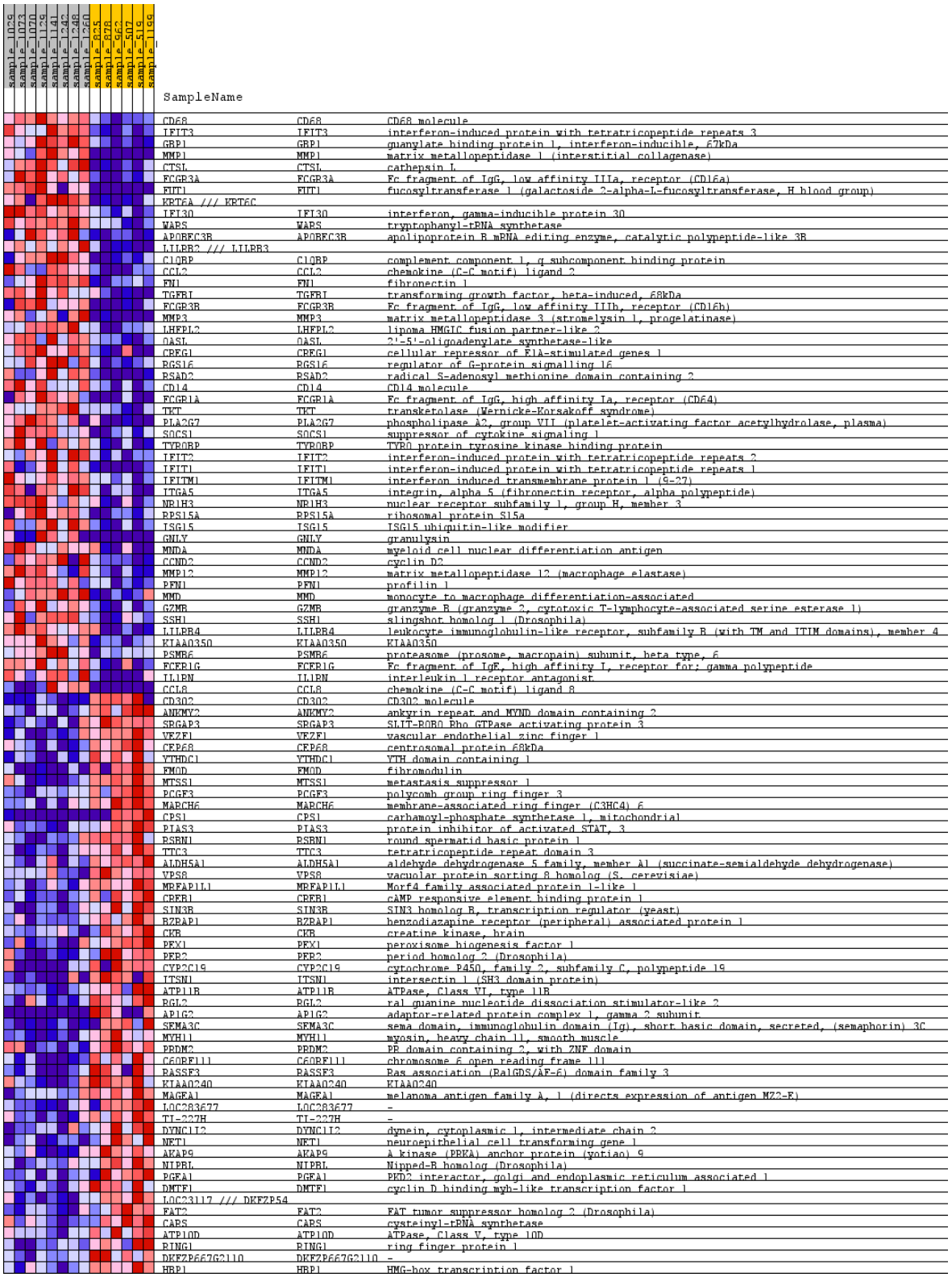

Fig 12. NPC type III vs. type II signature from an Affymetrix study of NPC biopsies

Figure 12. An NPC type III vs type II signature is constructed from an Affymetrix study of NPC biopsies. 8 NPC type III biopsies and 6 NPC type II biopsies were analyzed using Affymetrix GeneChip Human Genome U133 Arrays. The genes were rank-ordered by relative expression between the type III and type II phenotypes. We selected the top 50 up-regulated genes and the bottom 50 down-regulated genes in this list to comprise the signature that indirectly describes the molecular distinction between the type III and type II phenotypes. This signature was then used to interrogate the Connectivity Map constructed by the Broad institute.

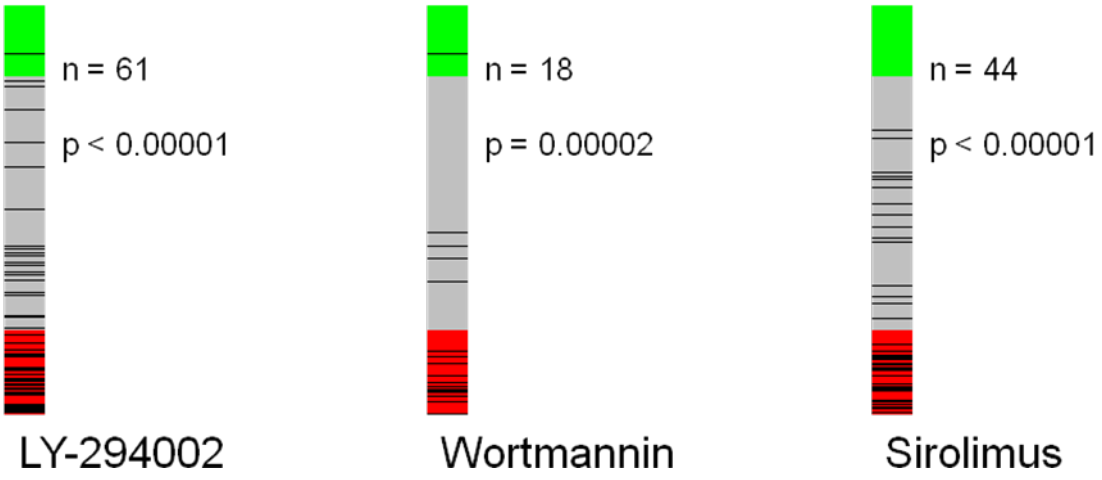

Figure 13. Connectivity Map results indicating a strong negative correlation between the NPC type III vs. type II signature and inhibitors of the PI3K-Akt-mTOR pathway. The type III vs. type II signature was compared to the results of 7000 "instances" in the Connectivity Map database. Each instance represents an experiment with a cell line exposed to one of 1300 compounds at a given concentration. Correlation to our type III vs. type II signature is calculated in each case and ranked. This is graphically presented as a colored vertical bar with the black lines indicating the location in the rank-ordered list of the instances of a given compound. The green region represents positive correlation; the red region represents negative correlation. The results shown here demonstrate a strong bias of instances for three inhibitors of the PI3K-Akt-mTOR pathway within the red region, indicating a strong negative correlation between the type III vs. type II signature and the response to PI3K-Akt-mTOR pathway inhibitors. The number of instances using each drug is indicated. The statistical chance of this overrepresentation occurring as a random event is estimated by permutation testing ($p < 0.0001$).

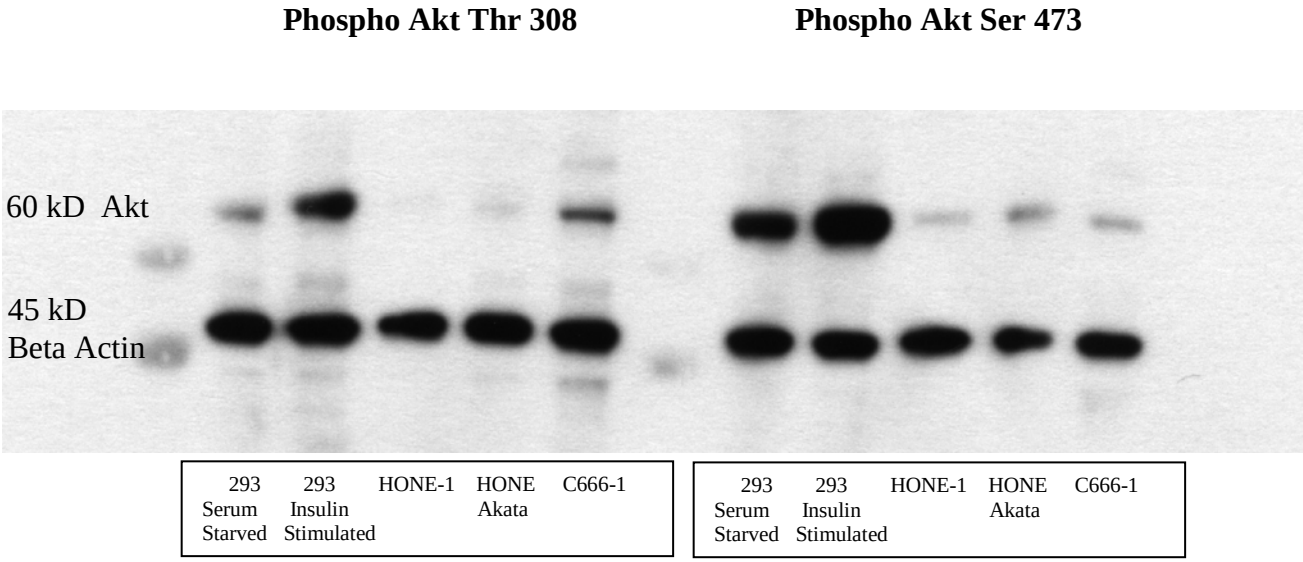

Figure 14. Western blots for phospho Akt and beta actin indicate that Akt activity may be higher in the type III C666-1 NPC cell line, compared to the type II HONE-1 and HONE Akata cell lines.

NPC cell lines cultured *in vitro* were used for Western analysis of Akt phosphorylation. Akt was phosphorylated at Thr 308 to a greater degree in the type III C666-1 line compared to the type II HONE-1 and HONE Akata lines. No difference was seen in the phosphorylation of Ser 473. 293 cells were either serum-starved or insulin-stimulated and used as controls to indicate that the 60 kD band is Akt. Comparative loading of samples is seen in the 45 kD band for beta actin. The blots shown are representative of four experiments.

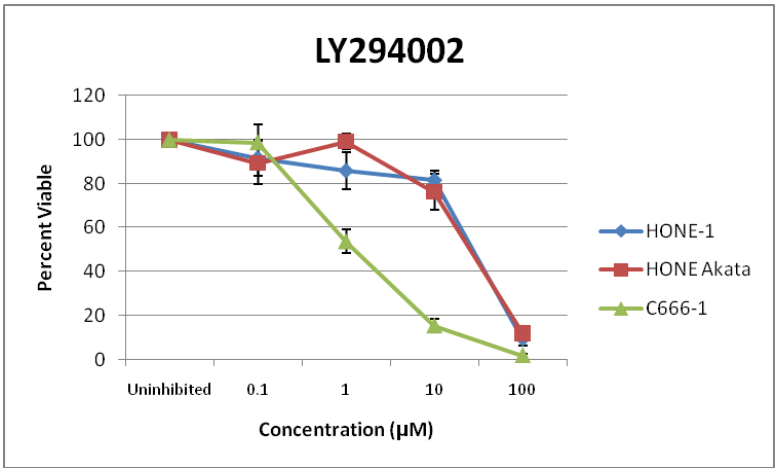

Fig 15a

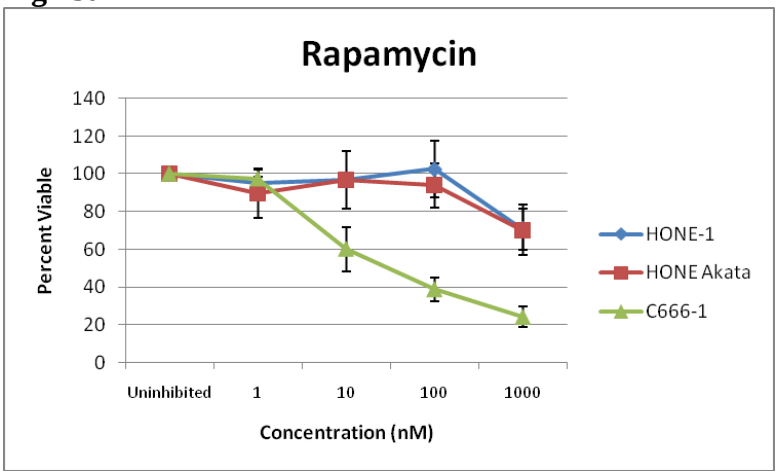

Fig 15b.

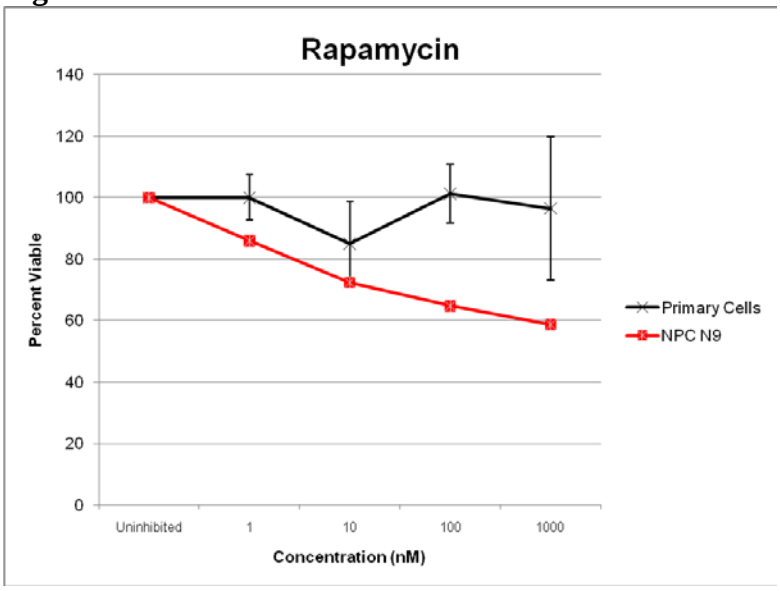

Fig 15c.

Figure 15. MTS proliferation/survival assays showing a greater sensitivity to PI3K and mTOR inhibitors for the NPC type III cell line compared to the type II cell lines. Greater sensitivity was also seen between a type III primary biopsy compared to primary tonsil epithelial cells. Type II NPC cell lines HONE-1 and HONE Akata, and the type III line C666-1 were cultured *in vitro* and exposed to various concentrations of (A) LY294002, a PI3K inhibitor, or (B) Rapamycin, an mTOR complex 1 inhibitor, for 72 hours. MTS proliferation assays were then performed to estimate the number of viable cells. The results indicate that the IC50 for these inhibitors is 70-100 times higher in the NPC type II cell lines compared to the type II C666-1 cell line. The results shown are representative of three experiments. (C) Cells cultured from a type III biopsy provided by Tufts Medical Center were also more sensitive to Rapamycin exposure than primary epithelial cells cultured from human tonsils.

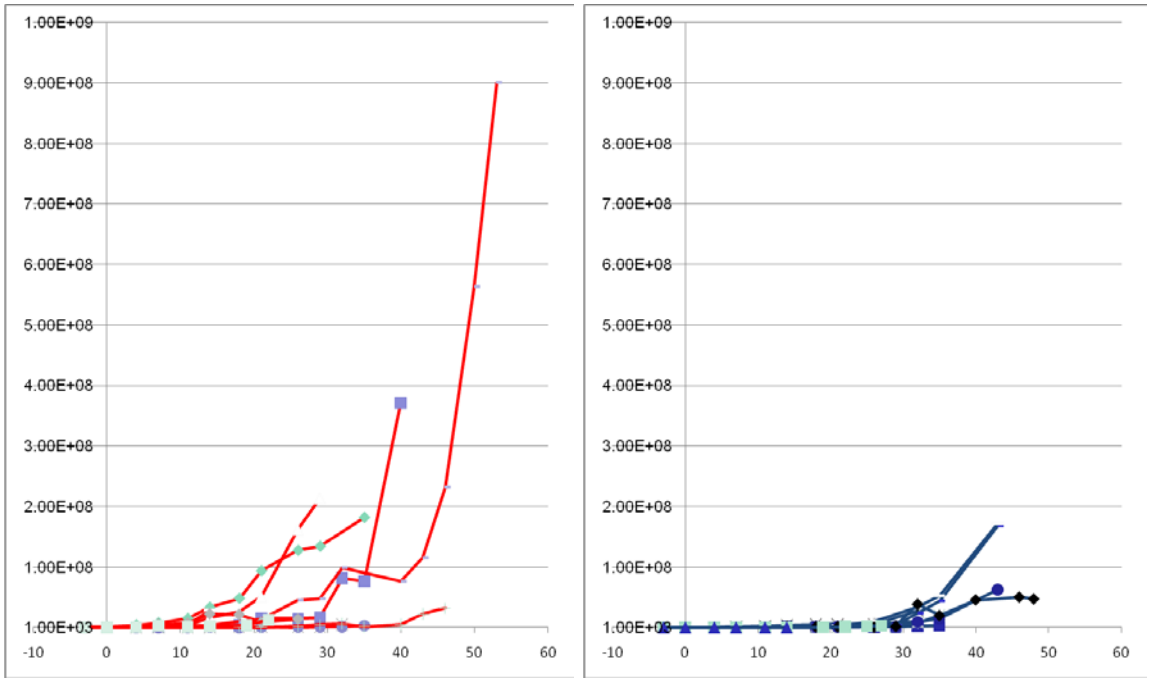

Figure 16. Growth of primary tumors in mice with orthotopic injection of type III C666-1 cells. Tumors in the placebo treated mice (red) grew at a higher rate than in the Rapamycin treated mice (blue.) Tumors were established in NOD scid gamma mice by orthotopic injection of 2.5×10^5 C666-1 cells. Growth of the primary tumors was monitored over time and calculated by quantifying the photon flux (photons per second) emitted by the tumors. Mice were either treated with a placebo (red) or treated with Rapamycin (blue.) Photon flux is indicated on the y-axis, days after the initiation of the treatment regimen is indicated on the x-axis.

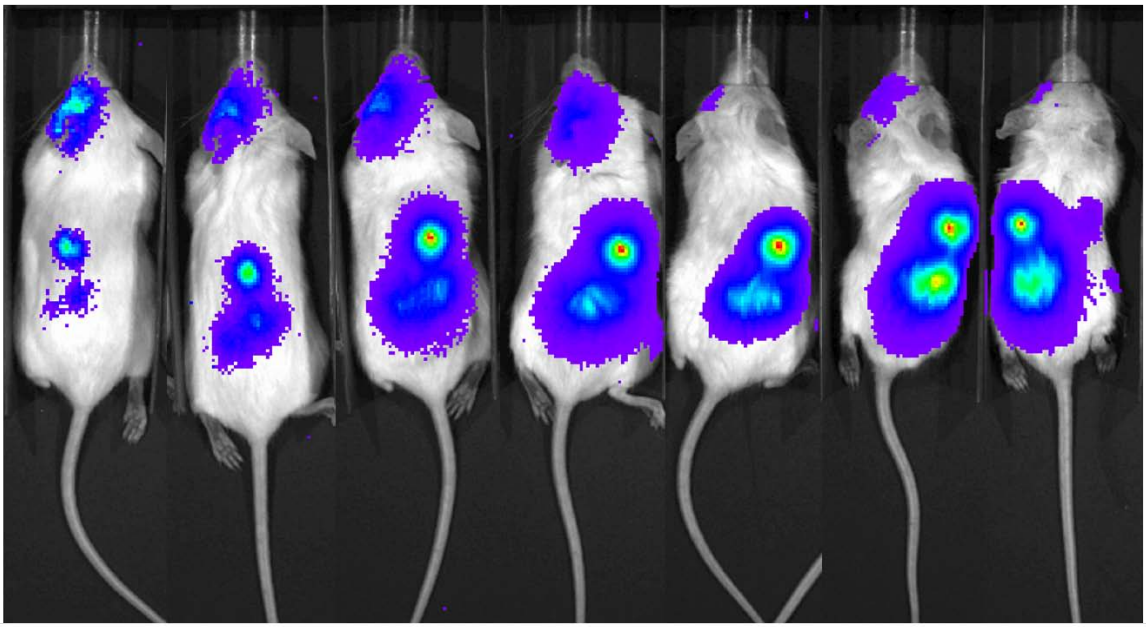

Figure 17. Growth of spine mets in a placebo-treated mouse. The development and growth of metastases in mice were tracked over time. Shown here are representative metastases in the spine of a placebo treated mouse.

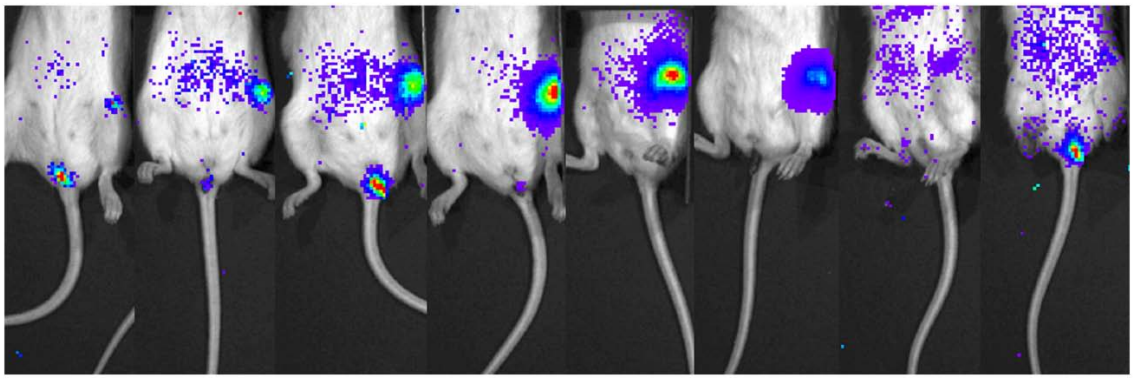

Figure 18. Growth and reduction of a femur met in a Rapamycin-treated mouse. This time sequence shows the development and regression of a representative metastasis in a mouse treated with Rapamycin. In contrast to the placebo-treated metastases in figure 17, the tumor in the Rapamycin-treated mouse initially grew at a relatively slow rate, then diminished until it could no longer be detected.

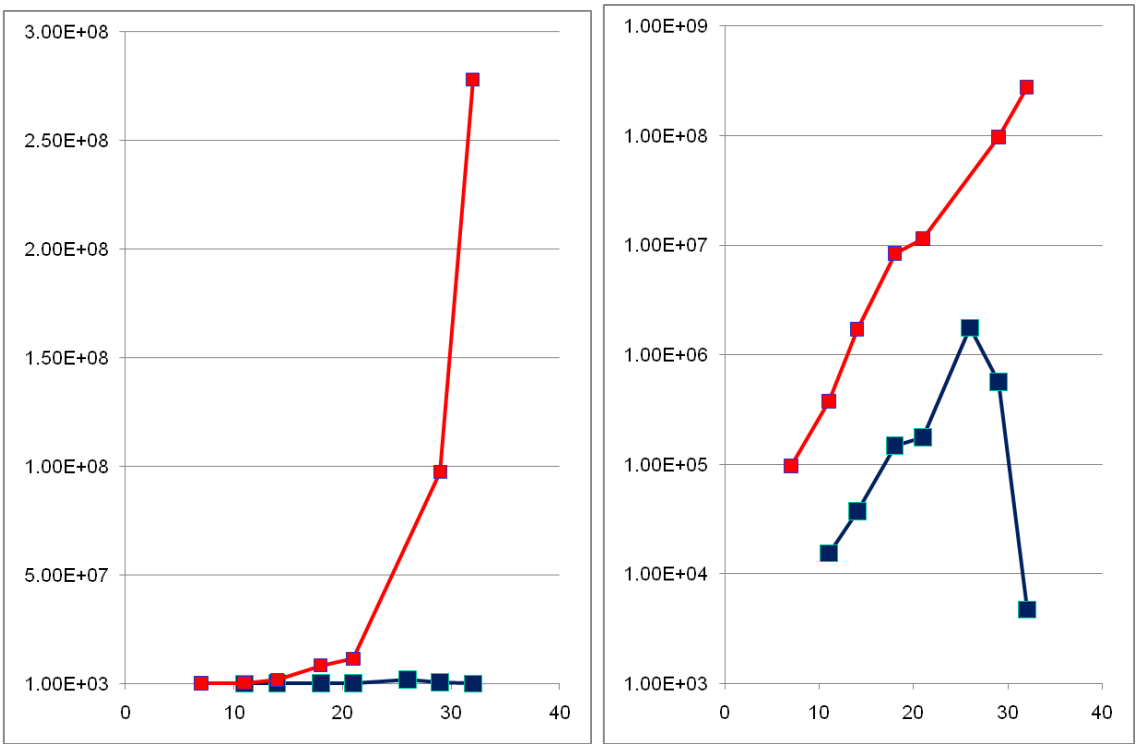

Figure 19. Growth over time of the spine met and the leg met in mice shown in figures 13 and 14. Linear scale on the left, log scale on the right. The sizes (estimated by photon flux) of the metastases shown in the previous figures are indicated. The spine metastases in the placebo-treated mouse (red) grew exponentially. In contrast, the leg metastasis in the Rapamycin-treated mouse grew at a relatively reduced rate and then diminished until it was undetectable. Photon flux is indicated on the y-axis; days after the initiation of treatment are indicated on the x-axis.

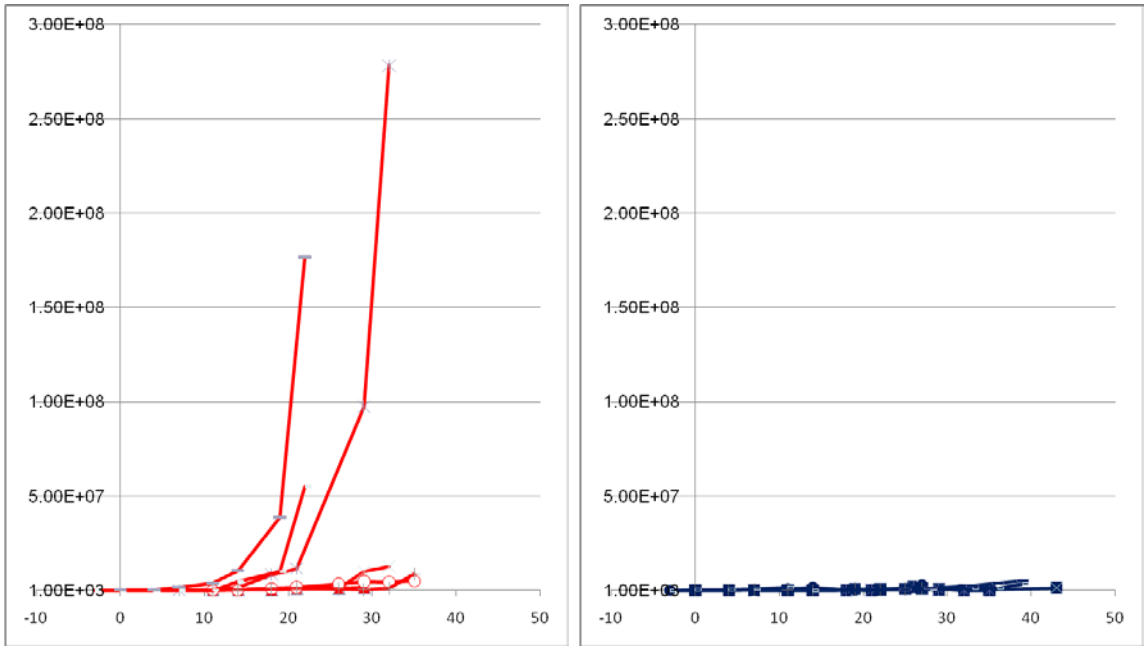

Fig 20. Growth of metastases in mice with orthotopic injection of type III C666-1 cells. Tumors in the placebo treated mice (red) grew at a higher rate than in the Rapamycin treated mice (blue.) Growth of metastases was monitored over time and calculated by quantifying the photon flux (photons per second) emitted by the tumors. Mice were either treated with a placebo (red) or treated with Rapamycin (blue.) Photon flux is indicated on the y-axis, days after the initiation of the treatment regimen is indicated on the x-axis. Growth rates in the Rapamycin treated mice were significantly lower than in the placebo treated mice ($p=0.04$).

Fig 21.

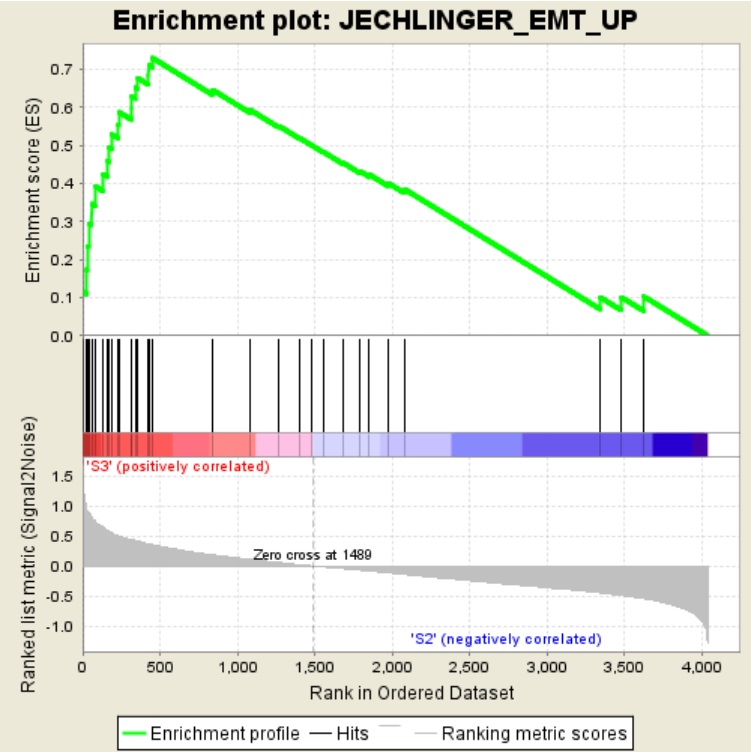
Enrichment plot: JECHLINGER_EMT_UP
Enrichment score (ES)
0.7
0.6
0.5
0.4
0.3
0.2
0.1
0.0
'S3' (positively correlated)
Ranked list metric (Signal2Noise)
1.5
1.0
0.5
0.0
-0.5
-1.0
Zero cross at 1489
'S2' (negatively correlated)
0
500
1,000
1,500
2,000
2,500
3,000
3,500
4,000
Rank in Ordered Dataset
Enrichment profile
Hits
Ranking metric scores

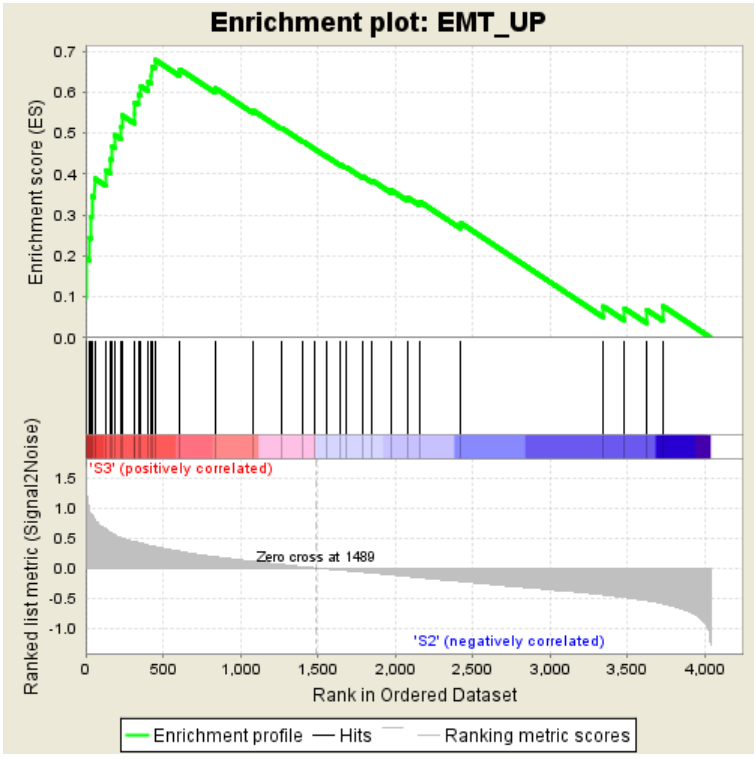
Enrichment plot: EMT_UP
Enrichment score (ES)
0.7
0.6
0.5
0.4
0.3
0.2
0.1
0.0
'S3' (positively correlated)
Ranked list metric (Signal2Noise)
1.5
1.0
0.5
0.0
-0.5
-1.0
Zero cross at 1489
'S2' (negatively correlated)
0
500
1,000
1,500
2,000
2,500
3,000
3,500
4,000
Rank in Ordered Dataset
Enrichment profile
Hits
Ranking metric scores

Figure 21. Gene Set Enrichment Analysis (GSEA) of primary NPC biopsies shows an overrepresentation of EMT associated genes in NPC type III.

Affymetrix data was analyzed using an algorithm called Gene Set Enrichment Analysis (GSEA). This is a computational method that determines whether an empirically derived set of genes shows statistically significant, concordant differences between two biological states. (In this case, NPC type III and NPC type II.) The results are illustrated above. The enrichment plot includes a color bar that depicts phenotype correlation based on ranking metric scores. Ranked from left to right (red to dark blue) is the rank-ordered gene list determined by the Affymetrix study, with genes highly up-regulated in type III NPC vs type II to the far left, genes down-regulated in type III vs. type II to the far right. The location of genes that comprise an experimentally-derived set of coordinately-regulated genes along the rank ordered gene list is indicated by the vertical black lines. If a set of genes is strongly correlated with one of the phenotypes vs. the other (such as type III vs. type II), the genes in that set will be skewed towards one side of the rank-ordered gene list.

With our analysis of NPC type III vs. type II, the two most statistically significant enriched gene sets were both comprised of genes that are up-regulated during epithelial-mesenchymal transition (EMT).

Results - Part II: CCL5/RANTES in NPC

Chapter 5: LMP1 induction of RANTES in epithelial cells

The Epstein-Barr virus is a risk factor for several human lymphoid and epithelial cancers. A central unresolved issue in understanding the development of nasopharyngeal carcinoma is the effect of EBV-encoded viral genes in epithelial cells and their contribution to oncogenesis. To address the role of EBV in the development of nasopharyngeal carcinoma, we analyzed the gene expression profiles of epithelial cells transduced to express viral proteins. In particular, we are interested in genes related to the recruitment of lymphocytes, since NPC tumors are characterized by a massive infiltration of T cells and macrophages. We hypothesize that EBV has a role in the development of NPC in part by inducing the expression of chemokines in transformed EBV-infected cells. The secreted chemokines would then attract T cells and macrophages to migrate to the tumor and provide growth signals to the tumor, possibly through cytokines.

We transduced the expression of LMP1 in an epithelial cell line (HaCat) by adenovirus infection, and then analyzed the induction of chemokine genes by microarray. The B95-8 coding sequence for LMP1 was cloned into the KpnI-NotI sites of the polylinker of a pShuttle vector. Recombinant adenovirus plasmids were produced by homologous recombination with the pAdEasy system (Quantum Biotechnologies.) These were used to transfect 293 cells, which produced recombinant adenovirus that could then be harvested by collecting the supernatants. A control virus that expressed only GFP was also produced in the same way using the original plasmid backbone without the additional LMP1 sequence. Virus supernatants were added to 80% confluent cultures of

HaCat epithelial cells. Within 36 hours, the cells could be seen to be positive for GFP. With a high MOI, the percentage of cells that were GFP positive was nearly 100% for both the LMP1 adenovirus-infected cells and the control cultures. After 72 hours, the cells were washed with PBS, and then used for RNA extraction by TRIZOL (Invitrogen). The RNA was reverse-transcribed to make cDNA, which in turn, was used to make biotinylated cRNA probes for a SuperArray microarray experiment. The SuperArray microarray that I used was printed with 113 chemokine and chemokine receptor gene sequences, as well as several housekeeping controls, such as GAPDH and Beta Actin. After overnight hybridization of the probes to the microarray, alkaline phosphatase-conjugated streptavidin was bound to the biotinylated probes, and a chemiluminescence substrate was used for detection (CDP-Star, SuperArray Biosciences). I scanned and analyzed the films using software (GEArray Expression Analysis Suite 2.0, SuperArray Biosciences) to quantify the relative expression levels between the LMP1-expressing samples and the GFP controls. By far the highest induction was for CCL5/RANTES, which is a chemoattractant for T cells and monocytes (fig 22).

The induction of RANTES by LMP1 was confirmed at the RNA level by quantitative real-time PCR, and at the protein level by ELISA in the HaCat epithelial cell line and in primary epithelial cells derived from human tonsils (fig 23-25). Cultures of HaCat cells were infected at 80% confluence with increasing titers of adenovirus to produce a dose range of increasing LMP1 expression. This was matched with GFP controls at the same MOI for each dose. After 72 hours, RNA was collected for each sample by TRIZOL (Invitrogen), and then reverse-transcribed to make cDNA (SuperScript II, Invitrogen). RANTES expression in each sample was analyzed by

quantitative real-time PCR using iTaq Supermix with Rox (Bio-Rad) and Real-Time PCR probes for RANTES and beta actin from Applied Biosystems. As indicated in figure 23, increasing expression of LMP1 induced increasing transcription of RANTES RNA in a dose-dependent manner. In contrast, increasing concentration of the control GFP virus had no effect on RANTES transcription. The same adenovirus infection protocol was used to generate LMP1-expressing samples and matched controls to study LMP1 induction of RANTES at the protein level. Supernatants were collected 72 hours after adenovirus infection and used for an ELISA specific for human RANTES (DuoSet, R&D Systems). The results confirmed that increasing LMP1 expression induced RANTES secretion in a dose-dependent manner, up to a point, after which secretion leveled-off and began to decline (figure 24). As before, increasing the concentration of the GFP control virus did not affect RANTES production.

I then studied the induction of RANTES by LMP1 in primary epithelial cells derived from human tonsils. These are the primary cells most similar to the cells infected by EBV in the nasopharynx that would eventually transform to malignant cancer cells in NPC that we could obtain. Tonsils from young children undergoing tonsillectomies were provided by surgeons from Tufts Medical Center. I sectioned the tonsils into small explants approximately 2-3 mm across, while intermittently washing the tonsil sections in DMEM/F12 media supplemented with penicillin, streptomycin and fungizone. Clusters of tonsil explants were then placed in 10 cm tissue culture dishes, over which transwell devices were placed in order to compress the explants to the plates. The tonsil epithelial cells require physical pressure in order to induce the cells to adhere to the plate and grow out in a monolayer. These cells were cultured in DMEM/F12 for four days, and then the

media was changed to a serum-free media, supplemented with Keratinocyte Growth Factor (KGF). This favored the outgrowth of epithelial cells over the typically more prolific fibroblasts from the tonsil explants. After two weeks in culture, the epithelial cells would be growing in monolayers emanating from the tissue beneath the transwell devices. These cells would then be trypsinized, and deposited in new plates to generate uniform monolayers of primary epithelial cells for experiments. I used several of these cultures for LMP1 adenovirus infection, followed by the preparation of samples for Quantitative Real-Time PCR and ELISA as described previously. In four separate experiments using cells from different donors, LMP1 expression induced significantly higher levels of RANTES RNA transcription and protein secretion compared to the GFP control virus infected cells (figure 25a and figure 25b).

We were interested in performing a functional chemotaxis assay to see if the induction of RANTES by LMP1 at the levels of LMP1 expression seen in NPC was great enough to influence the migratory behavior of T cells *in vitro*. We were concerned that HaCat cells would not be the best cell line to use for this since there was a baseline of RANTES expression in these cells with or without the expression of LMP1 (figure 24). Therefore, we decided to look at a panel of human epithelial cells in order to select one that had a low background level of RANTES expression. An ELISA for RANTES secretion indicated a wide range of background expression levels (figure 26). Furthermore, when three of these cell lines with low background levels of RANTES expression were selected for infection with the LMP1 adenovirus (BEAS-2B, CaCO2A, and HeLa), the responses to LMP1 expression varied. LMP1 induced RANTES expression in BEAS-2B and HeLa, but had no effect in CaCO2A (figure 27). This

suggests that context and differentiation state of an epithelial cell could have a dramatic impact on the downstream effects of LMP1 signaling.

Chemotaxis assays were performed with HeLa cells to demonstrate that the LMP1-induced expression of RANTES could promote lymphocyte migration (fig 28.) Cultures of HeLa cells were infected with either the LMP1 adenovirus or the GFP control virus and supernatants were collected. These supernatants were deposited in the lower chambers of a modified Boyden Chamber Assay (Neuro Probe). Anti-human CCL5 antibodies or isotype control antibodies were added to the supernatants (R&D systems). Then a membrane was placed over the lower chamber, and a cell suspension containing human T cells were placed above the membrane. If the contents of the supernatants included factors that attract the T cells, the T cells would then migrate into the membrane and get trapped. They were then extracted by centrifugation and quantified by an MTS assay, as described previously. LMP1 appeared to increase the number of T cells that migrated into the membrane (figure 28). When the anti-RANTES neutralizing antibody was added to the supernatant, this effect was reduced. These results suggest that the LMP1-induced chemotaxis of T cells was RANTES dependent.

In HONE-1, an NPC derived cell line that lost the EBV episome, CCL5 and two other chemokines previously linked to LMP1 siganling in our lab, CCL17 and CCL22, were all induced by LMP1 in a dose-dependent manner (fig 29-33). Expression of these chemokines is also induced by LMP1 in the B cell line, BJAB, suggesting that a similar process of LMP1 induced recruitment of lymphocytes to the tumor may be taking place in Hodgkin's lymphoma (fig 34-35).

Fig 22.

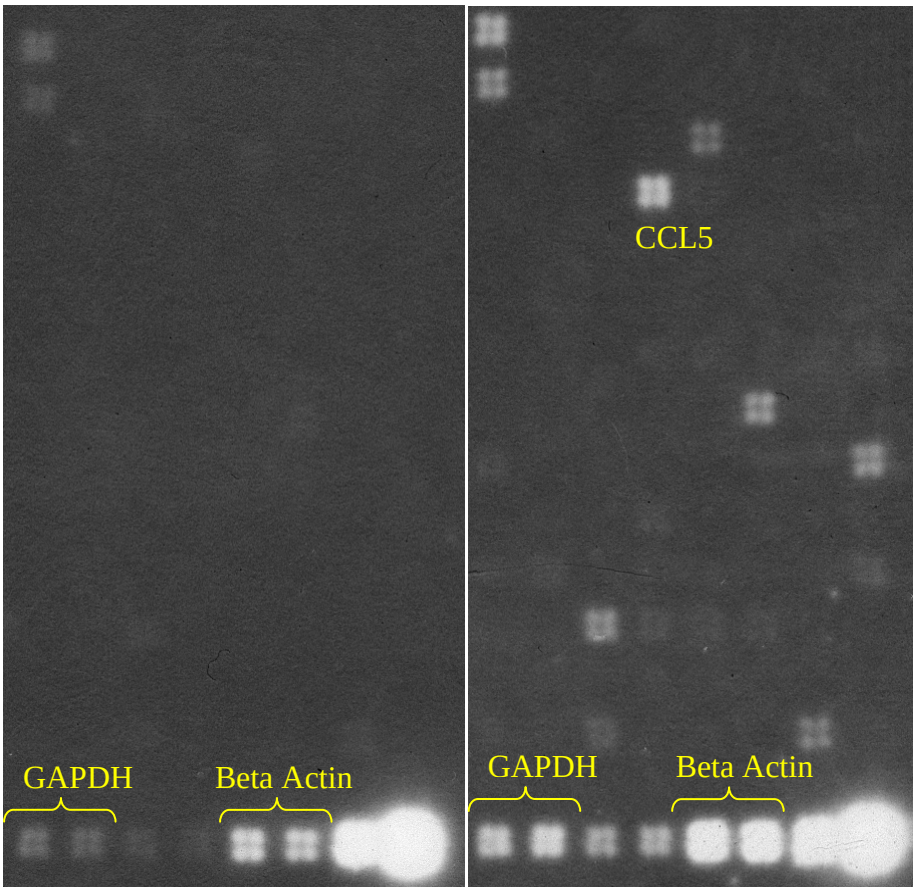
GAPDH
Beta Actin
CCL5
GAPDH
Beta Actin

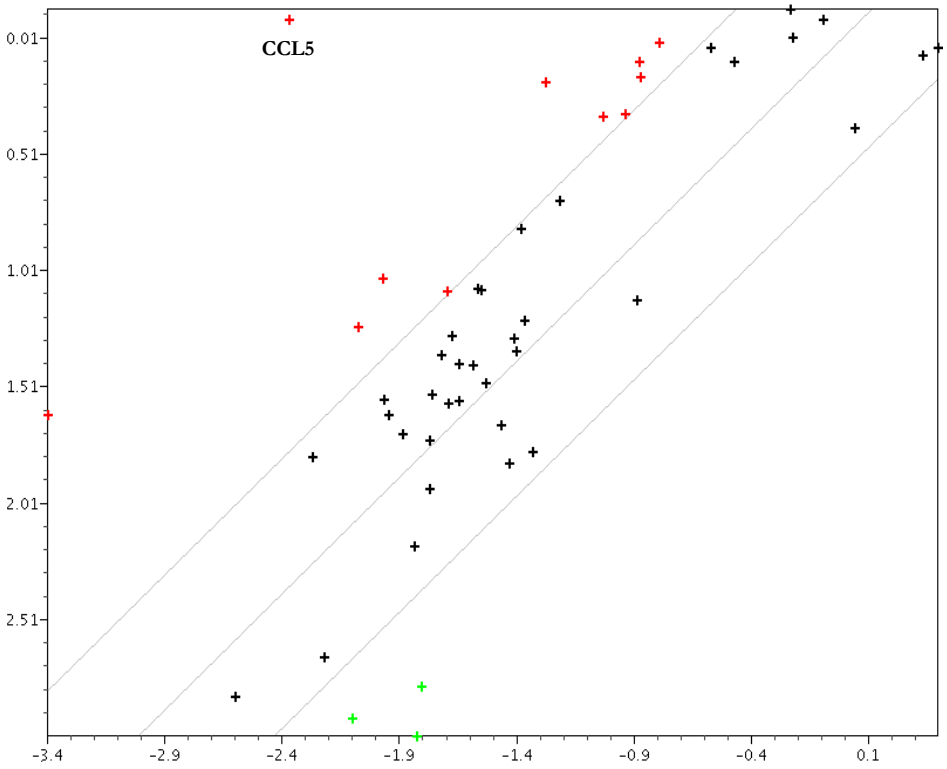
CCL5
0.01
0.51
1.01
1.51
2.01
2.51
-3.4
-2.9
-2.4
-1.9
-1.4
-0.9
-0.4
0.1

Figure 22. Microarray results indicate that CCL5/RANTES transcription is up-regulated in HaCaT cells transduced to express LMP1. The HaCaT epithelial cell line was cultured *in vitro* and infected with either an adenovirus encoding LMP1 and GFP or a mock control encoding only GFP. RNA was isolated from infected cells and used to synthesize cRNA probes which were hybridized to Chemokine microarrays (Superarray Biosciences). Signals for individual chemokine and chemokine receptor genes were normalized to housekeeping controls (GAPDH, beta actin) and compared between LMP1 expressing HaCaT (right) and the GFP control (left). The gene with the highest induction by LMP1 was CCL5/RANTES. Signals for genes, normalized to controls, were plotted in the lower figure (LMP1 on the y-axis; GFP on the x-axis). Deviation from the diagonal indicates an up-regulation (to the left) or down-regulation (to the right) of transcription in response to LMP1 expression.

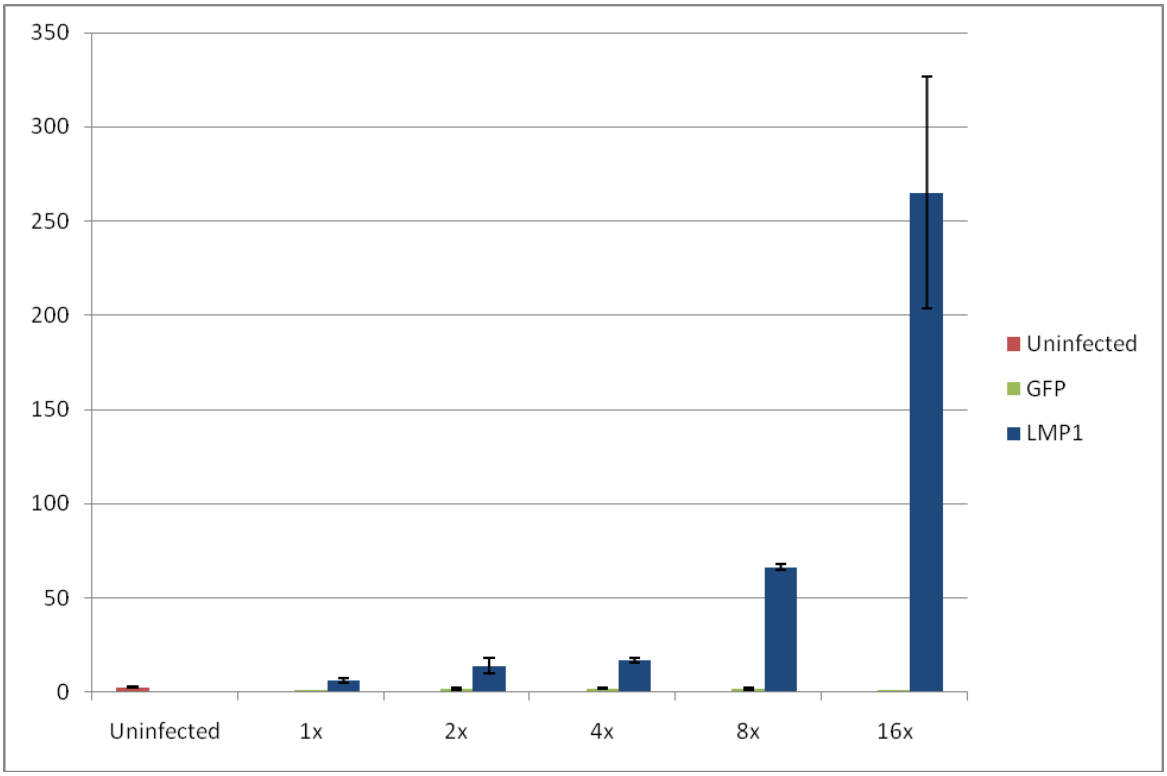

Figure 23. Real-time PCR for CCL5/RANTES in HaCaT. HaCaT epithelial cells were infected with increasing titers of adenovirus to generate a dose range of LMP1 expression (paired with GFP controls). Quantitative real-time PCR indicates that LMP1 induces CCL5/RANTES in a dose-dependent manner. Expression level is normalized to beta actin. These results are representative of four experiments.

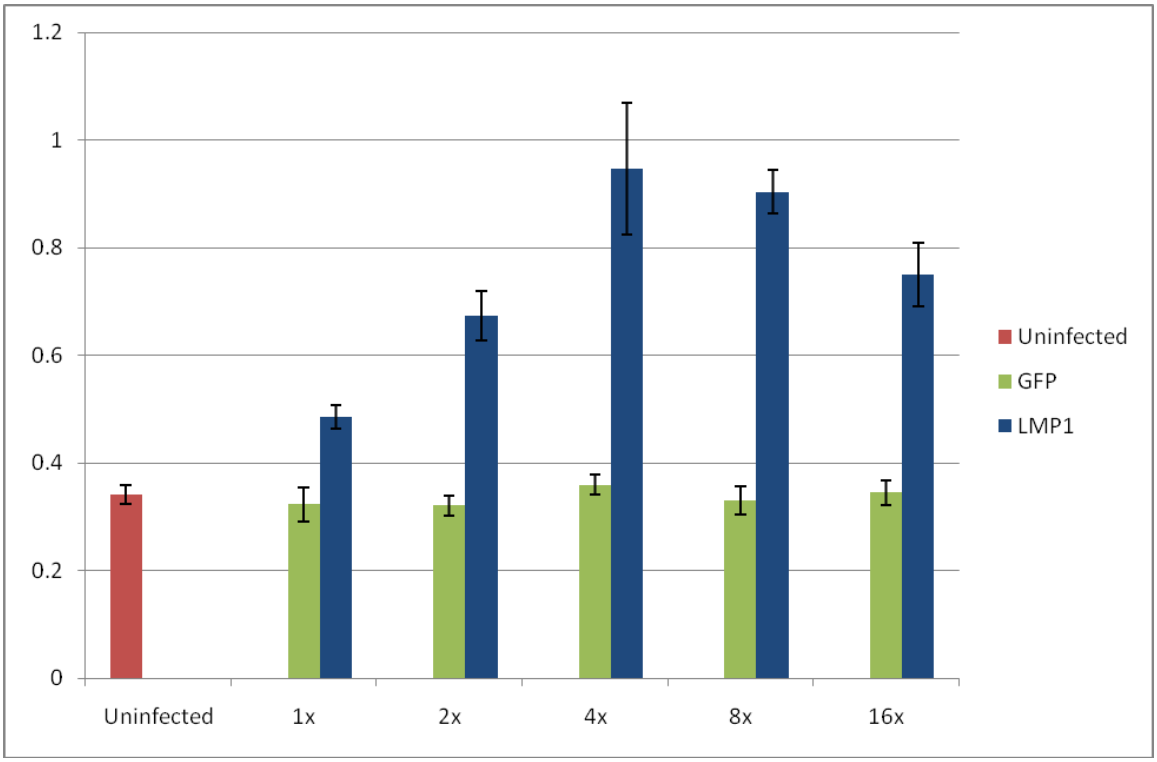

Figure 24. ELISA for CCL5/RANTES in HaCaT. HaCaT epithelial cells were infected with increasing titers of adenovirus to generate a dose range of LMP1 expression (paired with GFP controls). CCL5/RANTES protein secretion was measured by ELISA. Results confirm that LMP1 induces CCL5/RANTES in a dose-dependent manner. Concentration of RANTES in ng/ml is indicated on the y-axis. These results are representative of three experiments.

Fig 25a. Real-time PCR for CCL5/RANTES in primary epithelial cells

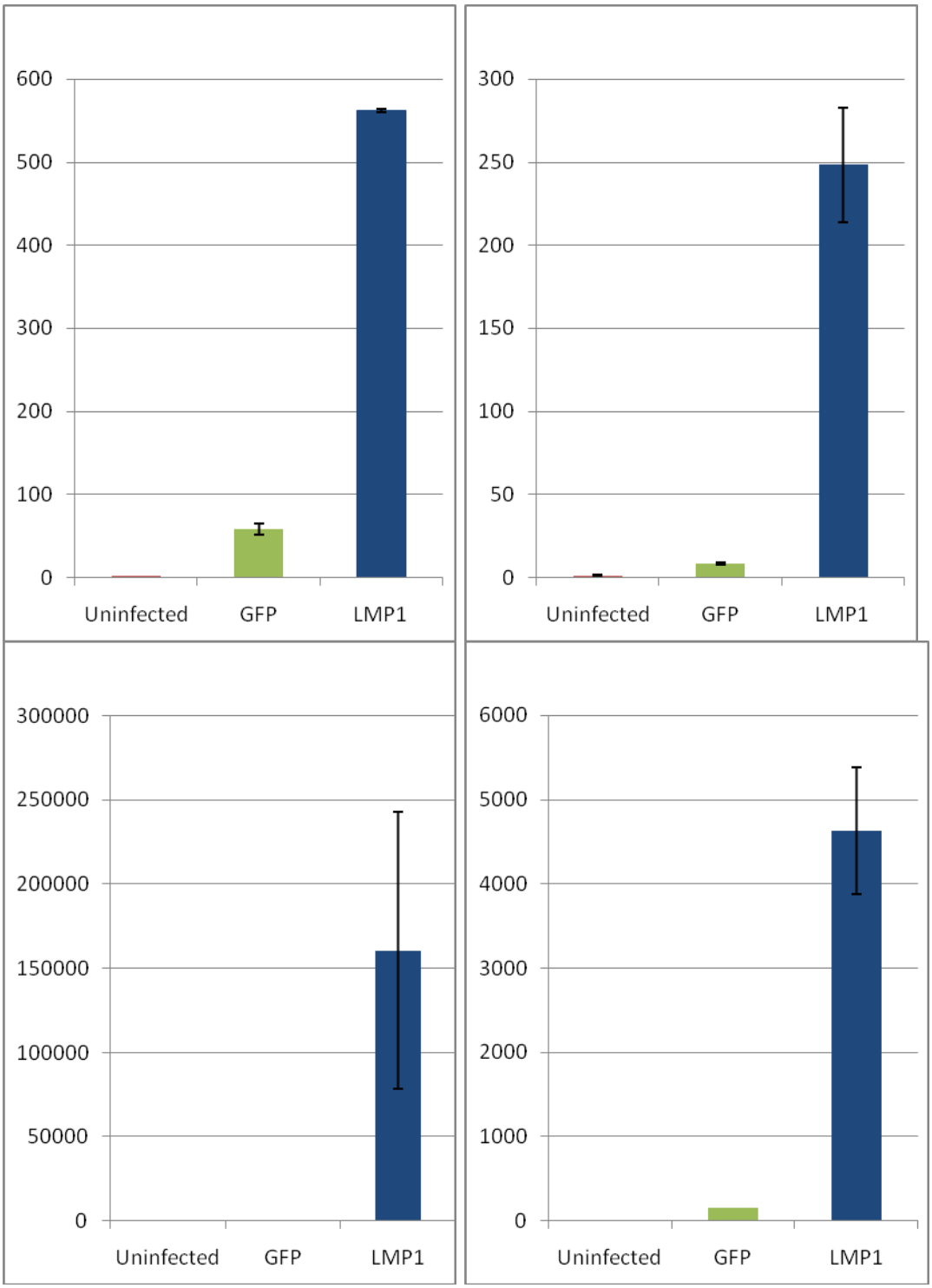

Fig 25b. ELISA for CCL5/RANTES in primary epithelial cells

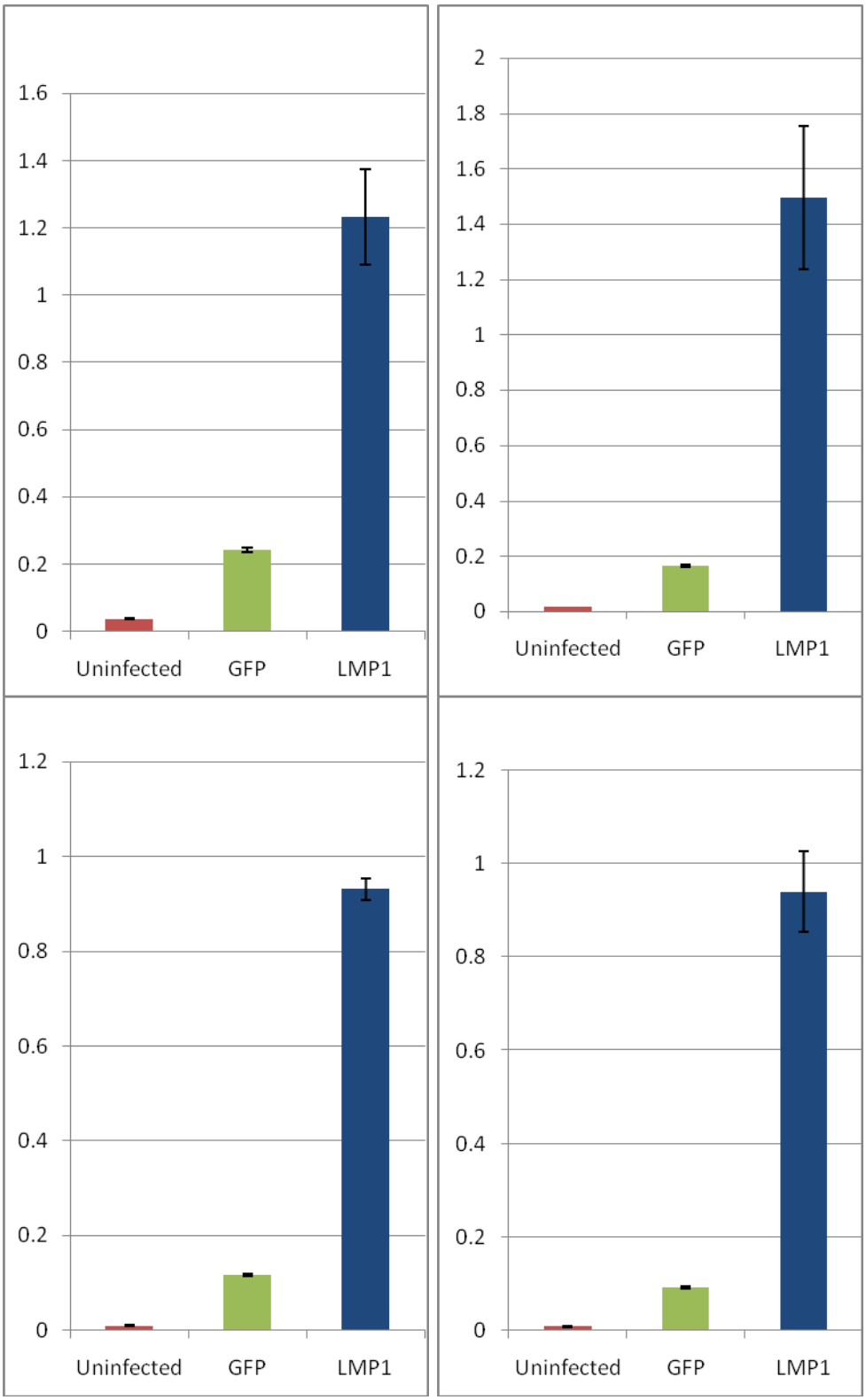

Figure 25. LMP1 induces CCL5/RANTES in primary tonsil epithelial cells. Primary epithelial cells derived from human tonsils were cultured *in vitro* and infected with the LMP1 adenovirus or the GFP control. (A) Quantitative real-time PCR indicates that LMP1 induces CCL5/RANTES transcription in epithelial cells from four different donors. Expression level is normalized to beta actin. (B) CCL5/RANTES protein secretion was measured by ELISA. Results confirm that LMP1 induces CCL5/RANTES secretion in primary epithelial cells from four different donors. Concentration of RANTES in ng/ml is indicated on the y-axis.

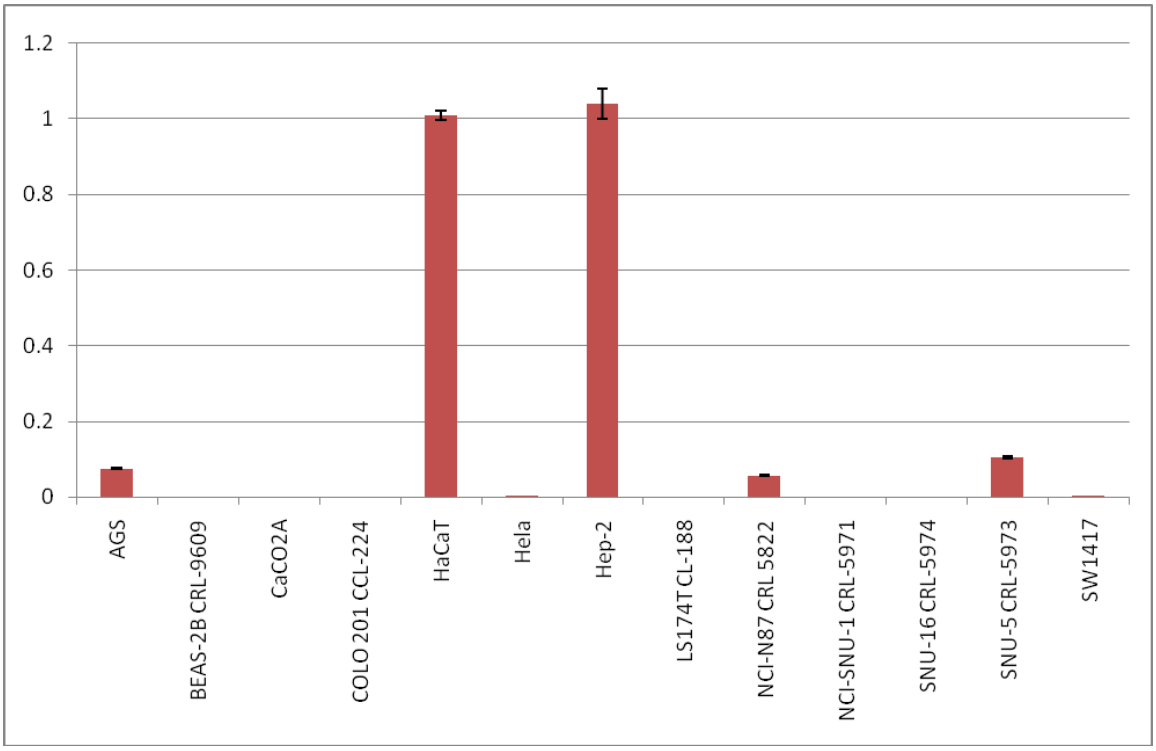

Figure 26. ELISA for CCL5/RANTES in epithelial cell lines. Endogenous expression levels of CCL5/RANTES was determined in a panel of epithelial cell lines. Results indicate that expression levels vary widely between different epithelial cell types.

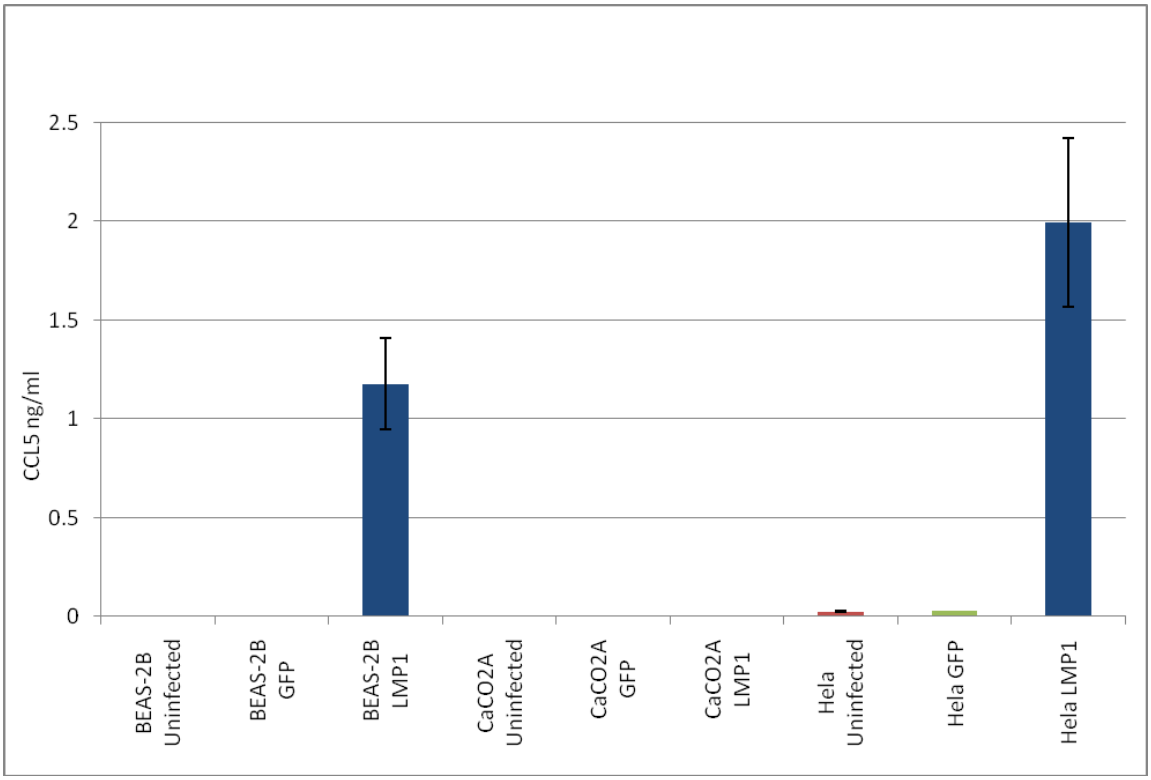

Figure 27. ELISA for CCL5/RANTES in epithelial cell lines. Three epithelial cell lines from the panel shown in Figure 26 which had low or undetectable levels of endogenous expression of CCL5/RANTES were selected to be infected with the LMP1 adenovirus and GFP controls. Results indicate that in two of these cell lines, HeLa and BEAS-2B, CCL5/RANTES was induced by LMP1.

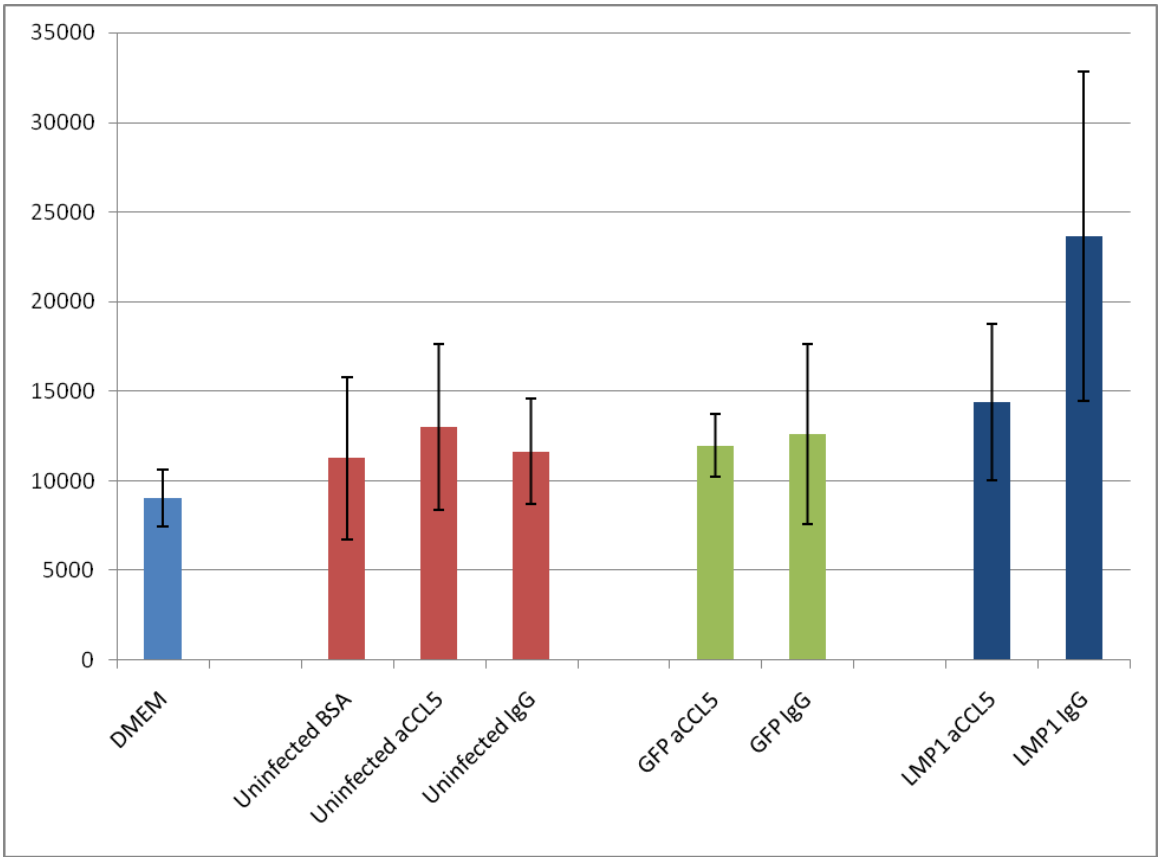

Figure 28. Chemotaxis Assay shows that LMP1 promotes T cell migration in a CCL5/RANTES-dependant manner. HeLa cells were infected with either the LMP1 adenovirus or the GFP control. Supernatants were placed in the lower chamber of a modified Boyden Chamber with either anti-CCL5 antibodies or isotype control antibodies added. A suspension containing T cells was placed over a membrane that separated the lower chamber from the suspension. The number of T cells that migrated into the membrane (in part driven by factors in the supernatants in the lower chamber) was quantified by an MTS assay. LMP1 increased the number of T cells that migrated into the membrane. This effect was negated by anti-CCL5/RANTES neutralizing antibodies, suggesting that the LMP1-induced chemotaxis of T cells was CCL5/RANTES-dependant.

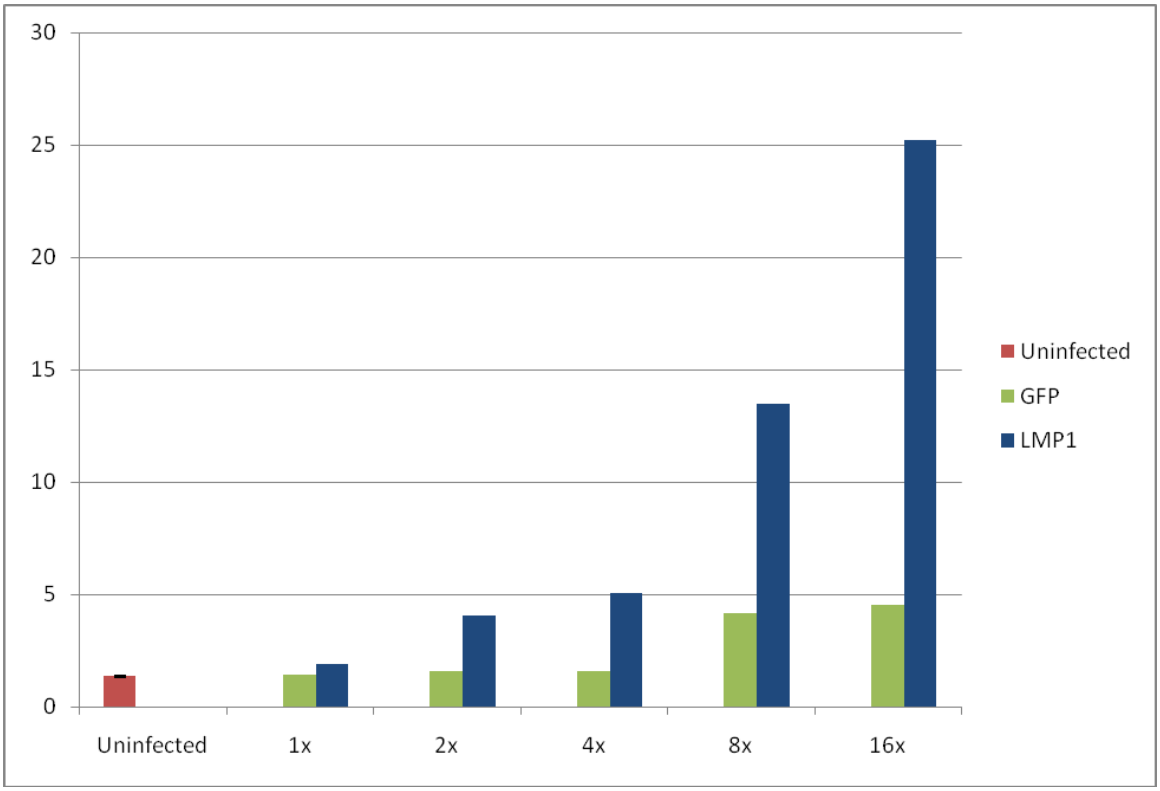

Figure 29. Real-time PCR for CCL5/RANTES in HONE-1. HONE-1 cells were infected with increasing titers of adenovirus to generate a dose range of LMP1 expression (paired with GFP controls.) Quantitative real-time PCR indicates that LMP1 induces CCL5/RANTES in a dose-dependent manner. Expression level is normalized to beta actin.

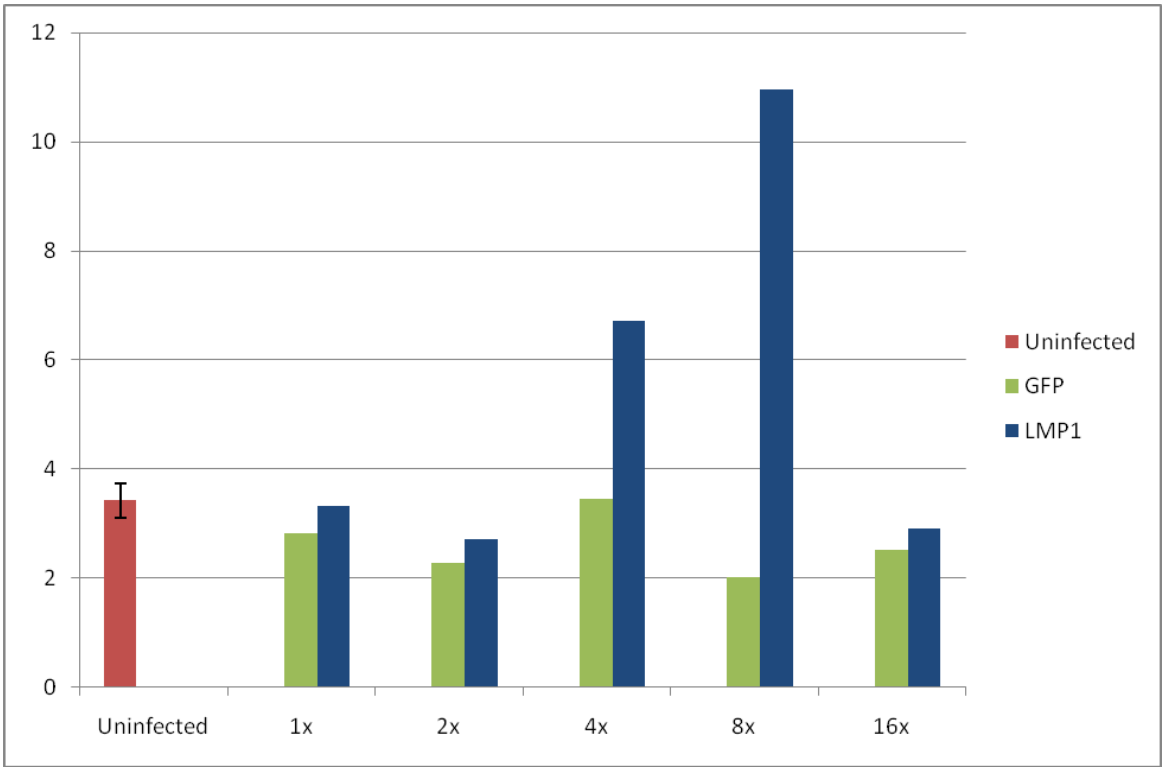

Figure 30. Real-time PCR for CCL17/TARC in HONE-1. HONE-1 cells were infected with increasing titers of adenovirus to generate a dose range of LMP1 expression (paired with GFP controls). Quantitative real-time PCR indicates that LMP1 induces CCL17/TARC, a chemokine that promotes chemotaxis of T cells. Expression level is normalized to beta actin.

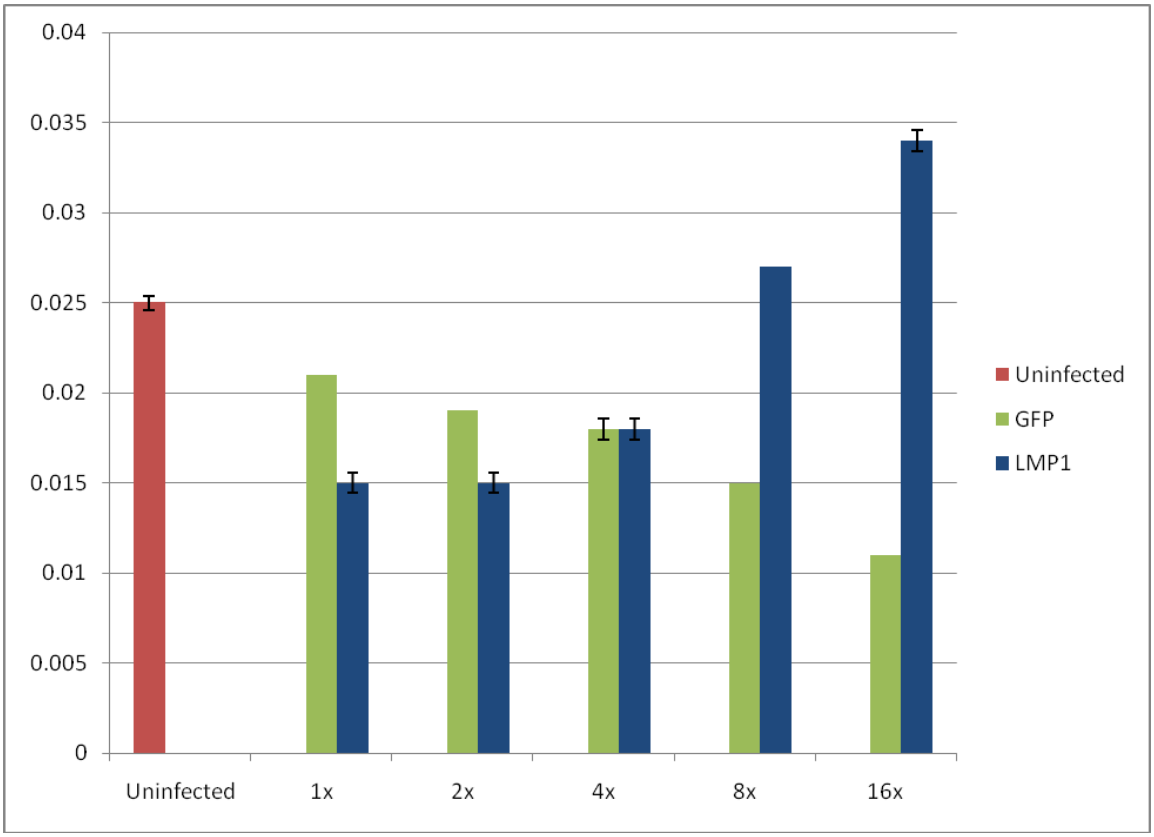

Figure 31. ELISA for CCL17/TARC in HONE-1. HONE-1 cells were infected with increasing titers of adenovirus to generate a dose range of LMP1 expression (paired with GFP controls). CCL17/TARC protein secretion was measured by ELISA. Results confirm that LMP1 induces CCL17/TARC in HONE-1. Concentration of CCL17/TARC in ng/ml is indicated on the y-axis.

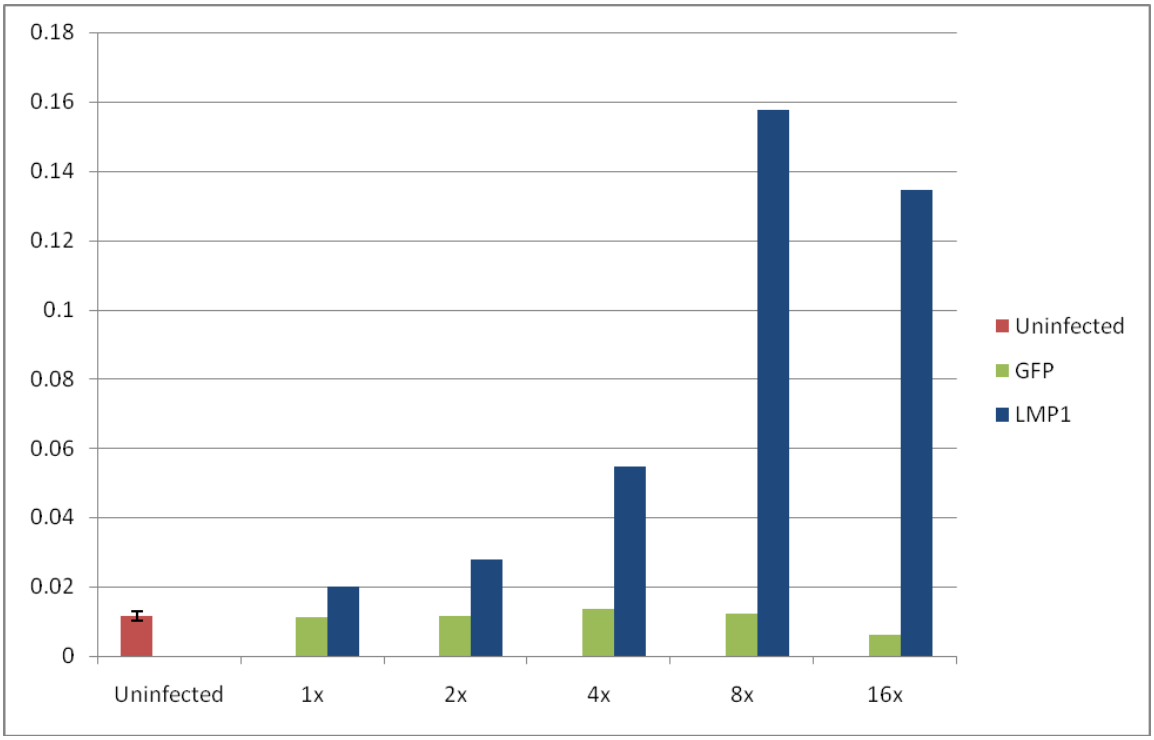

Fig 32. Real-time PCR for CCL22/MDC in HONE-1. HONE-1 cells were infected with increasing titers of adenovirus to generate a dose range of LMP1 expression (paired with GFP controls). Quantitative real-time PCR indicates that LMP1 induces CCL22/MDC, a chemoattractant for monocytes, monocyte-derived dendritic cells, and NK cells, in a dose-dependent manner. Expression level is normalized to beta actin.

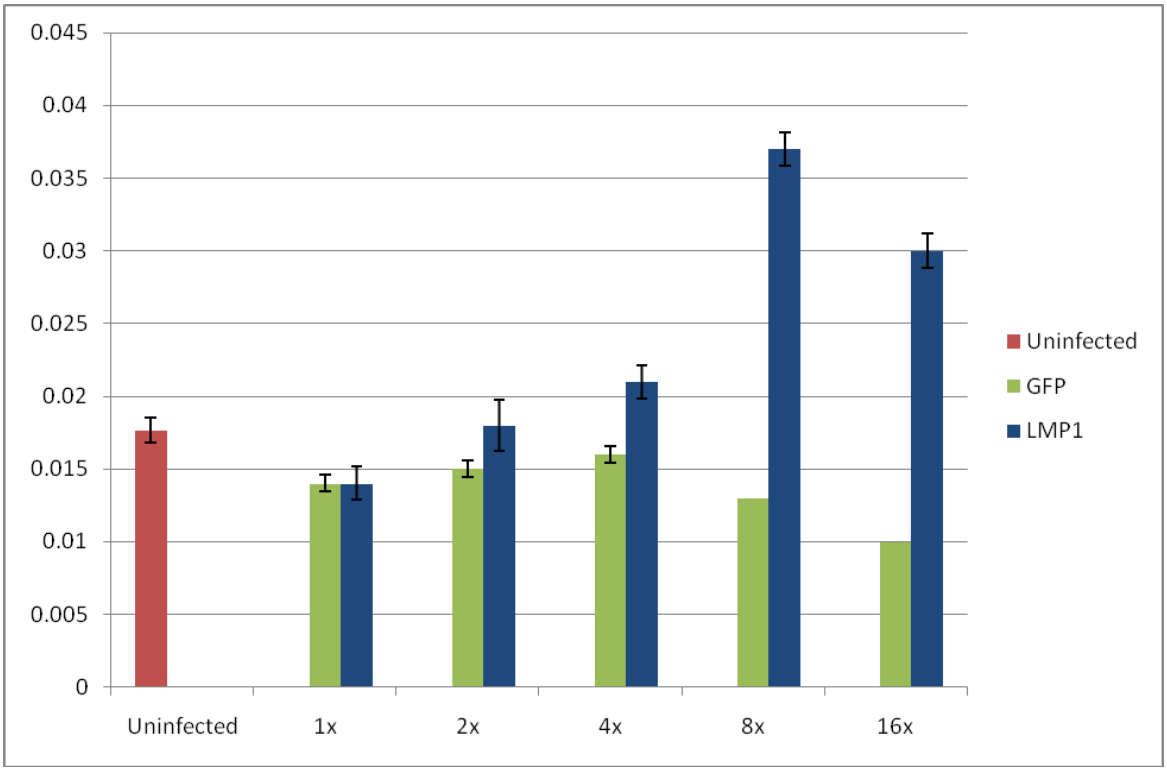

Figure 33. ELISA for CCL22/MDC in HONE-1. HONE-1 cells were infected with increasing titers of adenovirus to generate a dose range of LMP1 expression (paired with GFP controls). CCL22/MDC protein secretion was measured by ELISA. Results confirm that LMP1 induces CCL22/MDC in a dose-dependent manner. Concentration of CCL22/MDC in ng/ml is indicated on the y-axis.

Fig 34a. Real-time PCR for CCL5/RANTES in BJAB

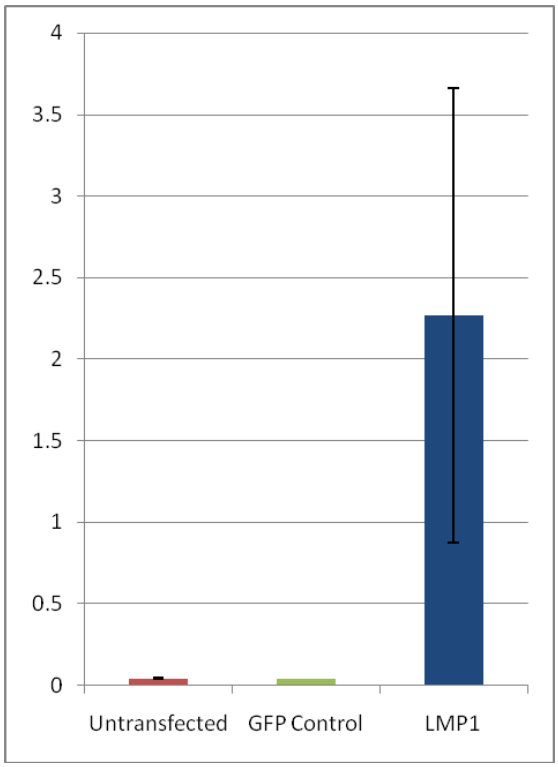

Fig 34b. Real-time PCR for CCL17/TARC in BJAB

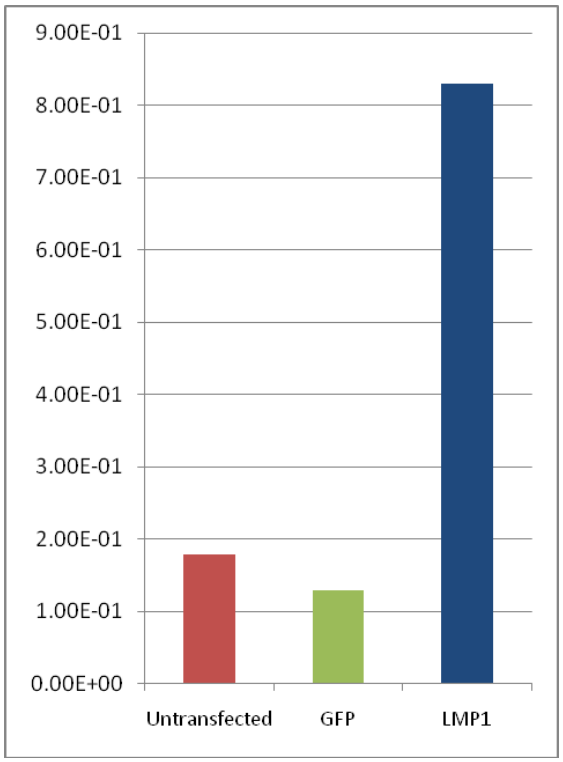

Fig 34c. Real-time PCR for CCL22/MDC in BJAB

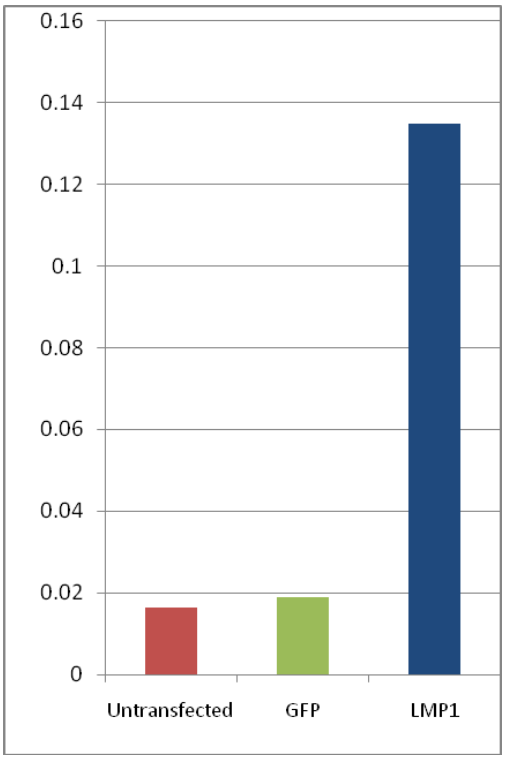

Figure 34. LMP1 induces CCL5, CCL17, and CCL22 transcription in BJAB. The B cell line, BJAB was transfected with a construct encoding LMP1 and GFP, or a mock control construct encoding only GFP. Quantitative real-time PCR indicates that LMP1 induces the transcription of (A) CCL5/RANTES, (B) CCL17/TARC, and (C) CCL22/MDC.

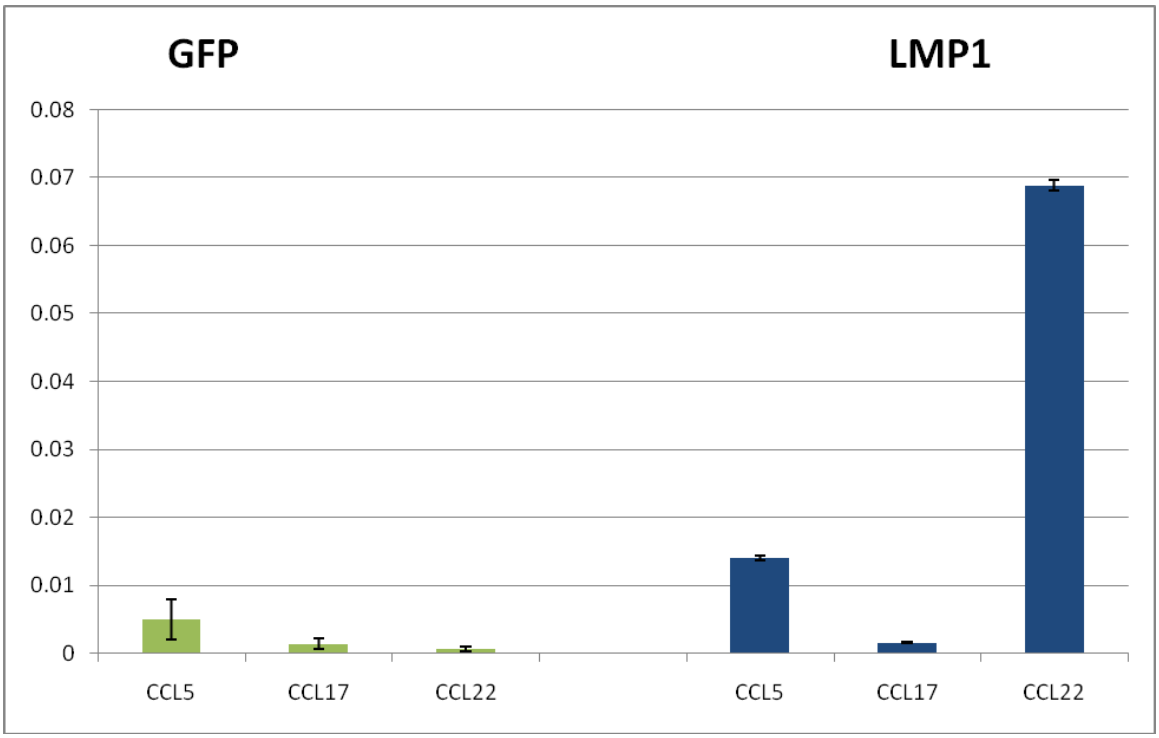

Figure 35. ELISA for Chemokine Expression in BJAB. The B cell line, BJAB was transfected with a construct encoding LMP1 and GFP, or a mock control construct encoding only GFP. Protein secretion of CCL5, CCL17 and CCL22 was measured by ELISA. Results confirm that LMP1 induces CCL5/RANTES and CCL22/MDC in BJAB, but not CCL17/TARC. Concentration of RANTES in ng/ml is indicated on the y-axis. These results are representative of three experiments.

Chapter 6: RANTES promotes migration and metastasis in Nasopharyngeal Carcinoma

Recent reports suggest that expression of RANTES promotes motility and migration of breast cancer cells (Karnoub, 2007). Furthermore, RANTES expression correlates with poor prognosis in studies of breast cancer and lung cancer (Luboshits, 1999, Niwa 2001, Azenshtein, 2002). Therefore, we investigated whether RANTES expression promotes motility, invasion and metastasis in NPC. We used scratch assays to determine whether RANTES promotes increased migration of NPC-derived cell lines. HONE Akata cells were grown in confluent monolayers in 6-well plates. I then used the tips of p200 pipette tips to create a scratch across the center of the monolayers. The size of the gap in the monolayers that this created was relatively uniform in each well. I then added either 1000 ng/ml of anti-RANTES neutralizing antibodies (R&D Systems), 1000 ng/ml of isotype control antibodies (R&D Systems), 128 ng/ml of recombinant human RANTES (R&D Systems) or left the cultures untreated. I then observed the closure of the gap in each well as HONE Akata cells migrated into the center, taking pictures under the microscope every three hours (figure 36). Compared to the cells in the isotype control cultures and in the untreated cultures, the cells in the anti-RANTES antibody-treated cultures converged at a decreased rate. Furthermore the gap in the wells treated with recombinant RANTES closed in less time than in the untreated wells. These results suggest that RANTES promotes increased migration of the HONE Akata NPC cell line *in vitro*.

I next repeated the same type of experiment using cells from biopsies of primary NPC tumors. The biopsies were sectioned and cultured using the same protocols that I used for culturing primary tonsil epithelial cells, described previously. I added anti-RANTES antibodies, isotype control antibodies, and recombinant RANTES protein or left the cultures untreated and then performed the scratch assays as before. I then observed the migration of cells into the scratch gap every 3 to 6 hours for up to 5 days. Again, the anti-RANTES antibody appeared to slow the migration of cells into the gap, whereas the recombinant protein appeared to accelerate the closure of the artificial wound, compared to the isotype control and untreated cultures (figure 37a and figure 37b).

The previous series of experiments used transformed NPC cells and NPC cell lines which presumably had undergone numerous genetic alterations during the process of tumorigenesis. I next wanted to determine whether the expression of LMP1 alone in primary tonsil epithelial cells would be sufficient to promote migration, and if so, whether this activity would be RANTES-dependent. EBV infection and the expression of virus-encoded proteins, such as LMP1, are believed to be early events in NPC development. The contributions of LMP1, including potentially increased motility via induced-RANTES expression, may be important early stage factors in NPC oncogenesis. Transducing the expression of LMP1 in primary epithelial cells would allow us to study this in the context of non-transformed cells, more similar to what would be found in a premalignant lesion. Therefore, I infected primary tonsil epithelial cells with the LMP1 adenovirus and the GFP control virus, allowed 72 hours to pass so that LMP1 would be expressed, and then performed scratch assays as described previously. Cultures were

treated with either the anti-RANTES neutralizing antibody, an isotype control antibody, recombinant human RANTES protein or were left untreated. After 48 hours, there appeared to be no difference among the cultures infected with the GFP control virus (fig 38). Cells were very slow to move into the gap. In comparison, LMP1-expressing cells treated with the isotype control antibody or untreated migrated into the gap to a greater degree. This appeared to be increased further with the addition of the recombinant RANTES protein. In contrast, the cells in the LMP1 adenovirus- infected culture treated with the anti-RANTES antibody appeared to have reduced motility, more similar to the cells in the control cultures. Interestingly, the control cells that were treated with recombinant RANTES did not appear to have increased motility. It is possible that the induced expression of CCL5/RANTES up-regulates the expression of one or more of its receptors, such as CCR5, and as a result, LMP1 expression not only increases the production of RANTES, it also sensitizes the cells to it. However, I did not perform the assays to confirm this.

LMP2A is also expressed in NPC tumors and has been reported to promote increased motility in infected epithelial cells. In order to determine the specific role of LMP1 and LMP2A in promoting RANTES-dependent migration of epithelial cells, primary epithelial cells derived from human tonsils were infected with adenoviruses to express LMP1, LMP2A and both LMP1 and LMP2A in combination. These cell cultures were then used for scratch assays as described previously. The results suggest that LMP1-induced migration is RANTES dependent but LMP2A-induced migration is not (fig 39). The concurrent expression of LMP1 and LMP2A has an additive effect on migration, closing the gap faster than LMP1 expression alone.

I then studied the role of RANTES-induced migration and the effect it may have in promoting metastasis in our mouse model, by establishing C666-1 tumors in mice, and then injecting 32 μg of anti-RANTES neutralizing antibodies or isotype control antibodies, by intraperitoneal injection, twice a week. I then tracked tumor development over several weeks and determined that blocking RANTES has an effect on the development of metastasis (figure 40). In the control mice, 10 out of 24 mice developed metastases (42%), whereas in mice receiving the neutralizing antibody, only 4 out of 25 mice developed metastases (15%). This suggests that CCL5/RANTES promotes metastasis in our NPC mouse model. Blocking RANTES appeared to also slow the progression of disease in the treated mice. The mice receiving the anti-RANTES antibody succumbed slower than the mice receiving the control antibody ($p=0.044$). The hazard ratio, a measure of the relative risk between each group, is 2.0677, indicating that the risk in the anti-RANTES group is approximately twice as high as in the isotype control group. (95% CI = 0.9001 to 04.7499) (fig 41). Ultimately, all the mice died however there was a delay of about seven to ten days between the two groups.

Fig 36. Scratch assay of HONE Akata NPC cell line

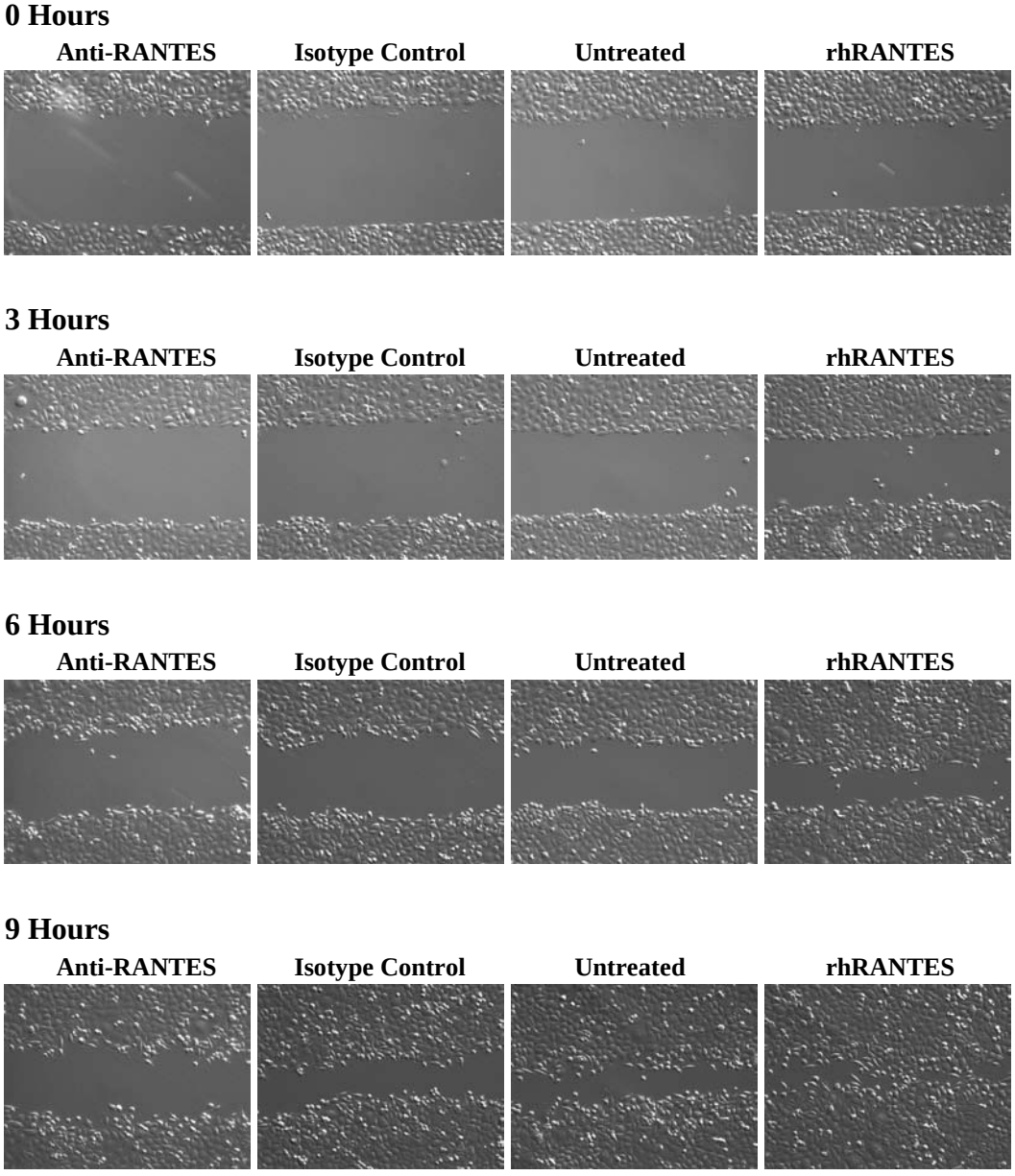

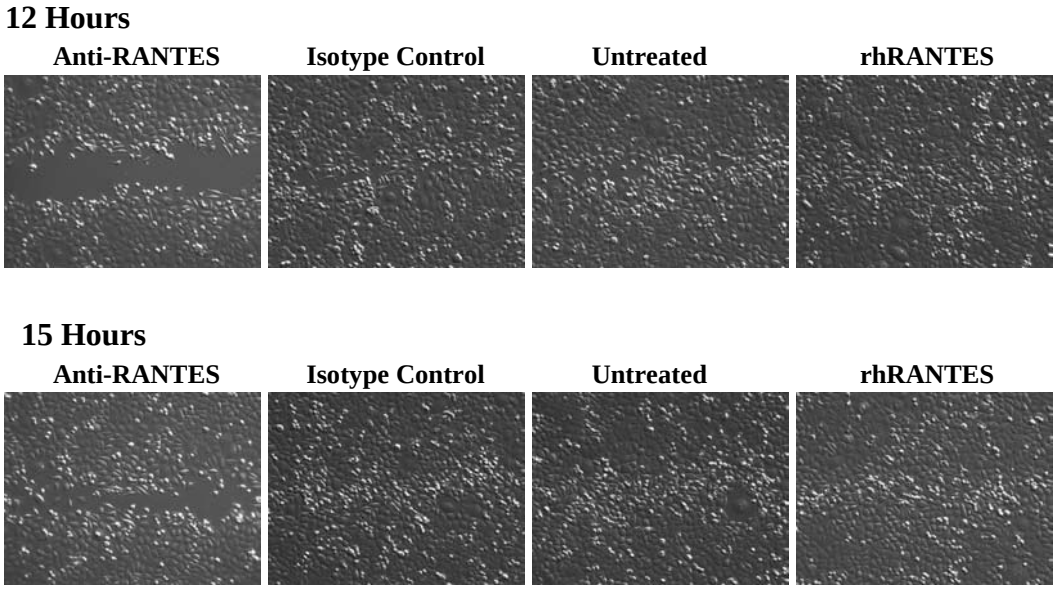

Figure 36. RANTES promotes motility of the HONE Akata NPC cell line. Hone Akata cells were cultured to form monolayers, then a pipet tip was used to create an artificial wound across the center of each well. Cells were either treated with an anti-RANTES neutralizing antibody, an isotype control antibody, recombinant human CCL5/RANTES protein, or were untreated. Images were taken every three hours to track the migration of cells and closing of the artificial wound. The data indicates that the cells receiving the neutralizing antibody had reduced motility compared to the isotype control. Cells exposed to exogenous recombinant RANTES displayed increased motility and closed the wound faster than in the antibody or untreated cultures. This data is representative of four experiments

Fig 37a. Scratch assay of Primary NPC biopsy cells (N7)

57 Hours

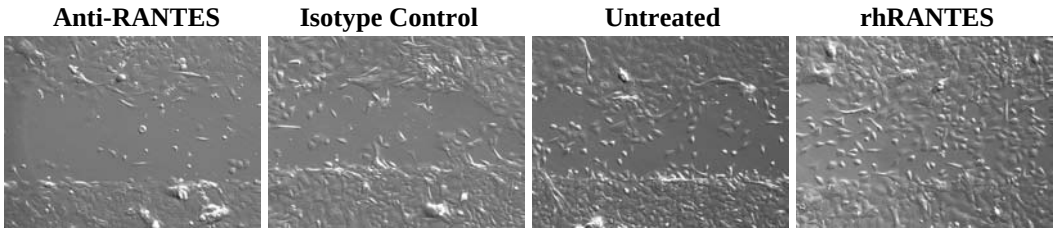

60 Hours

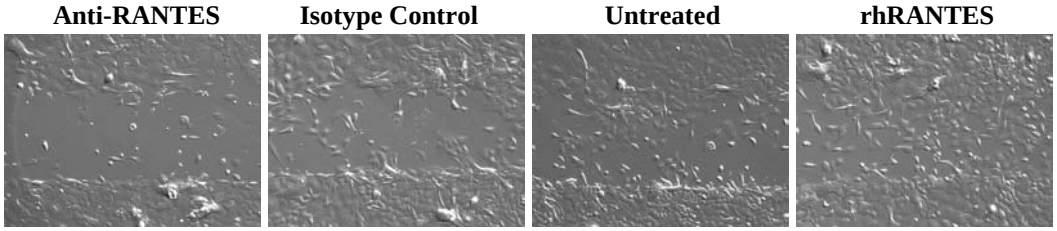

Fig 37b. Scratch assay of Primary NPC biopsy cells (N9)

18 Hours

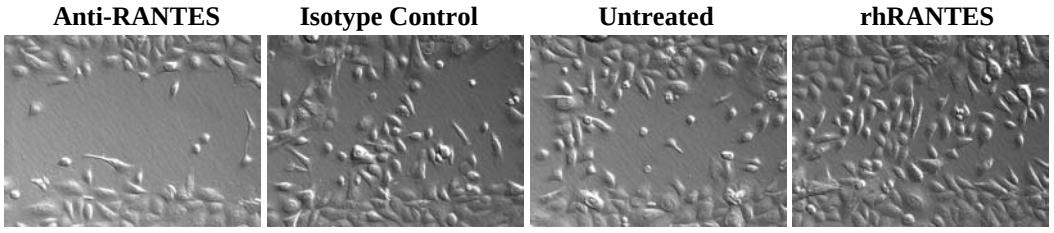

36 Hours

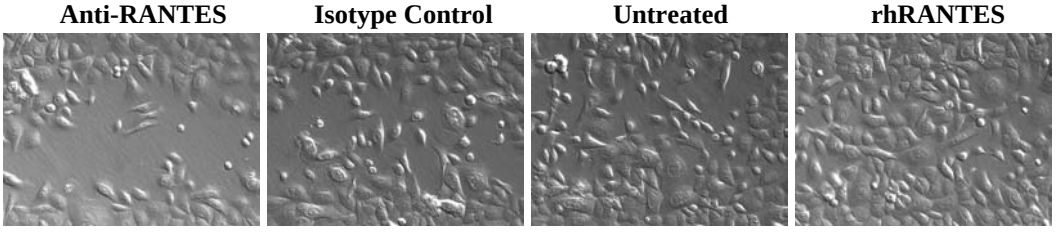

Figure 37. CCL5/RANTES promotes migration of primary NPC biopsy cells. NPC biopsies were sectioned and explants were cultured to generate uniform monolayers of cells from primary NPC tumors. Scratch assays were performed and cells were treated with an anti-RANTES neutralizing antibody, an isotype control antibody, recombinant human CCL5/RANTES protein, or were untreated. Images were taken at 3 or 6 hour intervals to track the migration of cells into the artificial wound. The data shown is from two of the four NPC tumors that were used for this series of experiments. In each case, the wells receiving the neutralizing antibody displayed reduced movement compared to the wells receiving the isotype control antibody. The addition of recombinant human RANTES increased motility.

Fig 38. LMP1 increases migration of human tonsil epithelial cells and migration is RANTES-dependent. Primary epithelial cells were cultured from human tonsils and infected with either an adenovirus that induces the expression of LMP1 or a control adenovirus. Scratch assays were performed and cells were treated with an anti-RANTES neutralizing antibody, an isotype control antibody, recombinant human CCL5/RANTES protein, or were untreated. Images were taken every six hours. In LMP1-expressing cells, migration appeared to be RANTES-dependent. In the control adenovirus cells, there was no endogenous expression of RANTES, and there was decreased motility of the cells, suggesting that LMP1 increases cell migration. There was no apparent difference between cells treated with the neutralizing antibody and those treated with the isotype control antibody. In the GFP control cells, there was no effect seen with the addition of the recombinant protein.

48 Hours

Control Adenovirus Infected

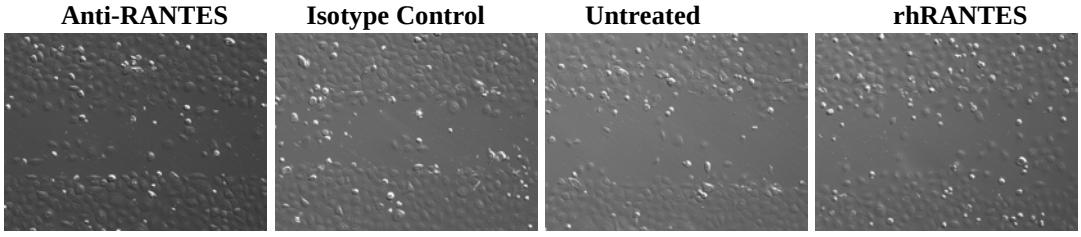

LMP1 Adenovirus Infected

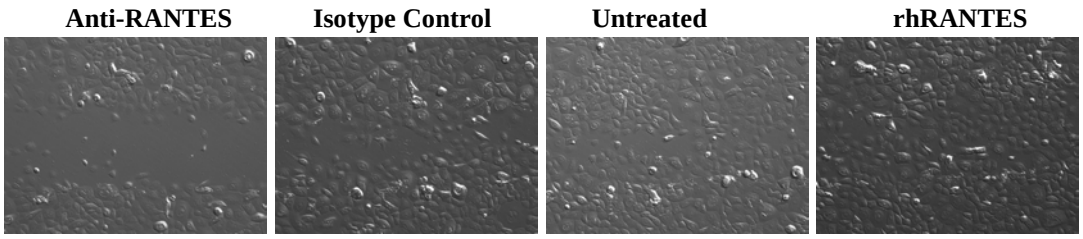

Fig 39. Scratch assay of primary human tonsil epithelial cells

48 Hours

Control Adenovirus Infected

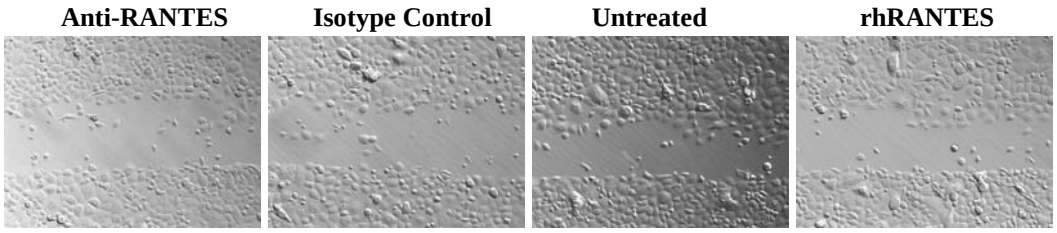

LMP1 Adenovirus Infected

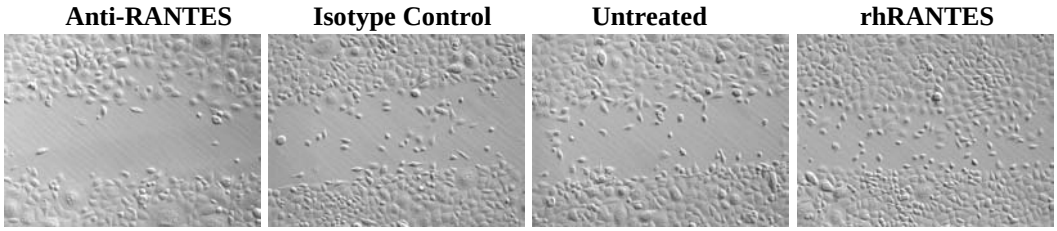

LMP2A Adenovirus Infected

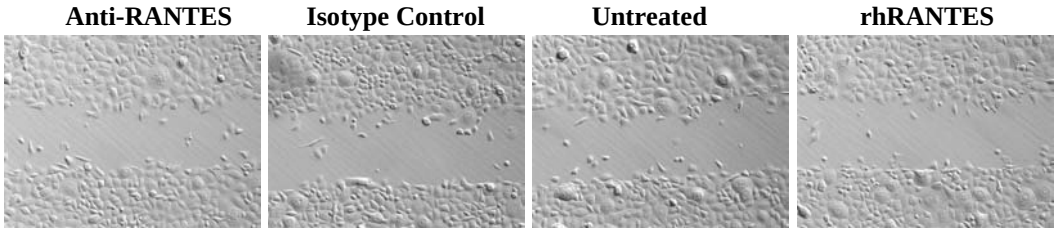

LMP1 and LMP2A Adenovirus Infected

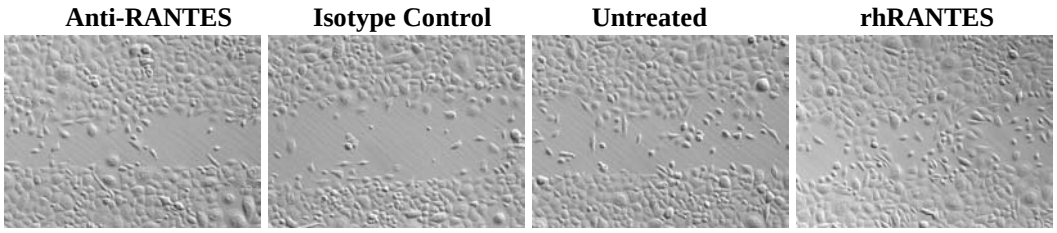

Primary Human Tonsil Epithelial Cells

72 Hours

Control Adenovirus Infected

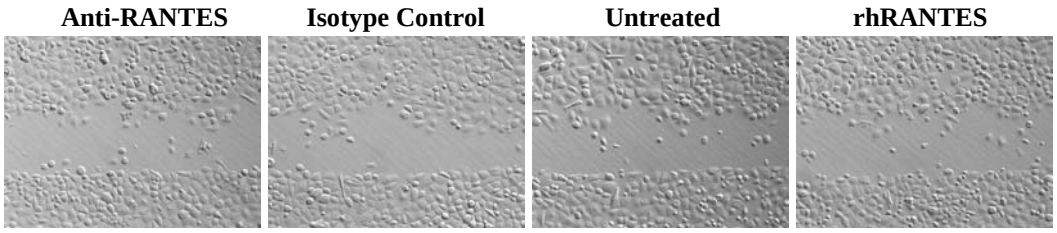

LMP1 Adenovirus Infected

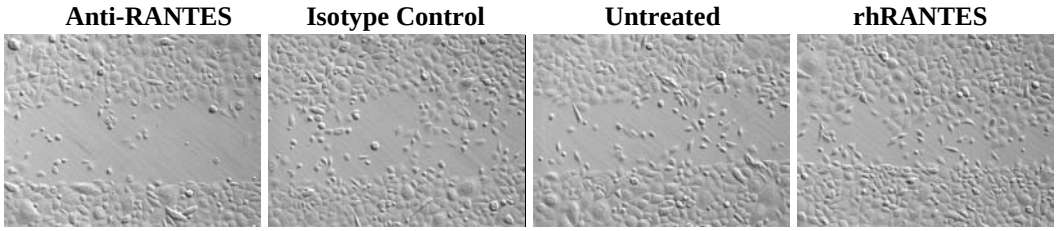

LMP2A Adenovirus Infected

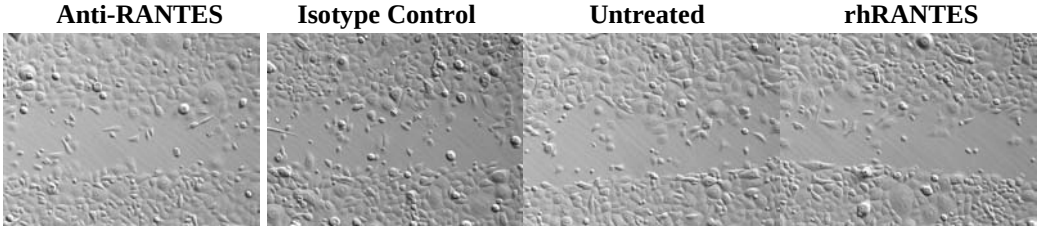

LMP1 and LMP2A Adenovirus Infected

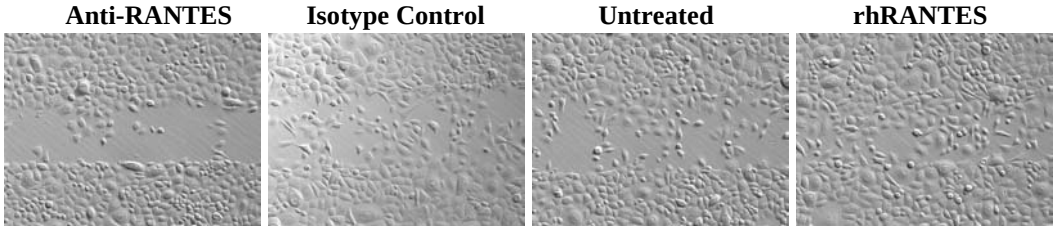

Figure 39. LMP1 and LMP2A each promote increased motility of primary tonsil epithelial cells, but LMP1 is RANTES-dependent, LMP2A is RANTES-independent. Primary epithelial cells derived from human tonsils were infected with adenoviruses to express LMP1, LMP2A, both in combination, or a mock control virus. Scratch assays were performed as before and cells were treated with an anti-RANTES neutralizing antibody, an isotype control antibody, recombinant human CCL5/RANTES protein, or were untreated. Images were taken every six hours. Compared to the control adenovirus-infected cells, the LMP1-expressing and LMP2A-expressing cells displayed increased motility. However, whereas there was a difference between the migration of LMP1-expressing cells exposed to the neutralizing anti-RANTES antibody and the isotype control antibody, there was no difference in LMP2A expressing cells to RANTES blockade. Total antibody titres were matched and cells receiving both the LMP1 and LMP2A adenoviruses displayed greater motility than either the LMP1 adenovirus or the LMP2A adenovirus alone.

Isotype Control IgG **Anti-RANTES IgG**

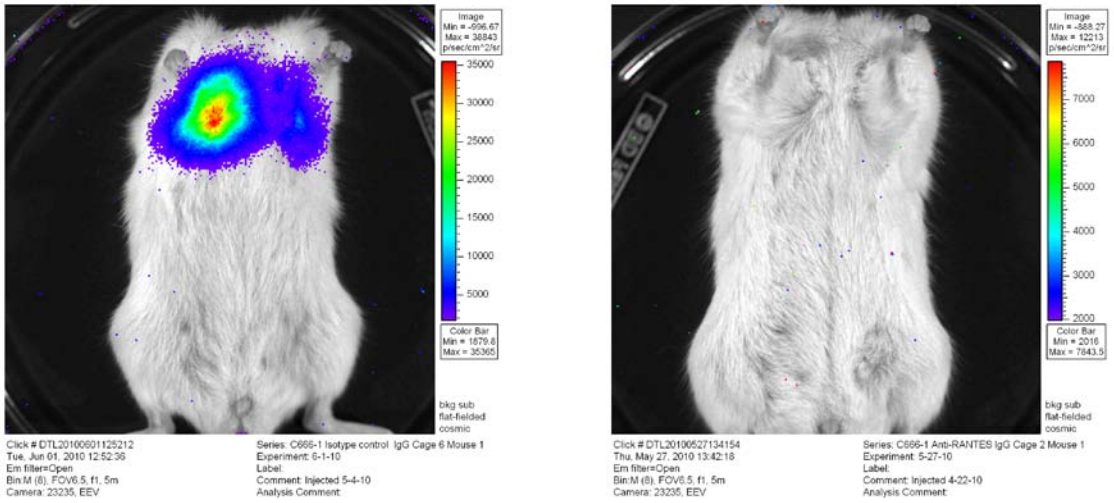

Incidence of metastasis

Isotype Control IgG: 10/24 (42%)

Anti-RANTES IgG: 4/26 (15%)

Figure 40. RANTES promotes metastasis in NPC *in vivo*. Xenograft tumors were established in NOD scid gamma mice by the orthotopic injection of C666-1 NPC cells in the nasopharynx of mice. The mice were then treated with either 32μg of anti-RANTES neutralizing antibody or an isotype control antibody, injected IP, twice a week. Tumor development in the mice was tracked for several weeks by luciferase imaging. Incidence of metastasis was reduced in mice receiving the anti-RANTES blocking antibody compared to mice receiving the isotype control antibody by the time that mice were sacrificed (15% compared to 42%, p=0.04).

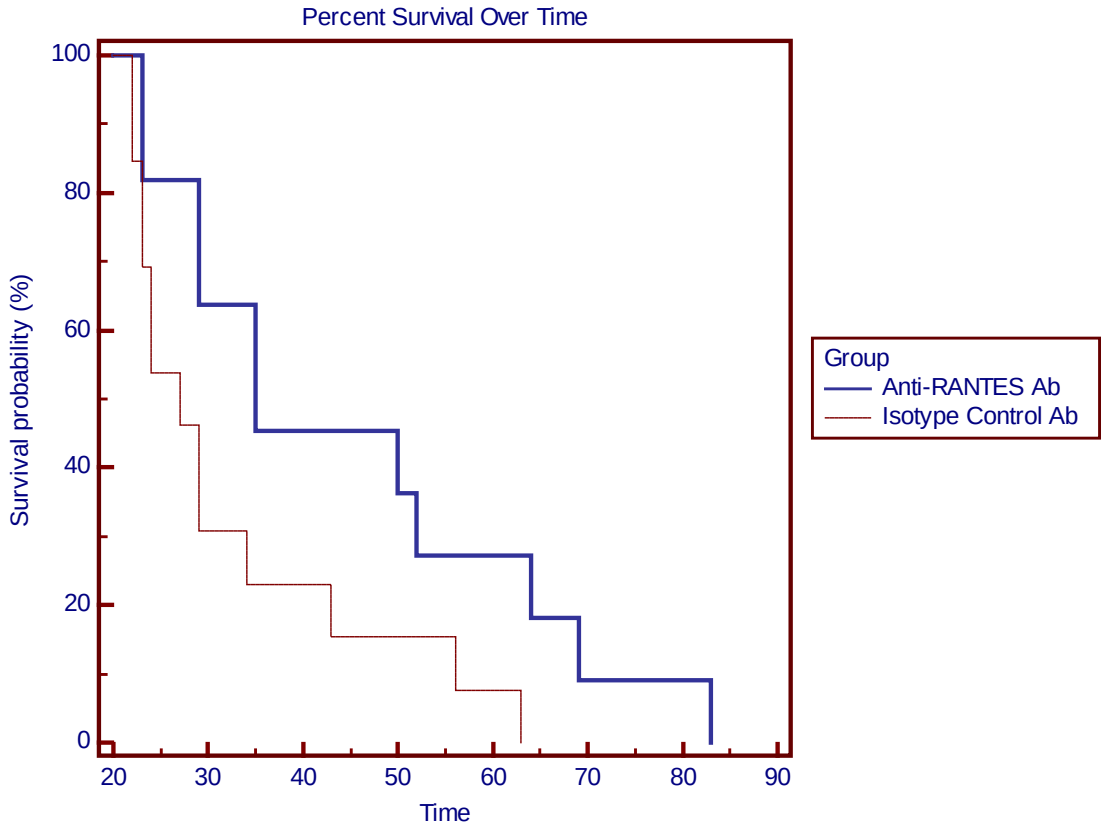

Figure 41. RANTES accelerates disease progression in NPC. Mice receiving the anti-RANTES antibody succumbed slower than mice receiving the isotype control antibody (p=0.0440). Assessment of when mice were to be euthanized was based on standard criteria for morbidity (weight loss, hunched appearance, inability to move or feed, etc.) by the Department of Laboratory Animal Medicine (DLAM) at Tufts.

Discussion

Chapter 7

The development of a novel model of nasopharyngeal carcinoma has allowed us to study factors that promote metastasis in NPC in an *in vivo* system that recapitulates disseminated disease. We analyzed the gene expression profiles of primary NPC biopsies and determined that the PI3K-Akt-mTOR pathway appeared to be more highly activated in tumors with the dedifferentiated NPC type III phenotype compared to the NPC type II phenotype. Targeting this pathway in mice decreased the formation and growth of metastases, suggesting that the PI3K-Akt-mTOR axis contributes to metastatic progression in NPC and that this pathway may be a potential target for therapy. We also showed that the EBV-encoded protein LMP1 induces the expression of CCL5/RANTES and that this chemokine may have a role in promoting invasion and metastasis in NPC.

The World Health Organization originally classified non-keratinizing NPC tumors as either NPC type II or NPC type III based on histology. This classification scheme was controversial since it was not clear whether these subtypes were derived from separate cellular origins or if the differences observed were the result of heterogeneity within the same tumor type, and perhaps reflected an aspect of progression in tumor development. “Poorly differentiated” type II tumors frequently appear to contain foci of “undifferentiated” type III cells within them, making characterization difficult and somewhat subjective. Furthermore, the standard for treatment and the prognosis for patients with respect to response to therapy and overall survival are similar. This has lead to the clinical reclassification of both type II and type III NPC as “undifferentiated.”

These treatment regimens, however, are not mechanistically targeted and as a result, would not be expected to have different responses to treatment between subtypes that may be driven by distinct underlying biochemical mechanisms.

Our results suggest that there are molecular distinctions that may account for the histological differences observed between type II and type III NPC and that the former classification scheme may have merit. Our analysis of gene expression profiles of primary NPC biopsies using the Connectivity Map suggests that NPC type III has a higher degree of activation of the PI3K-Akt-mTOR pathway. Furthermore, we have demonstrated in a xenograft model of NPC based on the type III C666-1 cell line that blocking mTORC1 signaling by the administration of Rapamycin inhibits the growth of metastases. Although patient data indicate that the incidence of metastasis and overall survival over time is similar for patients diagnosed with either NPC type II or NPC type III, we propose that this may be a reflection of histological heterogeneity within NPC tumors, specifically that within type II tumors, a foci of cells may develop after undergoing additional genetic events, resulting in a dedifferentiated type III morphology and leading to the acquisition of capabilities that increase the propensity for these cells to metastasize.

The subset of cells in the primary tumor that become competent for metastasis may become capable of colonizing distant organs, however, the malignant cells in the disseminated metastases may be mechanistically addicted to PI3K-Akt-mTOR signaling. This could explain why the formation and growth of metastases in our type III C666-1 based xenograft model appear to be dependent on mTORC1 signaling, whereas the effect of Rapamycin administration on the primary tumor is less pronounced. The difference

between the response to Rapamycin in the primary tumors and the metastases may be a reflection of different requirements for colonization that are provided in part by PI3K-Akt-mTOR signaling that are separate from the selective advantages provided by PI3K alterations earlier in tumor development that were necessary for oncogenic transformation in the primary tumor. This would argue that Rapamycin and other PI3K-Akt-mTOR inhibitors may have a significant therapeutic value for inhibiting the development of metastases in patients with non-keratinizing NPC, regardless of whether it is seen as type II or type III at the time of diagnosis. The apparent requirement for PI3K-Akt-mTOR signaling for metastatic progression is in agreement with clinical data which report that in NPC patients from Tunisia, PI3K amplification and increased Akt activity in the primary tumor correlates with poor prognosis due to higher rates of metastasis, irrespective of whether the tumors were classified as type II or type III at the time of diagnosis (Fendri, 2009).

Our proposal, that NPC tumors are heterogeneous and that a subset of type II NPC cells may undergo additional alterations to become more metastatically proficient type III cells, may explain why the injection of a pure population of type II HONE Akata cells into the nasopharynx of NOD scid gamma mice very rarely results in metastasis, whereas the injected type III C666-1 cells metastasize very efficiently.

Phenotypic and genetic divergence within a tumor has been reported in studies of other carcinomas. For example, in non-small cell lung cancer, adenomatous carcinoma and squamous cell carcinoma subtypes can be distinguished histologically (Bastide, 2009, West, 2009.) Both subtypes have historically received similar treatment in the clinic.

However, recently, genetic differences have been identified which may prove to be useful in directing targeted therapy (Ceppi, 2006, Monica, 2009.)

In addition to being less differentiated than type II NPC, type III NPC cells exhibit a more infiltrative pattern of growth with indistinct cell margins and dispersion amongst surrounding lymphoid and epithelial cells (Ali, 1967, Shanmugaratnam, 1993.) This description of dedifferentiation and increased invasiveness is consistent with the characteristics of malignant cells which undergo epithelial-mesenchymal transition (EMT). The possibility that type III NPC cells represent a population of NPC cells which are undergoing EMT is supported by our analysis of the gene expression profiles of primary NPC biopsies using Gene Set Enrichment Analysis. Our data shows a significant overrepresentation of genes associated with EMT in 8 NPC type III biopsies compared to 6 NPC type II biopsies.

The possibility that EMT may be a feature of type III NPC would be consistent with higher PI3K-Akt activity since PI3K-Akt activation has been reported to be a central feature of EMT (Larue, 2005). A potential link between increased PI3K-Akt activity and EMT in NPC is supported by evidence that overexpression of the polycomb group protein Bmi-1, which is frequently dysregulated in NPC and correlates with an invasive phenotype and poor prognosis, induces EMT characteristics in human nasopharyngeal epithelial cells. Bmi-1 suppresses PTEN, thereby increasing PI3K-Akt activity and stabilizes Snail, ultimately resulting in the downregulation of E-cadherin and promoting EMT (Song, 2009).

The demonstration that targeting the PI3K-Akt-mTOR pathway dramatically reduces the formation and growth of metastases in our mouse model can be seen as a

proof of concept that this mouse model is an effective tool for screening therapeutic agents and studying mechanisms that drive metastasis in an *in vivo* setting. Importantly, it demonstrates that molecular features that were identified in the gene expression analysis of primary biopsies were retained in the NPC cell lines used in the mouse model. It also provides preclinical data that suggests that Rapamycin and other PI3K pathway inhibitors should be considered for clinical trials for treatment of advanced disseminated NPC.

These results have significant clinical importance, since there is an urgent need for new therapeutic approaches to treat aggressively invasive and metastatic NPC. At the time of diagnosis, NPC most frequently has already progressed to advanced disease. Despite improvements in radiation and chemotherapy, survival at 5-years is less than 60% (Lee, 2005). The rate of recurrence after treatment is greater than 50% (Parkin, 1992) and of these, about half are solid organ metastases which tend to be refractory to further treatment. The median survival time after recurrence is less than 12 months (O'Sullivan, 2007). Therefore, novel therapeutics that are effective in targeting disseminated disease are critically needed, and our orthotopic xenograft mouse model provides a preclinical platform to evaluate drug efficacy.

The mediators and cellular effectors of inflammation are important constituents of the local environment of tumors. In some types of cancer, inflammatory conditions are present before a malignant transformation occurs. Conversely, in other types of cancer, oncogenic pathogenesis induces an inflammatory microenvironment that promotes the development of tumors. Inflammation in the tumor microenvironment has many tumor-

promoting effects. Cytokines and chemokines are components of an intensive dialog promoting angiogenesis, metastasis, and subversion of adaptive immunity.

CCL5/RANTES has been reported to be expressed at elevated levels in advanced breast cancer, where it correlates with poor prognosis (Luboshits, 1999, Niwa, 20001). It has been demonstrated to be a chemoattractant for stromal cells, including macrophages, which may have a role in promoting tumor development, and can improve vascularization in the tumor microenvironment, as well as act directly on breast cancer cells by inducing the expression of the matrix metalloproteinase MMP9 (Azenshtein, 2002). CCL5/RANTES has also been reported to contribute to neoplastic development in lung cancer (Borczuk, 2008) and in prostate cancer (Vaday, 2006).

Our finding that the EBV-encoded protein LMP1 induces the expression of RANTES in epithelial cells opens the possibility that this is a mechanism in which EBV may promote inflammation in premalignant nasopharyngeal lesions, leading to the recruitment of stroma which may contribute to cancer pathogenesis. A report that bone marrow derived mesenchymal stem cells (MSCs) stimulate breast cancer cells to metastasize via secreted CCL5/RANTES (Karnoub, 2007) prompted us to examine whether RANTES also enhances motility, invasive ability and metastatic potential of NPC cells. The results of *in vitro* scratch assays and *in vivo* experiments using our orthotopic xenograft NPC mouse model suggest that RANTES may provide a significant contribution to metastatic progression. This suggests that CCL5 analogues and CCR5 antagonists developed for anti-HIV therapy could potentially have therapeutic value in treating advanced NPC.

We have identified several key mechanisms which appear to support the development of metastasis in NPC. Based on our understanding of which stages these events appear to be crucial, we can incorporate these steps into our model of NPC pathogenesis (figure 42).

Figure 42. Proposed model of nasopharyngeal carcinoma pathogenesis

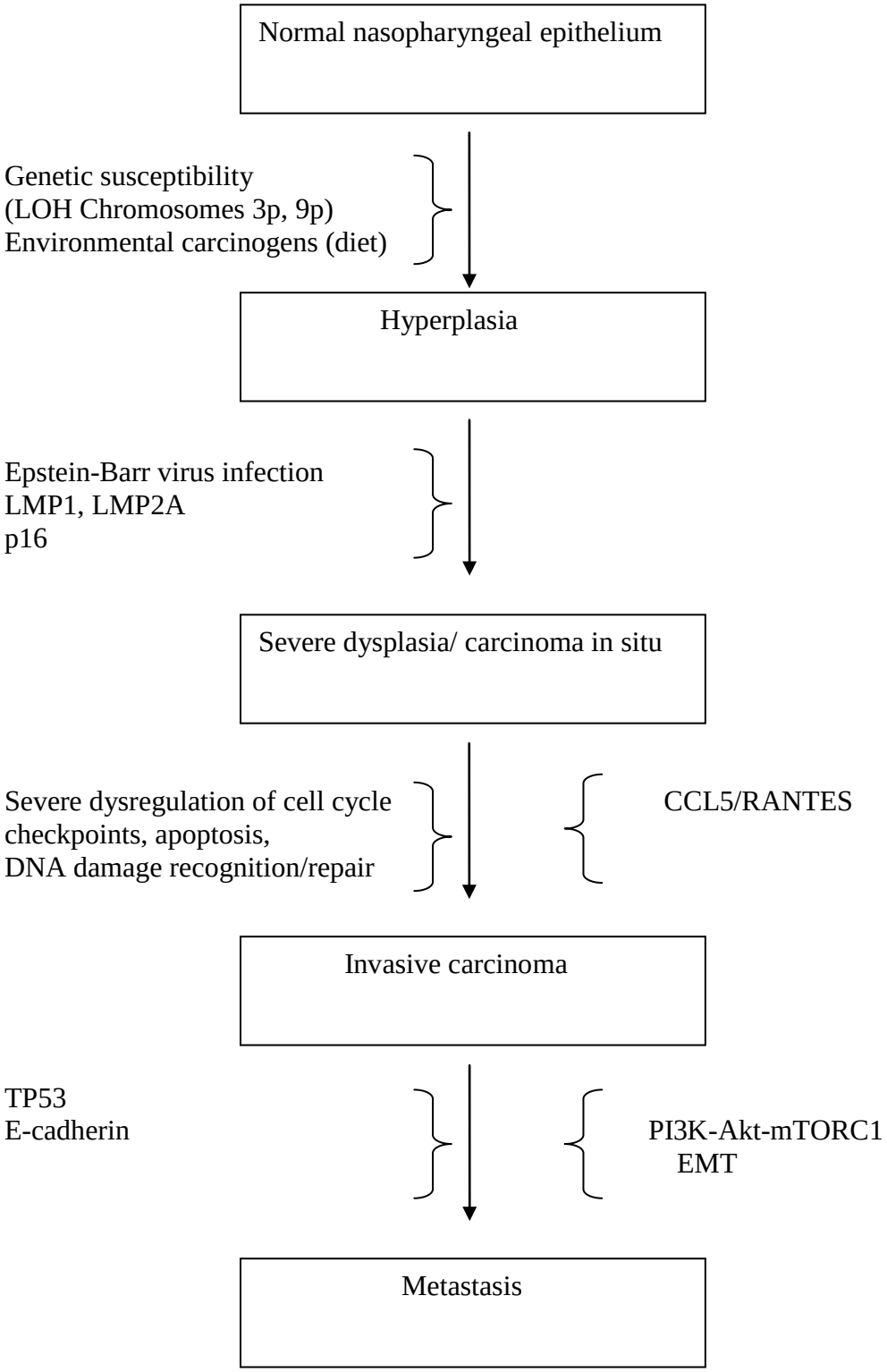

References

1. Ali, M. Y., Shanmugaratnam, K. (1967) Cytodiagnosis of nasopharyngeal carcinoma. Acta Cytol. 11. 54-60

2. Anderton, E., Yee, J., Smith, P., Crook, T., White, R.E., Allday, M.J. (2008) Two Epstein-Barr virus (EBV) oncoproteins cooperate to repress expression of the proapoptotic tumor suppressor Bim: clues to the pathogenesis of Burkitt's lymphoma. Oncogene. 27. 421-433

3. Azenshtein, E., Luboshits, G., Shina, S., Neumark, E., Shahbazian, D., Weil, M., Wigler, N., Keydar, I., Ben-Baruch, A. (2002) The CC chemokine RANTES in breast carcinoma progression: regulation of expression and potential mechanisms of promalignant activity. Cancer Res. 62, 1093–1102

4. Bastide, K., Ugolin, N., Levalois, C., Bernaudin, J. F., Chevillard. (2009) Are adenosquamous lung carcinomas a simple mix of adenocarcinomas and squamous cell carcinomas or more complex at the molecular level? Lung Cancer. 68. 1-9

5. Baum, B., Settleman, J., Quinlan, M. P. (2008) Transitions between epithelial and mesenchymal states in development and disease. Semin. Cell Dev. Biol. 19. 294-308

6. Borczuk, A. et al. (2008) Lung adenocarcinoma invasion in *TGFRII*-deficient cells is mediated by CCL5/RANTES. Oncogene 27**,** 557–564

7. Borza, C., Hutt-Fletcher, L. M. (2002) Alternate replication in B cells and epithelial cells switches tropism of Epstein-Barr virus. Nature Medicine. 8. 594-599

8. Busson, P., McCoy, R., Sadler, R., Gilligan, K., Turz, T., Raab-Traub, N. (1992) Consistent transcription of the Epstein-Barr virus LMP2 gene in nasopharyngeal carcinoma. Journal of Virology. 66. 3257-32-62

9. Caldwell, R. G., Wilson, J. B., Anderson, S. J., Longnecker, R. (1998) Epstein-Barr virus LMP2A drives B cell development and survival in the absence of normal B cell receptor signals. Immunity. 9. 405-411

10. Ceppi, P., Volante, M., Saviozzi, S., Rapa, I., Novello, S., Cambieri, A., Lo Iacono, M., Cappia, S., Papotti, M., Scagliotti, G. V. (2006) Squamous cell carcinoma of the lung compared with other histotypes shows higher messenger RNA and protein levels for thymidylate synthase. Cancer. 107. 1589-1596

11. Chambers, A. F., Groom, A. C., MacDonald, I. C. (2002) Dissemination and growth of cancer cells in metastatic sites. Nature Reviews Cancer. 2. 563-572.

12. Chesnokova L.S., Nishimurs S.L., Hutt-Fletcher, L.M. (2009) Fusion of epithelial cells by Epstein-Barr virus proteins is triggered by binding of viral glycoproteins gHgL to integrins αvβ6 or αvβ8. PNAS. 106(48). 20464-20469

13. Cohen, J.I., Wang, F., Mannick, J., Kieff, E. (1989) Epstein-Barr virus nuclear protein 2 is a key determinant of lymphocyte transformation. PNAS. 86. 9558-9562

14. de Visser, K. E., Eichten, A., Coussins, L. M. (2006) Paradoxical roles of the immune system during cancer development. Nature Reviews Cancer. 6. 24-37

15. DiNitto, J. P., Cronin, T. C., Lambright, D. G. (2003) Membrane recognition and targeting by lipid-binding domains. Science Signaling. 2003. re 16

16. Dumont, N., Wilson, M. B., Crawford, Y. G., Reynolds, P. A., Sigaroudinia, M., Tisty, T. D. (2008) Sustained induction of epithelial to mesenchymal transition activates DNA methylation of genes silenced in basal-like breast cancers. PNAS. 105. 14867-14872

17. Engelman, J. A. (2009) Targeting PI3K signaling in cancer: oppurtunities, challenges and limitations. Nature Reviews Cancer. 9. 550-562

18. Fendri, A., Khabir, A., Mnejja, W., Sellami-Boudawara, T., Daoud, J., Frikha, M., Ghorbel, A., Gargouri, A., Mokdad-Gargouri, R. (2009) PIK3CA amplification is

predictive of poor prognosis in Tunisian patients with nasopharyngeal carcinoma. Cancer Sci. 100. 2034-2039

19. Franke, T. F., Kaplan, D. R., Cantley, L. C., Toker, A. (1997) Direct regulation of Akt proto-oncogene product by phosphatidylinositol-3,4-bisphosphate. Science. 275. 665-668

20. Gires, O., Zimber-Strobl, U., Gonnella, R., Ueffing, M., Marschall, G., Zeidler, R., Pich, D., Hammerschmidt, W. (1997) Latent membrane protein 1 of Epstein-Barr virus mimics a constitutively active receptor molecule. EMBO J. 16. 6131-6140

21. Guo, C., Sah, J. F., Beard, L., Wilson, J. K., Markowitz, S. D., Guda, K. (2008) The noncoding RNA miR-126 suppresses the growth of neoplastic cells by targeting phophatidylinositol 3-kinase signaling and is frequently lost in colon cancers. Genes Chromosomes Cancer. 47. 939-946

22. Gupta, G. P., Massague, J. (2006) Cancer metastasis: building a framework. Cell. 127. 679-695.

23. Grossman, S.R., Johannsen E., Tong, R., Yalamanchili, R., Kieff, E. (1994) The Epstein-Barr virus nuclear antigen 2 transactivator is directed to response elements by the Jκ recombination signal binding protein. PNAS. 91. 7568-7572

24. Hammerschmidt, W., Sugden, B. (1989) Genetic Analysis of immortalizing functions of Epstein-Barr virus in human B lymphocytes. Nature. 340. 393-397

25. Heussinger, N., Buttner, M., Ott, G., Brachtel, E., Pilch, B. Z., Kremmer, E., Niedobitek. (2004) Expression of the Epstein-Barr virus (EBV)-encoded latent membrane protein 2A (LMP2A) in EBV-associated nasopharyngeal carcinoma. J Pathol. 203. 696-699

26. Hui, A. B., Lo, K. W., Teo, P. M., To, K. F., Huang, D. P. (2002) Genome wide detection of oncogene amplifications in nasopharyngeal carcinoma by array based comparative genomic hybridization. Int J Oncol. 20. 467-73

27. Hsieh, J.J., Hayward, S.D. (1995) Masking of the CBF1/RBPJκ transcriptional repression domain by Epstein-Barr virus EBNA2. Science. 268. 560-563

28. Hu, G., Chong, R. A., Yang, Q., Wei, Y., Blanco, M. A., Li, F., Reiss, M., Au, J. L., Haffty, B. G., Kang, Y. (2009) MTDH activation by 8q22 genomic gain promotes chemoresistance and metastasis of poor-prognosis breast cancer. Cancer Cell. 15. 9-20

29. Humme S, Reisbach G, Feederle R, Delecluse HJ, Bousset K, Hammerschmidt W, Schepers A. (2003) The EBV nuclear antigen 1 (EBNA1) enhances B cell immortalization several thousandfold. PNAS. 100(19). 10989-94

30. Inoki, K., Li, Y., Zhu, T., Wu, J., Guan, K. L. (2002) TSC2 is phosphorylated and inhibited by Akt and suppresses mTOR signalling. Nature Cell Biology. 4. 648-657

31. Jia, W.H. (2004) Familial risk and clustering of nasopharyngeal carcinoma in Guangdong, China. Cancer. 101. 363-369

32. Kang Y., Siegel, P. M., Shu, W., Drobnjak, M., Kakonen, S. M., Cordon-Cardo, C., Guise, T. A., Massague, J. (2003) A multigenic program mediating breast cancer metastasis to bone. Cancer Cell. 3. 537-549

33. Karboub, A. E., Dash, A. B., Vo, A. P., Sullivan, A., Brooks, M. W., Bell, G. W., Richardson, A. L., Polyak, K., Tubo, R., Weinberg, R. A. (2007) Mesenchymal stem cells within tumor stroma promote breast cancer metastasis. Nature. 449. 557-563

34. Kaye, K.M., Izumi, K.M., Kieff, E. (1993) Epstein-Barr virus latent membrane protein 1 is essential for B lymphocyte growth transformation. PNAS. 90. 9150-9154

35. Kieff, E., Rickinson, A.B. (2001) Fields Virology. Lippincott Williams and Wilkins, Philadelphia. 2511-2574

36. Kilger, E., Kieser, A., Baumann, M., Hammerschmidt, W. (1998) Epstein-Barr virus mediated B cell proliferation is dependent upon latent membrane protein 1, which simulates an activated CD40 receptor. EBMO. 17. 1700-1709

37. Klein, C. A. (2003) The systemic progression of human cancer: a focus on the individual disseminated cancer cell - the unit of selection. Adv. Cancer Res. 89. 35-67

38. Larue, L., Bellacosa, A. (2005) Epithelial-mesenchymal transition in development of cancer: role of phosphatidylinositol 3' kinase/Akt pathways. Oncogene. 24. 7443-7454

39. Lee A.W., Foo, W., Law, S.C., Poon, Y.F., Sze, W.M., O,S.K., Tung, S.Y., and Lau, W.H., (1997) Nasopharyngeal carcinoma: presenting symptoms and duration before diagnosis. Hong Kong Med J. 3. 355-361

40. Lee A. W., Foo W, Mang O, Sze WM, Chappell R, Lau WH, Ko WM. (2003) Changing epidemiology of nasopharyngeal carcinoma in Hong Kong over a 20-year period (1980-99): an encouraging reduction in both incidence and mortality. Int J Cancer. 103(5). 680-685

41. Lee, A. W., Sze W.M. (2005) Treatment results for nasopharyngeal carcinoma in the modern era: the Hong Kong experience. Int J Radiat Oncol Biol Phys. 61. 11071116

42. Levitskaya J., Coram, M., Levitsky, V., Imreh, S., Steigerwald-Mullen, P.M., Klein, G., Kurilla, M.G., Masucci, M.G. (1995) Inhibition of antigen processing by the internal repeat region of the Epstein-Barr virus nuclear antigen-1. Nature. 375. 685-688

43. Lin, E. Y., Li, J. F., Gnatovskiy, L., Deng, Y., Zhu, L., Grzesik, D. A., Qian, H., Xue, X. N., Pollard, J. W. (2006) Macrophages regulate the angiogenic switch in a mouse model of breast cancer. Cancer Res. 66. 11238-11246

44. Lo, K. W., Huang, D. P. (2002) Genetic and epigenetic changes in nasopharyngeal carcinoma. Semin. Cancer Biol. 12. 451-462

45. Longnecker, R. (2000) Epstein-Barr latency: LMP2, a regulator or means for Epstein-Barr virus persistence? Adv Cancer Res. 79. 175-200

46. Luboshits, G. et al. (1999)Elevated expression of the CC chemokine regulated on activation, normal T cell expressed and secreted (RANTES) in advanced breast carcinoma. Cancer Res. 59, 4681–4687

47. Majumder, P. K., Febbo, P. G., Bikoff, R., Berger, R., Xue, Q., McMahon, L. M., Manola, J., Brugarolas, J., McDonnell, T.J., Golub, T.R., Loda, M., Lane, H.A., Sellers, W. R. (2004) mTOR inhibition reverses Akt-dependent prostate intraepithelial neoplasia through regulation of apoptotic and HIF-1-dependent pathways. Nature Medicine. 10. 594-601

48. Mannick, J.B., Cohen, J.I., Birkenbach, M., Marchini, A., Kieff, E. (1991) The Epstein-Barr virus nuclear protein encoded by the leader of the EBNA RNAs is important in B lymphocyte transformation. Journal of Virology. 65. 6826-6837

49. Mantovani, A., Allanvena, P., Sica, A., Balkwill, F. (2008) Cancer-related inflammation. Nature 454. 436-444

50. Marks, J.E., Phillips, J.L. Menck, H.R. (1998) The National Cancer Database report on the relationship of race and national origin to the histology of nasopharyngeal carcinoma. Cancer. 83. 582-588

51. Massague, J. (2008) TGFβ in cancer. Cell. 134. 215-230

52. Medzhitov, R. (2008) Origing and physiological roles of inflammation. Nature. 454. 428-435

53. Minna, J. D., Kurie, J. M., Jacks, T. (2003) A big step in the study of small cell lung cancer. Cancer Cell. 4. 163-166

54. Monica, V., Sagliotti, G. V., Ceppi, P., Righi, L., Cambieri, A., Lo Iaccono, M., Saviozzi, S., Volante, M., Novello, S., Papotti, M. (2009) Differential thymidylate synthase expression in different variants of large-cell carcinoma of the lung. Clin Cancer Res. 15. 7547-7552

55. Moody, S. E., Sarkisian, C. J., Hahn, K. T., Gunther, E. J., Pickup, S., Dugan, K. D., Innocent, N., Cardiff, R. D., Schnall, M. D., Chodosh, L. A. (2002) Conditional activation of Neu in the mammary epithelium of transgenic mice results in reversible pulmonary metastasis. Cancer Cell. 2. 451-461

56. Mori, S., Chang, J. T., Andrechek, E. R., Matsumura, N., Baba, T., Yao, G., Kim, J. W. Gatza, M., Murphy, S., Nevins, J. R. (2009) Anchorage-independent cell growth signature identifies tumors with metastatic potential: Expression signature for anchorage independence. Oncogene. 28. 2796-2805

57. Mosialos, G., Birkenbach, M., Yalamanchili, R., Van Arsdale, T., Ware, C., Kieff. (1995) The Epstein-Barr virus transforming protein LMP1 engages signaling proteins for the tumor necrosis factor receptor family. Cell. 80. 389-399

58. Mullen, M.M., Haan, K.M., Longnecker, R., Jardetzky, T.S., (2002) Structure of the Epstein-Barr Virus gp42 protein bound to the MHC class II receptor HLA-DR1. Molecular Cell. 9. 375-385

59. Nanbo, A., Inoue, K., Adachi-Takasawa, K., Takada, K. (2002) Epstein-Barr virus RNA confers resistance to interferon-α-induced apoptosis in Burkitt's lymphoma. EMBO J. 21. 954-965

60. Nemerow, G.R., Mold, C., Schwend, V.K., Tollefson, V., Cooper, N.R., (1987) Identification of gp350 as the viral glycoprotein mediating attachment of Epstein-Barr virus (EBV) to the EBV/Cd3 receptor of B cells: sequence homology of gp350 and C3 complement fragment Cd3. Journal of Virology. 61. 1416-1420

61. Neshat, M. S., Mellinghoff, I. K., Tran, C., Stiles, B., Thomas, G., Petersen, R., Frost, P., Gibbons, J. J., Wu, H., Sawyers, C. L. (2001) Enhanced sensitivity of PTEN-deficient tumors to inhibition of FRAP/mTOR. PNAS. 98. 10314-10319

62. Nguyen, D. X., Massague, J. (2007) Genetic determinants of cancer metastasis. Nature Reviews Genetics. 8. 341-352

63. Nguyen, D. X., Bos, P. D., Massague, J. (2009) Metastasis: from dissemination to organ-specific colonization. Nature Reviews Cancer. 9. 274-284

64. Niwa, Y. et al. (2001) Correlation of tissue and plasma RANTES levels with disease course in patients with breast or cervical cancer. Clin. Cancer Res. 7, 285–289

65. Nozawa, H., Chiu, C., Hanahan, D. Infiltrating neutrophils mediate the initial angiogenic switch in a mouse model of multistage carcinogenesis. (2006) PNAS 103. 12493-12498

66. Or, Y. Y,, Hui, A. B., Tam, K. Y., Huang, D.P., Lo, K. W. (2005) Characterization of chromosome 3q and 12q amplicons in nasopharyngeal carcinoma cell lines. Int J Oncol. 26. 49-56

67. O'Sullivan, B. (2007) Nasopharynx cancer: therapeutic value of chemoradiotherapy. Int J Radiat Oncol Biol Phys. 69. S118-21

68. Ozdamar, B., Bose, R., Barrios-Rodiles, M., Wang, H. R., Zhang, Y., Wrana, J. L. (2005) Regulation of the polarity protein Par6 by TGF beta receptors controls epithelial cell plasticity. Science. 307. 1603-1809

69. Parker, G.A., Crook, T., Bain, M., Sara, E.A., Farrell, P.J., Allday, M.J. (1996) Epstein-Barr virus nuclear antigen (EBNA)3C is an immortalizing oncoprotein with similar properties to adenovirus E1A and papillomavirus E7. Oncogene. 13. 2541-2529

70. Parker, G.A., Touitou, R., Allday, M.J. (2000) Epstein-Barr virus EBNA3C can disrupt multiple cell cycle checkpoints and induce nuclear division divorced from cytokinesis. Oncogene. 19. 700-709

71. Parkin, D. M., Muir, C. S. (1992) Cancer incidence in five continents, comparability and quality of data. IARC Sci Publ. 120. 45-173

72. Pathmanathan, R., Prasad, U., Sadler, R., Flynn, K., Raab-Traub, N. (1995) Clonal proliferations of cells infected with Epstein-Barr virus in preinvasive lesions related to nasopharyngeal carcinoma. New England Journal of Medicine. 333. 693-698

73. Pegtel, D. M., Middeldorp, J., Thorley-Lawson, D. A. (2004) Epstein-Barr virus infection in ex vivo tonsil epithelial cell cultures of asymptomatic carriers. Journal of Virology. 78. 12613-12624

74. Podsypanina, K., Lee, R. T., Politis, C., Hennessy, I., Crane, A., Puc, J., Neshat, M., Wang, H., Yang, L., Gibbons, J., Frost, P., Dreisbach, V., Blenis, J., Gaciong, Z., Fisher, P., Sawyers, C., Hedrick-Ellenson, L., Parsons, R. (20001) An inhibitor of mTOR reduces neoplasia and normalizes p70/S6 kinase activity in Pten+/- mice. PNAS. 98. 10320-10325

75. Potter, C. J., Pedraza, L. G., Xu, T. (2002) Akt regulates growth by directly phosphorylating Tsc2. Nature Cell Biology. 4. 658-665

76. Raab-Traub, N., Flynn, K. (1986) The structure of the termini of the Epstein-Barr virus as a marker of clonal cellular proliferation. Cell. 47. 883-889

77. Robertson, E., Lin, J., Kieff, E. (1996) The amino-terminal domains of Epstein- Barr virus nuclear proteins 3A, 3B and 3C interact with RBP- Jκ. Journal of Virology. 70. 3068-3074

78. Ruf, I. K., Ryne, P. W., Yang, C., Cleveland, J. L., Sample, J. T. (2000) Epstein-Barr virus small RNAs potentiate tumourigenicity of Burkitt lymphoma cells independently of apoptosis. Journal of Virology. 74. 10223-10228

79. Scholle, F., Bendt, K.M., Raab-Traub, N. (2000) Epstein-Barr virus LMP2A transforms epithelial cells, inhibits cell differentiation, and activates Akt. Journal of Virology. 74. 10681-10689

80. Slamon, D. J., Leyland-Jones, B., Shak, S., Fuchs, H., Paton, V., Bajamonde, A., Fleming, T., Eiermann W., Wolter, J., Pegram, M., Baselga, J., Norton, L. (2001) Use of Chemotherapy plus a monoclonal antibody against HER2 for metastatic breast cancer that overexpresses HER2. The New England Journal of Medicine. 344. 783-792

81. Shanmugaratnam, K., Sobin, L. H. (1993) The World Health Organization histological classification of tumors of the upper respiratory tract and ear. A commentary on the second edition. Cancer. 71. 2689-2697

82. Sinclair, A.J., Palmero I., Peters, G., Farrell, P.J. (1994) EBNA-2 and EBNA-LP cooperate to cause G0 and G1 transition during immortalization of resting human B lymphocytes by Epstein-Barr virus. EMBO J. 13. 3321-3328

83. Song, L. B., Li, J., Liao, W.T., Feng, Y., Yu, C. P., Hu, L. J., Kong, Q. L., Xu, L.H., Zhang, X., Liu, W. L., Li, M. Z., Zhang, L., Kang, T. B., Fu, L. W., Huang, W.L., Xia, Y. F., Tsao, S. W., Li, M., Band, V., Band, H., Shi, Q. H., Zeng, Y. X., Zeng, M. S. (2009) The polycomb group protein Bmi-1 represses the tumor suppressor PTEN and induces epithelial-mesenchymal transition in human nasopharyngeal epithelial cells. J Clin Invest. 119. 3626-3636

84. Stein, U., Walther, W., Arlt, F., Schwabe, H., Smith, J., Fichtner, I., Birchmeier, W., Schlag, P. M. (2009) MACC1, a newly identified key regulator of HGF-MET signaling, predicts colon cancer metastasis. Nature Medicine. 15. 59-67

85. Sutkowski, N., Chen, G., Calderon, G., Huber, B. T. (2004) Epstein-Barr virus latent membrane protein LMP-2A is sufficient for transactivation of the human endogenous retrovirus HERV-K18 superantigen. Journal of Virology. 78. 7852-7860

86. Tavazoie, S. F., Alarcon, C., Oskarsson, T., Padua, D., Wang, Q., Bos, P. D., Gerald, W. L., Massague, J. (2008) Endogenous human microRNAs that suppress breast cancer metastasis. Nature. 451. 147-152

87. Thiery, J. P., Sleeman, J. P. (2006) Complex networks orchestrate epithelial-mesenchymal transitions. Nature Reviews Molecular Biology. 7. 131-142

88. Thorley-Lawson, D.A. (2001) Epstein-Barr virus: exploiting the immune system. Nature Reviews Immunology. 1. 75-82

89. Tomkinson, B., Robertson, E., Kieff, E. (1993) Epstein-Barr virus nuclear proteins EBNA-3A and EBNA-3C are essential for B lymphocyte transformation. Journal of Virology. 67. 2014-2025

90. Uchida, J., Yasui, T., Takaoka-Shichijo, Y., Muraoka, M., Kulwichit, W., Raab-Traub, N., Kikutani, H. (1999) Mimicry of CD40 signals by Epstein-Barr virus LMP1 in B lymphocyte responses. Science. 286. 300-303

91. Vaday, G. G., Peehl, D. M., Kadam, P. A., Lawrence, D. M. (2006) Expression of CCL5 (RANTES) and CCR5 in prostate cancer. Prostate. 66. 124-134

92. Vincan, E., Barker, N. (2008) The upstream components of the Wnt signaling pathway in the dynamic EMT and MET associated with colorectal cancer progression. Clin. Exp. Metastasis. 25. 657-663

93. Vokes, E.E. Liebowitz, D.N. and Weicheselbaum, R.R. (1997) Nasopharyngeal Carcinoma. Lancet. 350. 1087-1091

94. Wang, Z., Banergee, S., Li, Y, Rahman, K. M., Zhang, Y., Sarkar, F. H. (2006) Down-regulation of notch-1 inhibits invasion by inactivation of nuclear factor-kappaB, vascular endothelial growth factor, and matrix metalloproteinase-9 in pancreatic cancer cells. Cancer Res. 66. 2778-2784

95. Wang, D., Liebowitz, D., Kieff, E. (1985) An EBV membrane protein expressed in immortalized lymphocytes transforms established rodent cells. Cell. 43. 831-840

96. West, H., Harpole, D., Travis, W. (2009) Histologic considerations for individualized systemic therapy approaches for the management of non-small cell lung cancer. Chest. 136. 1112-1118

97. Wilson, J.B., Bell, J. L., Levine, A.J., (1996) Expression of Epstein-Barr virus nuclear antigen-1 induces B cell neoplasia in transgenic mice. EMBO J. 15. 3117-3126

98. Yang, J., Weinberg, R. A. (2008) Epithelial-mesenchymal transition: at the crossroads of development and tumor metastasis. Dev. Cell. 14, 818-829

99. Yin, J. J., Selander, K., Chirgwin, J. M., Dallas, M., Grubbs, B. G., Wieser, R., Massague, J., Mundy, G. R., Guise, T. A. (1999) TGF-beta signaling blockade inhibits PTHrP secretion by breast cancer cells and bone metastases development. Journal of Clinical Investigation. 103. 197-206

100. Yu, M.C. and Yuan, J.M. (2002) Epidemiology of nasopharyngeal carcinoma. Semin Cancer Biol. 12. 421-429

101. Zhao, B., Marshall, D.R., Sample, C.E. (1996) A conserved domain of the Epstein-Barr virus nuclear antigens 3A and 3C binds to a discrete domain of Jk. Journal of Virology. 70. 4228